ATM and p400: Characterisation of a novel interaction between a DNA repair enzyme and a chromatin remodeler

A thesis presented to Massey University in partial fulfilment of the requirement for the degree of Doctor of Philosophy in Biochemistry.

Rebecca Jane Smith

2014

Just keep swimming…

Dory, Finding Nemo 2003

Acknowledgements

They say that the acknowledgements are often the hardest part of a thesis to write. Often they are the only part of a thesis read and yet they can never truly express how you feel. I shall try to give it my best shot, but realise that my way with words is not the best and I owe everyone more than I can say.

First and foremost I must thank my supervisor, Jeong Park. You took me on as a student fresh out of undergraduate study and have turned me into a scientist. You never gave up on me and together we waded our way through some trials. I will forever be grateful for the skills you have taught me and I will take them with me though my science career.

To Kathryn Stowell, you have been much more than just a cosupervisor to me. Your encouragement, support and insight were more than I could have ever expected. I hope you know how much I appreciate everything you have done for me.

To my lab members past and present, please forgive me for being a grump on those bad days and for laughing with me on the good ones. Clare, you and your 'purple' shorts will always make me smile. To the members of the Twilite Zone, your kindness and patience will always be remembered.

Thanks to the New Zealand Federation of Graduate Women, the Institute of Fundamental Science and Massey University for the financial support.

To my friends and family for your continued support: Bob, Neroli, Kim, Mark, Dan, Alex and Leah, thanks for making home a place where I could relax and escape the stress of the lab when needed; Stacey, for being the ray of sunshine on a gloomy day; Patrick and Remai, for making uni so much more enjoyable and always having time for a laugh; Rebecca Bloomer, particularly in these last few months while I have been writing, your daily pep talks have been vital; Ems and Steph, you are by far the best friends anyone could ever ask for.

Finally to Mum and Dad. You have always believed in me and given me the greatest support. I hope I have made you proud. Love you.

Abstract

The ability to maintain genomic integrity prevents unrestricted cell proliferation and the progression of cancer. DNA repair pathways such as the DNA double-strand break (DSB) response are essential in maintaining this integrity. This system requires activation of the serine/threonine kinase ataxia telangiectasia mutated (ATM) through acetylation by TIP60, a histone acetyl transferase, and subsequent ATM autophosphorylation. During DNA repair, activated ATM phosphorylates the histone variant H2AX several kilobases either side of the break site. This phosphorylation acts a signal for additional repair proteins and chromatin remodeling complexes which repairs DNA.

In a previous study, H2AX phosphorylation was induced through the over expression of TIP60 or the SWI3-ADA2-N-CoR-TFIIIB (SANT) domain of p400. It was hypothesised that over expressed TIP60 or SANT domain was able to sequester a putative negative regulator from the ATM-TIP60 complex and artificially induce activation. This study aimed to investigate if a single domain of TIP60 or if a single helix from the three helix SANT domain was responsible for the activation of the ATM-TIP60 complex. Here, the ability of the chromo domain and zinc domain of TIP60 individually and the combined zincHat domain of TIP60 to induce H2AX phosphorylation as well as three helix deletion mutants of the SANT domain of p400 was examined. While all constructs were able to be expressed in human cell lines, the induction of H2AX was variable and non-reproducible.

ATM belongs to the phosphatidylinositol 3-kinase-related kinase family (PIKK). Members of the PIKK family show domain homology, where the domain of one protein is replaced with the homologous domain of another member and the function of the protein is not altered. As p400 has been previously shown to interact with TIP60 and also Transformation/transcription domain-associated protein (TRRAP), a member of the PIKK family, it was hypothesised that p400 could interact with ATM (which also interacts with TIP60). This study confirms this novel interaction between ATM and p400 through the use of co-immunoprecipitation and protein localisation using confocal microscopy. This study provides a platform to further investigate the involvement of an ATM-p400 complex during DNA repair.

Abbreviations

-ve	Negative
A	Ampere
ADA2	Adaptor 2
Amp	Ampicillin
APS	Ammonium persulphate
AP	Apurnic or Apyrimidic
AT	Ataxia Telangiectasia
ATM	Ataxia Telangiectasia Mutated
ATP	Adenosine triphosphate
ATR	ATM and Rad3-related
BAF53	BRG1-associated factor of 53 kDa
bp	Base pair
BSA	Bovine Serum Albumin
c-Abl	Abelson murine leukemia viral oncogene homolog 1
ChIP	Chromatin ImmunoPrecipitation
CiP	Claf intestinal phosphatase
CMV	Cytomegalovirus
DAPI	4',6-diamidino-2-phenylindole
ddH_2O	Double distilled water
DDR	DNA damage response
DMEM	Dulbecco's Modified Eagle Medium
DNA	Deoxyribose nucleic acid
DNA-PKcs	DNA-dependent protein kinase catalytic subunit
dNTPs	Deoxyribonucleotide triphosphate
DSB	Double strand break
dTIP60	Drosophila TIP60 homologue
DTT	Dithiothreitol
E.coil	*Escherichia coli*
EDTA	Ethylene diamine tetra-acetic acid
EtOH	Ethanol
FAT	FRAP-ATM-TRRAP
FAT-C	FAT domain located at the C-terminus of the protein
FBS	Fetal bovine serum
FRAP	Fluorescence recovery after photobleaching
FRET	Fluorescence resonance energy transfer
g	Gram
GAS41	Glioma-amplified-sequence 41
GST	Glutatione S-Transferase
h	Hours
H2Av	Drosophila H2AZ and H2AX homologue

H2AX-P	H2AX phosphorylated at serine 139
H3K9me	Methylated H3K9
HA	Hemagglutinin
HAT	Histone acetyl transferase
HEK293T	Human embryonic kidney cell line
HD	High definition
HF	High fidelity
HDAC	Histone deacetylase
HP1	Heterochromatin binding protein 1
HRP	Horse radish peroxidase
HSA	Helicase and SANT Associated
IB	Immunoblot
IgG	Immunoglobulin G
IP	Immunoprecipitation
IPTG	Isopropyl β-D-1-thiogalactopyranoside
ISWI	Imitation SWI
K	Lysine
kb	Kilo bases
kDa	Kilo dalton
L	Liter
L	Ladder
LB	Luria Bertani bacteriological media
M2 agarose	α-FLAG antibody immobilized on agarose beads
mA	miliampere
Mb	megabase
mCi	Millicurie
mg	Milligram
min	Minute
mL	Milliliter
mM	Millimol
MRN	Mre11-Rad3-Nsb1
Mre11	Meiotic recombination 11
mTOR/FRAP	FKBP adarapamycin associated protein / mammalian target of rapamycin
MYST	MOZ, YBF2/SAS3, SAS2 and TIP60
NBS	Nijmegen breakage syndrome
NEB	New England Biolab
ng	Nano gram
NLS	Nuclear localization sequence
nm	nano meter
NP-40	Igapal CA-630
nt	Nucleotide
P1	Generation 1 of baculovirus
PBS	Phosphate buffered saline
PCR	Polymerase chain reaction

PHYRE2	Protein Homology/analogY Recognition Engine V 2.0
PI3K	phosphatidylinositol 3-kinase
PIKK	phosphatidylinositol 3-kinase-like protein kinases
pmol	Picomol
PMSF	Phenylmethanesulfonylfluorise solution
PVDF	Polyvinylidenine fluoride
Q	Glutamine
RNA	Ribose nucleic acid
S	Serine
s	second
SANT	SWI3-ADA2-N-CoR-TFIIIB
SDS	Sodium dodecylsulphate
SDS-PAGE	Sodium dodecylsulphate polyacrylamide gel electrophoresis
SF9	clonal isolate of Spodoptera frugiperda Sf21 cells
siRNA	small interfering RNA
SV40	Simian virus 40
SWI2/SNF2	switch 2/sucrose non-fermentable 2
TAT	Transactivator of transcription
TBE	Tris Boric acid EDTA
TBS/T	Tris-buffered saline with tween 20
TEMED	N, N, N', N'- Tetramethylethylene diamie
TIP48	transactivation-domain interacting protein of 48 kDa
TIP49	transactivation-domain interacting protein of 49 kDa
TIP60	HIV-I TAT interacting protein of 60 kDa
Tris	2-amino-2-hydromethyl-1,3-propanidol
TRRAP	transformation/transcription domain-associated protein
µg	microgram
µL	microliter
UV	Ultraviolet light
V	volts
WT	Wild Type
X-gal	5-bromo-4-chloro-3-indolyl-beta-D-galacto-pyranoside

List of Figures

List of Tables

Table of Contents

1 Introduction

1.1 Chromatin dynamics

Each cell of an organism contains an entire genomic complement of DNA. To ensure that this DNA fits into the cell, it must be packaged into a higher-ordered structure called chromatin. The most basic unit of chromatin is the nucleosome, where 147 nucleotides of DNA wrap around an octomer of histone proteins consisting of two histone H2A/H2B dimers and a tetramer of histone H3 and H4 (Luger, 1997). A histone has two major domains, the globular domain and the histone tail. The globular domains make up the central core of the nucleosome with the histone tails protruding out from the nucleosome core. The histone tails are capable of being modified by a large range of enzymes including kinases and histone acetyl transferases and these types of modifications facilitate different chromatin structures (Luger, 1998).

There are several orders of chromatin folding which are schematically represented in figure 1.1. The most basic form of folding is known as the 'bead on a string' or the 10 nm fibre where nucleosomes are connected by linker DNA (Luger, 1997). The second level of organisation is the 30 nm fibre where the 10 nm fibre is folded together using histone H1 to maintain this higher level of folding (P. J. J. Robinson, Fairall, Huynh, & Rhodes, 2006). The 30 nm fibre is able to fold into even higher levels of chromatin structure. These higher levels of organisation require the use of architectural proteins such as histone H1 and heterochromatin protein 1 (HP1) to maintain the highly organised folding (Canzio et al., 2011).

There are two main folding states of chromatin, euchromatin and heterochromatin. Euchromatin is an open chromatin structure that is associated with active regions of transcription and is promoted by the presence of specific histone modifications. One of the best characterised examples of a histone modification promoting the euchromatic state is acetylation of histone H4 on lysine 16. This acetylation on the positively charged lysine residue neutralises its overall charge which eliminates a charge interaction between the lysine residue and DNA phosphate group promoting a more open structure (Shogren-Knaak et al., 2006). Conversely, heterochromatin is a highly folded state of chromatin that is associated with regions of DNA that are not actively

transcribed. These regions assume the 30 nm chromatin structure, higher order chromatin folding and require a different set of chromatin modifications to maintain folding. For example, trimethylation of histone H3 at lysine 9 acts as a docking site for heterochromatin protein 1 (HP1) which help maintain a heterochromatic state (Fischle et al., 2005).

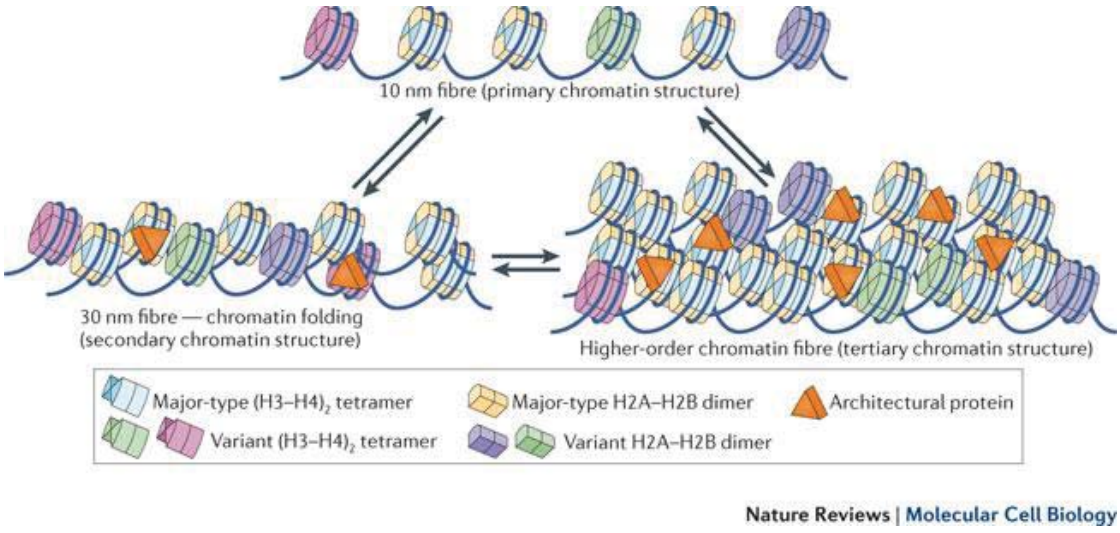

Figure 1.1 States of chromatin folding. Chromatin adopts different levels of folding depending on a number of factor including post-translational modification and the presence of architectural proteins. The basic chromatin structure is the 10 nm fibre with nucleosomes connected by linker DNA. Higher levels of chromatin folding include the 30 nm fibre and the higher-order chromatin fibre. These higher levels are maintained by the presence of post-translational modifications and architectural proteins. Reprinted by permission from Macmillan Publishers Ltd on behalf of Cancer Research UK: [Nature Reviews Molecular Cell Biology] (13, 436-447), copyright 2012.

The post-translational modifications found on histone tails are highly dynamic and reversibly added and removed by a variety of proteins. These include histone acetyl transferases and histone deacetylases to add and remove acetylation marks, methylases and demethylases to add and remove methyl groups, kinases and phosphatases to add and remove phosphate groups and a range of other proteins involved in ribosylation, sumoylation and ubiquitination. Each type of modification has different effects on chromatin structure. Acetylation results in neutralisation of lysine's positive charge which has been known to prevent the folding of chromatin to the 30 nm structure (Philip J. J. Robinson et al., 2008). Phosphorylation adds an additional negative charge to the nucleosome and is often the site for protein binding (Stucki et al., 2008). Methylation

does not alter the charge on proteins and acts as a binding site for proteins such as HP1 (Fischle et al., 2005). Ribosylation, sumoylation and ubiquitination also act as binding motifs for a number of targeting proteins (Messner & Hottiger, 2011; Shiio & Eisenman, 2003; Zhang, 2003). This study focuses on protein complexes that are involved in the modification of histones and other proteins that occurs upon DNA damage. Thus the dynamic state of chromatin applies not only to replication, transcription and recombination, but also to the DNA repair process.

1.2 Histone Variants

In addition to the regular core histones, H2A, H2B, H3 and H4, there are several histone variants that have roles in various specific functions. One such example is the histone variant H3.3. This variant is enriched in actively transcribed genes where it was shown to destabilize H3.3/H4 tetramers in nucleosomes and facilitate a more open chromatin structure for the access of transcription factors (Elsaesser, Goldberg, & Allis, 2010). Of interest to this study are the H2A variants, particularly H2AX and H2AZ.

H2AZ is a histone variant that was first identified in 1980 and has been shown to be deposited at specific sites in the genome by chromatin remodeling complexes including the p400 ATPase and accounts for approximately 10% of the total H2A in a cell (Chan, Narita, Lowe, & Livingstone, 2005; West & Bonner, 1980). H2AZ has 64% sequence homology to the canonical H2A and contains an extended acidic patch in its C-terminal region which may help to stabilize higher order chromatin structures (Hardy et al., 2009). H2AZ deposition at promoters has been shown to have both positive and negative effects on transcription. In *Saccharomyces cerevisiae*, H2AZ deposition is increased in promoter regions of genes where it is thought to interact with transcriptional machinery or RNA polymerase II itself (Adam, Robert, Larochelle, & Gaudreau, 2001; Larochelle & Gaudreau, 2003; Wong, Cox, & Chrivia, 2007). A study conducted in 2003 examined the global deposition of H2AZ in *Saccharomyces cerevisiae* and showed that 107 promoters containing H2AZ were repressed while 214 promoters containing H2AZ were induced (Meneghini, Wu, & Madhani, 2003). Interestingly, the type of post-translational modification may be essential in determining the action of H2AZ during transcription. For example, acetylated H2AZ has been associated with transcriptional activation due to its ability to promote a more open chromatin structure while ubiqutination of H2AZ is found throughout heterochromatin

and provides a binding site for heterochromatin promoting factors (Draker, Sarcinella, & Cheung, 2011; Sarcinella, Zuzarte, Lau, Draker, & Cheung, 2007; Valdes-Mora et al., 2012). Interestingly, H2AZ has the ability to be methylated at specific sites which prevents acetylation making methylation and acetylation mutually exclusive (Zilberman, Coleman-Derr, Ballinger, & Henikoff, 2008).

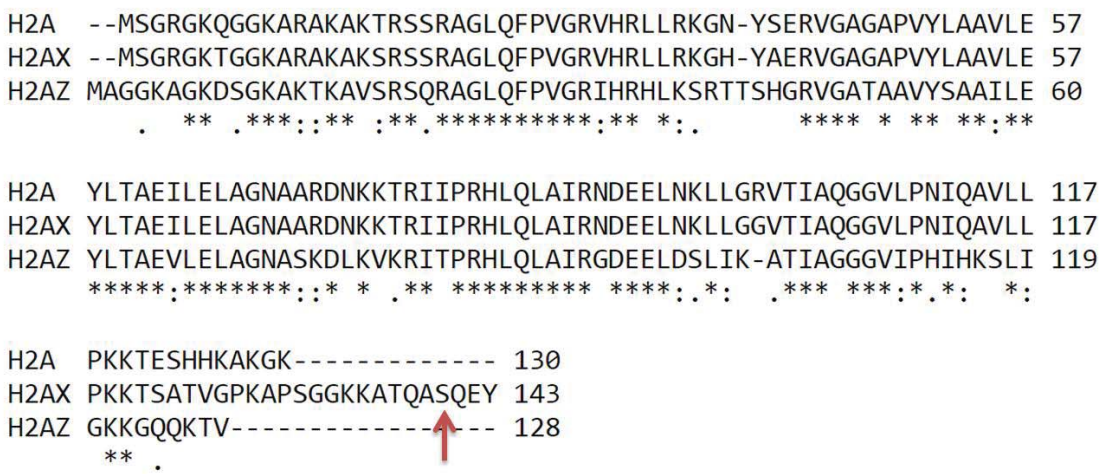

Figure 1.2 H2A variant protein alignment. Sequences for H2A (M60752.1), H2AX (NM_002105.2) and H2AZ (AH006891.1) were aligned using ClustalW. Stars (*) denote conserved residues between all three proteins while dots (.) denote conserved residues between two proteins. Serine 139 in H2AX which is phosphorylated by members of the PIKK family of kinases during DNA repair is shown by the red arrow.

The second histone H2A variant of interest to this study if H2AX. H2AX is a variant that found throughout the genome and is incorporated randomly into chromatin during DNA replication. H2AX shows 95% homology to canonical H2A and contains a C terminal extension with a SQ motif that is recognized by serine/threonine kinases (Pinto & Flaus, 2010). Serine 139, positioned within the C terminal extension (indicated in Figure 1.2 by a red arrow), is readily phosphorylated around DNA break sites which acts as an identification signal for sites of DNA repair as exemplified by the fact that knockdown of H2AX results in decreased accumulation of repair proteins at these break sites (Celeste et al., 2003; Rogakou, Pilch, Orr, Ivanova, & Bonner, 1998). Interestingly, H2AX knockout mice show an increase in chromosomal aberrations, deficiencies in double-strand break repair and an overall increase in sensitivity to DNA damage highlighting the importance of H2AX in DNA repair (Bassing et al., 2002; Celeste et al., 2003; Kao et al., 2006). Additionally, inability to acetylate H2AX inhibits the exchange of modified H2AX for unmodified H2AX during DNA repair and leads to an

overall reduction in repair efficiency (X. Jiang, Y. Xu, & B. D. Price, 2010) illustrating acetylation of H2AX is one of a number of post-translational modification that are essential in H2AXs role in DNA repair.

1.3 DNA repair

The importance of maintaining DNA integrity is possibly best exemplified by an increased risk of cancer development with unrepaired DNA aberrations. The changes to the genome through unrepaired DNA lead to mutations that can result in unrestricted cell growth, promoting malignancies (Stratton, Campbell, & Futreal, 2009). In order to maintain DNA integrity, cells have evolved a number of repair systems which can be grouped into two main categories of single-strand break repair and double-strand break repair. Single-strand break repair consists of base excision repair, nucleotide excision repair and mismatch repair while double-strand break repair consists of homologous recombination and non-homologous end joining.

1.3.1 Single-strand break repair

Each of the single-stand break repair systems recognize and repair different types of single strand malformations. Mismatch repair occurs primarily during replication and acts on incorrectly incorporated bases and loops formed from insertions and deletions. This system relies on being able to recognize the parent strand and hence removal of the incorrectly incorporated nucleotides on the daughter strand (Jiricny, 2006). In *E.coli* this type of mechanism uses methylation on the parent strand as a means of recognition, however, the mammalian recognition system is less well understood (Acharya, Foster, Brooks, & Fishel, 2003; Kramer, Kramer, & Fritz, 1984; Lahue, Au, & Modrich, 1989).

Base excision repair is used for the repair of subtle DNA changes which include alkylation and oxidation. A lesion is first recognized by sensor proteins, particularly DNA glycosylases which are capable of removing the nitrogenous base by cleaving the N-glycosidic bond between the base and the deoxyribose sugar. This leaves an AP (apurinic or apyridimic) gap. The DNA backbone is then cleaved creating a single strand break that contains a 3’ hydroxyl group and a 5’ phosphate group. The break is filled by a polymerase and the backbone is repaired by a ligase (David, O'Shea, & Kundu, 2007).

Nucleotide excision repair is required for bulkier adducts that tend to cause distortions in the helical structure. One such example of this is pyrimidine dimers that are produced due to UV exposure. While there are a variety of different types of distortions and a number of repair systems, in general the adduct is identified and targeted for removal of 20-30 nucleotides. The gap which is created is then refilled using general replication machinery (Batty & Wood, 2000; de Laat, Jaspers, & Hoeijmakers, 1999).

1.3.2 Double-strand break repair

While all damage to DNA needs to be recognized and repaired, DNA double-strand breaks are potentially more harmful lesions compared to single-strand breaks as they have the potential to cause chromosomal translocations or loss of chromosomal fragments (Halazonetis, Gorgoulis, & Bartek, 2008). Two well-studied pathways in double-strand break repair are homologous recombination and non-homologous end joining.

Homologous recombination is a method of error-free double-strand break repair where there is no loss or gain of DNA. This occurs primarily during DNA replication and the G2 stage of the cell cycle. Homologous recombination requires the break site to be processed into single-strand DNA which is then used to search by strand invasion for the homologous region in the sister chromatid. This region is then used as a template to complete repair (Filippo, Sung, & Klein, 2008). The second type of double-strand break repair is non-homologous end joining. This repair system can occur at any stage of the cell cycle. It works by simply religating the DNA ends with limited processing and as such, is an error-prone mechanism of repair (Lieber, 2008). Interestingly, these repair systems show similarities in their initial steps. The double-strand break is first recognized by a phosphatidylinositol 3-kinase-related kinase (PIKK) family member will phosphorylate H2AX around break sites. ATM (Ataxia telangiectasia mutated), ATR (ATM and Rad3-related) and DNA-PKcs are used interchangeable for H2AX phosphorylation in response to different stresses (Falck, Coates, & Jackson, 2005; Stiff et al., 2004). The phosphorylation of H2AX will promote the accumulation of repair proteins with each pathway requiring a different complement of proteins (Stucki et al., 2005; I. M. Ward, Minn, Jorda, & Chen, 2003). Homologous recombination uses a larger number of proteins that will process DNA to produce single-stranded DNA before these are used in strand invasion to locate homologous regions that can be used as a template for completing repair (Filippo et al., 2008). Non-homologous end joining,

with minimal trimming, predominantly uses the MRN complex (Mre11, Rad50 and NSB1) to tether the two ends and proceeds to ligate these together using a DNA ligase (Lieber, 2008). Chromatin remodeling complexes are involved in the final stages of both types of double-strand break repair through exchanging modified nucleosomes for unmodified nucleosomes to return chromatin to a pre-break state (Doyon & Cote, 2004; Kusch et al., 2004).

The DNA DSB response is an essential process for maintaining cellular integrity and requires an orchestrated effort of many proteins that must to work synergistically to promote repair. An exact blueprint of the order of events however, is unknown. While DNA double-strand breaks are repaired by both homologous recombination and non-homologous end joining, multi-subunit protein complexes which include TIP60, ATM and p400 have conserved roles in both processes. The roles these proteins during transcription and DNA repair are addressed below.

1.4 TIP60- A Histone Acetyl Transferase

TIP60 (TAT interacting protein) was originally identified through an interaction with the HIV protein TAT (Transactivator of transcription) (Kamine, Elangovan, Subramanian, Coleman, & Chinnadurai, 1996) where it was shown to slightly enhance the activation of specific HIV promoters. TIP60 was subsequently shown to acetylate H2A, H3 and H4 of the core histones (Yamamoto & Horikoshi, 1997) as well as non-histone proteins such as p53 and ATM (Chailleux et al., 2010; Sun, Jiang, Chen, Fernandes, & Price, 2005; Tang, Luo, Zhang, & Gu, 2006). TIP60 is a member of the MYST family of acetyl transferases which are named after the four founding members, MOZ, YBF2/SAS3, SAS2 and TIP60. These proteins are characterised by the inclusion of the MYST domain which is a 200 amino acid stretch in TIP60 that contains both a zinc finger domain and an acetylCoA binding site. The zinc finger domain has been associated with protein-protein interactions and is considered essential for the acetylase function of TIP60 (Nordentoft & Jorgensen, 2003; Xiao, Chung, Kao, & Yang, 2003). TIP60 also contains a chromodomain, a domain commonly found in proteins that bind or modify chromatin (Cavialli & Paro, 1998). In the case of TIP60, the chromodomain has been shown to bind methylated H3K9 which is enriched in heterochromatic regions of the genome (Hlubek et al., 2001; Sun et al., 2009).

TIP60 is known to have a variety of functions within a cell including roles in transcriptional activation and the DNA repair. These different processes require TIP60 to be in complex with specific binding partners. The TIP60 complex is one of these larger complexes, containing at least 14 subunits including two large molecular weight proteins TRRAP (transformation/transcription domain-associated protein) and p400, along with GAS41 (glioma-amplified-sequence 41), two helicases TIP48 (transactivation-domain interacting protein of 48 kDa) and TIP49 (transactivation-domain interacting protein of 49 kDa), β-actin and a β-actin like protein BAF53 (BRG1-associated factor of 53 kDa) (T. Ikura et al., 2000). This complex serves as a chromatin remodeling complex with implications in transcriptional activation and DNA repair.

1.4.1 TIP60 as a transcriptional coactivator

A transcriptional coactivator can act in a variety of ways to promote transcription, including acting on chromatin or other proteins to elicit an effect. TIP60 can act as a transcriptional coactivator through acetylating both histones and non-histone proteins.

An example of TIP60 as a transcriptional coactivator through non-histone proteins comes through the examination of the tumor suppressor p53. In the absence of DNA damage, p53 is maintained at a low level without modification. This is mainly facilitated through an interaction with the E3 ubiquitin ligase mdm2 (murine double minute 2) which targets p53 for proteosomal degradation, keeping p53 levels at a minimum (Oliner et al., 1993). Additionally, the lack of post-translational modifications on p53 acts to maintain it in an inactive state. In the presence of low levels of DNA damage, p53 dissociates from mdm2 and become phosphorylated by kinases such as ATM which phosphorylates p53 on serine 15 (Shieh, Ikeda, Taya, & Prives, 1997). This action prevents reassociation of p53 with mdm2 and promotes p53 stabilisation and binding to the promoter of genes, such as the cell cycle inhibitor p21, to enhance cell cycle arrest as opposed to apoptosis (Li, Jenkins, Nichols, & Xiong, 1994). In cases of extensive DNA damage, the apoptosis pathway is activated. Here, p53 dissociates from mdm2 and binds to TIP60. TIP60 can then acetylate p53 at lysine 120, which is located within the DNA binding domain of p53 (Figure 1.3 A). This modification promotes p53 binding to promoters of pro-apoptotic genes such as *PUMA*, a key player in the progression of apoptosis (Tang et al., 2006). It has been found that lysine 120 (K120) mutants of p53 are unable to bind to promoters of these pro-apoptotic genes and consequently are apoptosis deficient. Additionally, ChIP data from H1299 lung

carcinoma cells presented by Sykes *et al*, 2006, show that p53 K120 mutants bind to the promoter of cell cycle inhibitors (for example p21) with higher affinity compared with pro-apoptotic genes, supporting the hypothesis that acetylation at K120 of p53 by TIP60 is required for transcription of pro-apoptotic genes (Sykes et al., 2006).

TIP60 also acts on histones in chromatin while serving as a transcriptional coactivator. One example of this occurs in conjunction with the oncogene MYC. MYC has been shown to recruit TIP60 as part of the TIP60 complex to gene promoters where TIP60 acetylates H4 promoting an open chromatin structure for binding of transcriptional machinery (Frank et al., 2003; Tyteca, Vandromme, Legube, Chevillard-Briet, & Trouche, 2006). This function of TIP60 is reliant on the TIP60 complex as a whole (Figure 1.3 B). Several members of the TIP60 complex have been shown to co-localise at promoter regions. Additionally, TIP60 isolated without the other members of the TIP60 complex can acetylate free histones but lack the ability to acetylate nucleosomes. When isolated as part of the TIP60 complex, the nucleosome acetylase function is restored (Kimura & Horikoshi, 1998).

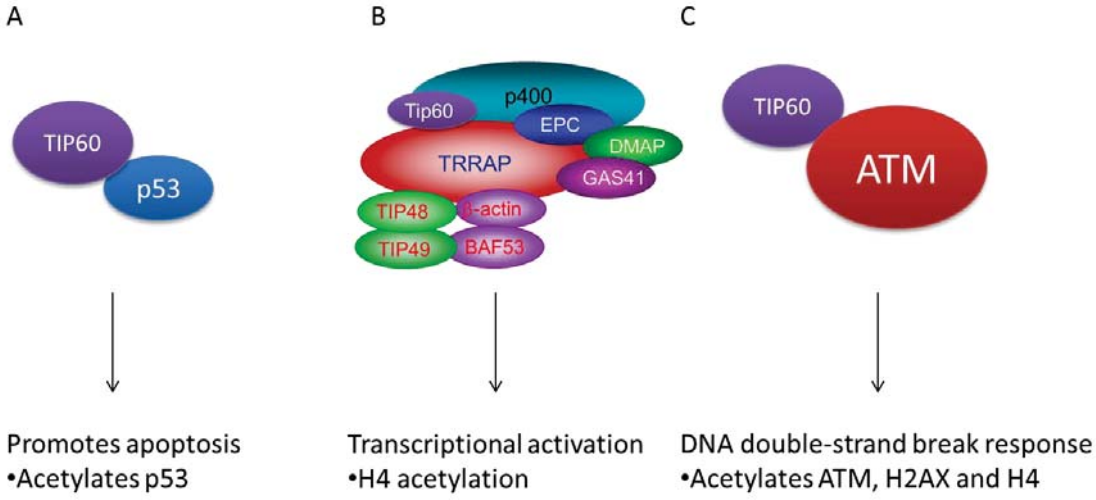

Figure 1.3 TIP60 complexes and their functions. A. TIP60 acetylates p53 in the presence of extensive DNA damage promoting apoptosis. B. TIP60 as part of the TIP60 complex to promote transcription through acetylating histone H4. C. TIP60 will acetylate ATM in the presence of DNA damage promoting ATM autophosphorylation needed for ATM activation. TIP60 will also acetylate histone H2AX and histone H4 during DNA repair.

1.4.2 TIP60 in DNA repair

DNA damage presents one of the biggest threats to cell survival. There is coordination between a vast array of proteins in the cell to ensure DNA is repaired correctly. TIP60 is involved in several key processes during which this repair protein acts to acetylate both histone and non-histone targets. Involvement of TIP60 in activation of ataxia telangiectasia mutated (ATM) kinase is possibly its most well-known function. TIP60 is associated with a dimer of inactive ATM proteins in the absence of DNA damage. In the presence of DNA damage, TIP60 is activated and will acetylate ATM at lysine 3016, promoting ATM autophosphorylation at residue 1981 (Figure 1.3 C) (Sun et al., 2005). This autophosphorylation of ATM promotes the monomerisation of ATM producing an active protein which will then phosphorylate histone H2AX around break sites, acting as a signal for the accumulation of DNA repair proteins (Burma, Chen, Murphy, Kurimasa, & Chen, 2001). The ATM-TIP60 complex appears to be a distinct complex from the larger TIP60 complex. How the ATM/TIP60 recognises DNA damage and signals activation of the down-stream repair process is currently unknown. Recently, the involvement of a tyrosine kinase, c-Abl, has been implicated in the signalling of DNA damage by phosphorylating TIP60 at tyrosine 44, activating TIP60 and promoting acetylation of ATM (Kaidi & Jackson, 2013).

In addition to its role in ATM activation, TIP60 also plays a role in DNA repair as part of the TIP60 complex. Just as TIP60 acetylates histone H4 in its role as a transcriptional activator, TIP60 as part of the TIP60 complex acetylates histone H4 of nucleosomes around DNA double-strand break sites (R. Murr et al., 2006). The involvement of the TIP60 complex in DNA repair has been validated through the depletion of a major member of the TIP60 complex and through the use of a TIP60 acetylase deficient mutant. Depletion of TRRAP, the largest scaffolding protein in the TIP60 complex, results in a marked reduction in histone H4 acetylation in response to DNA damage. Additionally, the introduction of a TIP60 acetylase deficient mutant also shows a reduction in H4 acetylation with the reduction in H4 acetylation resulting in reduced repair efficiency. Acetylation of histone H4 is particularly important in DNA repair as it allows chromatin structure to take a more open conformation, presumably for the assembly of repair proteins at the break site (R. Murr et al., 2006). The chromodomain of TIP60 is particularly important in DNA repair as it has been shown to bind to the heterochromatic mark tri-methyl H3K9, providing a mechanism for TIP60 to bind to

heterochromatin regions and promote an open chromatin structure for DNA repair (Sun et al., 2009).

TIP60 also shows a role in acetylation of H2AX which is essential for histone exchange at break sites. In Drosophila, the acetylation of H2Av (a H2AX/H2AZ homologue) is needed for the exchange of modified H2Av for unmodified H2Av. This exchange is thought to restore chromatin to its original state before DNA damage occurred. In Drosophila, this exchange is catalysed by the chromatin remodeler Domino of which the human homologue is known as p400 (X. F. Jiang, Y. Xu, & B. D. Price, 2010; Kusch et al., 2004).

1.5 p400

p400 was initially described in 2001 by Fuchs et al as a part of a protein complex that is essential for transformation with the adenovirus E1A oncoprotein (Fuchs et al., 2001). p400 is a multidomain protein that contains a HSA (Helicase and SANT Associated) domain, a SWI2/SNF2 (switch 2/sucrose non-fermentable 2) homology domain, a poly-Q (poly-glutamine) domain and a SANT (SWI3-ADA2-N-CoR-TFIIIB) domain (Aasland, Stewart, & Gibson, 1996). While the SWI2/SNF2 domain has been shown to exhibit ATP dependent histone exchange, there is little information available regarding the function of the remaining domains within p400 (Fuchs et al., 2001). p400 exists as part of two multi-protein complexes known as the TIP60 complex and the p400 complex (Fuchs et al., 2001; T. Ikura et al., 2000). These two complexes have the same composition of subunits except for TIP60 which does not reside in the p400 complex. The additional proteins found in these complexes include TRRAP, BAF53 (53 kDa BRG1/human BRG1-associated factor), TIP60 associated proteins TAP53α and β, as well as TIP49 (TATA binding protein (TBP)- interacting protein). The similarity between the two complexes suggests a possible dynamic exchange between the p400 and TIP60 complexes where the p400 complex lacks histone acetylase activity (Fuchs et al., 2001; T. Ikura et al., 2000; Park, Sun, & Roeder, 2010).

1.5.1 H2AZ exchange by p400

The importance of p400 and its function can be highlighted through the retention of homologues throughout evolution. *Saccharomyces cerevisiae* contains a homologue of p400 known as Swr1p (Swi2/Snf2 related). Swr1p is shown to deposit the histone variant H2AZ in eurochromatic regions that flank heterochromatic regions (Kobor et al.,

2004). Silencing of Swr1p showed a marked decrease in H2AZ deposition and spread of heterochromatic regions. Swr1p is also found within a functionally conserved complex of proteins known as the SWR1 complex which shares common subunits with the yeast NuA4 complex (Doyon & Cote, 2004; Doyon, Selleck, Lane, Tan, & Cote, 2004). These two complexes are homologous to the TIP60 complex in humans and carry many of the same functions. The p400 homologue in drosophila is known as Domino and is found in the drosophila TIP60 complex, dTIP60-Domino. Importantly, this protein has been shown to catalyse the exchange of H2A for H2Av, the drosophila H2AX/H2AZ homologue, at sites of DNA damage (Kusch et al., 2004). When p400 was first isolated, it was assumed to be involved in histone exchange due to the inclusion of the SWI2/SNF2 ATPase homology domain (Fuchs et al., 2001). The H2AZ exchange of p400 in human cells was initially described through the p21 promoter. In the presence of DNA damage, H2AZ was removed from the promoter of the p21 gene which resulted in an increase in expression of p21 (Gevry, Chan, Laflamme, Livingston, & Gaudreau, 2007).

1.5.2 The SANT domain

While the ATPase function of p400 has been associated with the SWI2/SNF2 domain, there is little information regarding the function of the additional domains (Fuchs et al., 2001). The SANT domain motif is part of the MYB family of proteins, where the MYB domain, the MYB-like domain and the SANT domain share the familiar helix-turn-helix motif that manifests as a three helix bundle (Boyer, Latek, & Peterson, 2004). There is debate regarding the function of the SANT domain. It has been suggested that the SANT domain has a DNA binding role as it shares a similar structure MYB and MYB-like domains which are known DNA binding domains (Mohrmann, Kal, & Verrijzer, 2002). The second role proposed is that it is necessary for protein-protein interactions (Humphrey et al., 2001; Sterner, Wang, Bloom, Simon, & Berger, 2002).

Interestingly, the SANT domain is a common motif within chromatin remodeling proteins. A SWI/SNF (switch deficiency/sucrose non-fermentable) family member, Swi3, and RSC (remodel the structure of chromatin) are both ATP dependent chromatin remodelers that have a dependency on the SANT domain for their function (Barbaric, Reinke, & Horz, 2003; Boyer et al., 2002). Small deletions within the each of the three helices result in a reduction in activity with deletions in the third helix resulting in the greatest reduction in activity (Barbaric et al., 2003; Boyer et al., 2002). This function

appears to be conserved across the MYB and MYB-like domains with the third helix being considered the recognition helix (Barbaric et al., 2003; Boyer et al., 2002; Pinson, Sagot, Borne, Gabrielsen, & Daignan-Fornier, 1998; Sterner et al., 2002).

While little information regarding the function of the SANT domain of p400 is available, there has been some evidence provided that it is important in protein-protein interactions. The SANT domain of p400 has been described to interact with the histone acetyl transferase, TIP60 and cause a robust inhibition of TIP60 acetylase activity (Park et al., 2010). A second protein interaction was suggested in a study completed in 2010. Here, overexpression of the SANT domain of p400 induced an increase in H2AX phosphorylation (Smith, 2010). It was suggested that a putative negative regulator associated with the TIP60-ATM complex becomes sequestered by the overexpressed SANT domain promoting TIP60 activation. This putative interaction appears to have a protective effect on cells against DNA damage, and overexpression of the SANT domain appears to increase cell viability when faced with a lethal dose of UV irradiation (Smith, 2010). Understanding the role of the p400 SANT domain, whether it be a chromatin interaction or function in DNA repair, may provide valuable information to how the DNA DSB repair pathway could possibly be manipulated during cancer treatment.

1.5.3 p400 in DNA repair

While the deposition of H2AZ by p400 has been shown to have an effect on transcription (Gevry et al., 2007), p400 also shows an important role in DNA repair. Chromatin is a highly dynamic structure and shows changes during both transcriptional regulation and DNA repair. Examination of chromatin after DNA repair shows expansion of the chromatin adjacent to double-strand breaks. This expansion presumably helps to facilitate efficient DNA repair by allowing repair proteins access to DNA breaks. Interestingly, a study conducted in 2010 showed that p400 was involved in destabilisation of nucleosomes at break sites where the use of knockdowns and the loss of p400 activity resulted in an overall increase in cell radiosensitivity and chromosomal aberrations (X. Jiang et al., 2010; Ye Xu et al., 2010). Additionally, it has been shown that p400 of the TIP60 complex is required for the acetylation of both histones H4 and H2AX at DNA break sites, consequently promoting a relaxed chromatin structure (Bird et al., 2002; R. Murr et al., 2006). Finally, the role of p400 homologues in both *S. cerevisiae* and Drosophila demonstrate that the p400 ATPase

can enable exchange of modified H2AX nucleosomes around DNA break sites and facilitate the incorporation of unmodified nucleosomes, thereby presumably promoting restoration of pre-damaged chromatin structure (Kobor et al., 2004; Kusch et al., 2004).

1.6 ATM

Ataxia telangiectasia mutated (ATM) is a member of the phosphatidylinositol 3-kinase-like protein kinases (PIKK) family which are members of the larger phosphatidylinositol 3-kinase (PI3K) superfamily of kinases. Unlike PI3Ks that phosphorylate lipid moieties, PIKKs, with the exception of mTOR (mammalian target of rapamycin), phosphorylate protein substrates at a [S/T]Q sequence. There are currently six members of the PIKK family, ATM, ATR (ATM and Rad3-related), SMG1 (suppressor with morphological effect on genitalia family member 1), mTOR/FRAP (FKBP adarapamycin associated protein / mammalian target of rapamycin), TRRAP (transformation/transcription domain-associated protein) and DNA-PKcs (DNA-dependent protein kinase catalytic subunit). All members of this PIKK family contain a similar domain structure with the possession of a FAT (FRAP-ATM-TRRAP) domain, a FAT-C domain (a FAT domain located at the C-terminus of the protein), a PIKK regulatory domain and a PI3K kinase domain (Shiloh, 2003). In addition, all members of the PIKK family have active kinase activity with the exception of TRRAP which lacks a functional kinase domain.

Ataxia telangiectasia mutated (ATM) was initially identified as the gene product that causes the genetic disease Ataxia Telangiectasia (AT). This is a homozygous recessive disease that presents early in life with ataxia, a miscoordination of muscle movement, and also telangiectasia, the grouping of small blood vessels. Patients with AT have an increased risk of developing lymphatic malignancies (Lavin & Shiloh, 1997) and show an increase in chromosomal breakages and sensitivity to DNA-damaging agents. Additionally, the possession of one mutated allele of ATM does not result in AT symptoms, however, there is a large increase in the risk for developing cancers. This is presumably due to ATM having a significant role in DNA damage repair (Lavin & Shiloh, 1997). ATM was shown to be localised in the nucleus of a cell and does not appear to be altered in the presence or absence of DNA damage (Dar, Biton, Shiloh, & Barzilai, 2006; Gately, Hittle, Chan, & Yen, 1998; Watters et al., 1997).

ATM is one of the key proteins in the double-strand break response where in the absence of double-strand breaks, ATM exists as a homodimer facilitated by an interaction between the kinase domain and FAT domain with the sequences flanking residue serine 1891 essential for the interaction. The ATM homodimer is also in complex with TIP60. Dimerised ATM is inactive but in the presence of DNA damage, TIP60 will acetylate ATM at lysine 3016 promoting ATM autophosphorylation on serine 1981 allowing monomerisation (Bakkenist & Kastan, 2003). It is this active form of ATM that is essential for DNA repair through phosphorylating a myriad of DNA repair proteins (Canman et al., 1998). One prime example of ATM kinase activity during DNA repair is H2AX phosphorylation. H2AX phosphorylation by ATM is a marker of DNA damage and acts as a docking signal for repair protein assembly (Burma et al., 2001). Phosphorylation of histone H2AX at serine 139 by ATM spreads several kilobases either side of the break site and is instrumental in the accumulation of repair proteins at break sites. ATM is also involved in phosphorylation of a number of additional repair proteins such as Mre11 and Rad50, part of the MRN complex vital in DSB repair (Lee & Paull, 2004; Uziel et al., 2003).

There has been debate regarding the way in which ATM recognizes DNA damage and is subsequently activated. Changes in chromatin structure induced by DNA damage have been suggested to promote activation of ATM. Specifically, incubation of cells in a hypotonic solution, the presence of chloroquine or a HDAC inhibitor (all methods known to alter the structure of chromatin) results in the activation of ATM (Figure 1.4 B) (Bakkenist & Kastan, 2003). It has also been suggested that ATM binding directly to broken DNA is required for ATM activation (Figure 1.4 D) (Shiotani & Zou, 2009; You, Bailis, Johnson, Dilworth, & Hunter, 2007) or through binding to other DNA repair proteins (Figure 1.4 C) (Soutoglou & Misteli, 2010). While TIP60 acetylation of ATM is essential for activation, how TIP60 was activated in the presence of DNA damage remained a question. Recently it was found that the tyrosine kinase c-Abl phosphorylated TIP60 in the presence of DNA double-strand breaks or changes to chromatin structure which induced acetylation of ATM and subsequent autophosphorylation (Figure 1.4 E) (Kaidi & Jackson, 2013).

In addition to the involvement of ATM in the DNA damage response, ATM is also a key player in cell cycle arrest where it can control progression to several stages. In the presence of DNA damage, ATM is activated and phosphorylates various key proteins in

the G1/S checkpoint, the intra-S phase checkpoint and the G2-M phase checkpoint. This is essential to prevent the replication of cells that contain damaged regions of DNA. These phosphorylation events can facilitate changes in gene expression and degradation of checkpoint proteins, facilitating cell cycle arrest at the various checkpoints (Geng, Zhang, Zheng, & Legerski, 2007; Kastan & Lim, 2000; Lim et al., 2000; B. Xu, Kim, Lim, & Kastan, 2002).

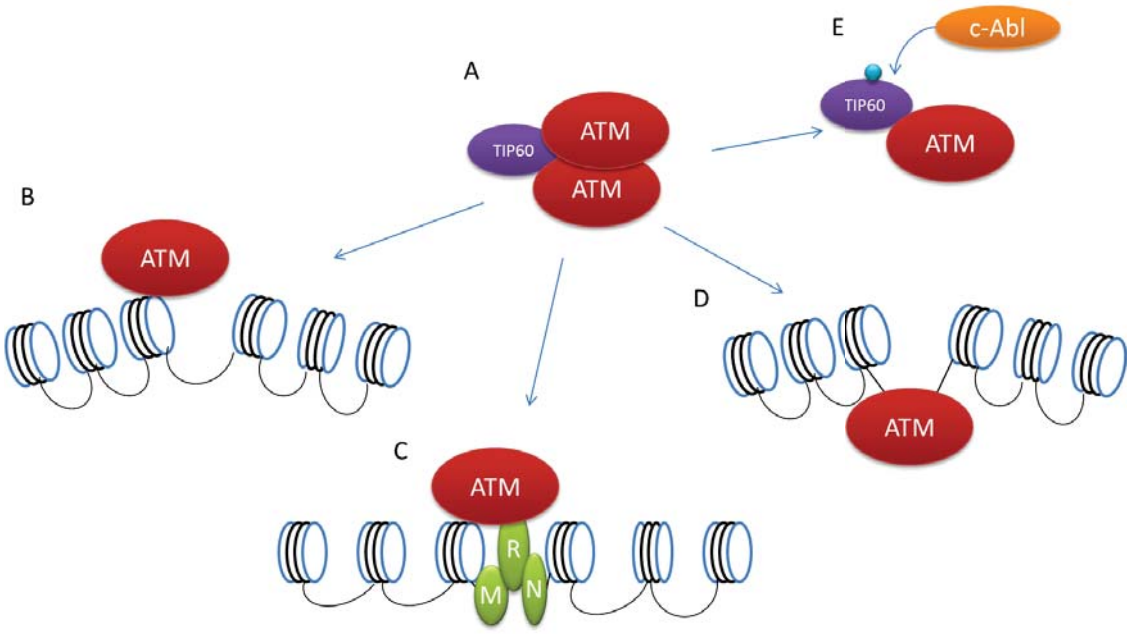

Figure 1.4 ATM activation methods. A) In its inactive state, ATM exists as a homodimer in complex with TIP60. In order to have a positive effect on DNA repair, ATM must be activated. This can occur through a variety of methods including B) through binding to distorted chromatin, C) binding to DNA repair proteins such as Mre11 from the MRN complex, D) binding directly to DNA ends and E) when TIP60 is phosphorylated by c-Abl which in turn acetylates ATM promoting autophosphorylation.

1.7 DNA double-strand break repair

The DNA double-strand break (DSB) response is an essential process for maintaining cellular integrity. Typically three events occur rapidly after the induction of DNA damage. These are the activation of ATM kinase, the phosphorylation of H2AX and the accumulation of the MRN complex at break sites.

As mentioned previously, ATM has an important role in DNA damage and is activated through acetylation by TIP60 and subsequent autophoshoryaltion (Bakkenist & Kastan, 2003; Sun et al., 2005). These posttranslational modifications on ATM result in monomerisation of the previously inactive dimer with the active monomer being able to phosphorylate a large array of proteins including numerous DNA repair proteins such as the histone variant H2AX (Figure 1.5 B) (Burma et al., 2001; Lee & Paull, 2004; Nakagawa, Taya, Tamai, & Yamaizumi, 1999). Additional targets of ATM include all three members of the MRN (Mre11, Rad50 and NSB1) complex (Gatei et al., 2011; Lim et al., 2000; Yuan et al., 2002).

The MRN complex consists of three proteins, Mre11, Rad50 and NSB1. Accumulation of this complex at the break sites occurs rapidly after the production of double-strand breaks. MRE11 contains two DNA binding domains and has been shown to bind to single strand regions of DNA that occur at break sites (de Jager et al., 2001). Rad50 and NSB1 bind to Mre11 and form the MRN complex at break site (Hopfner et al., 2001; Williams et al., 2009) NSB1 appears to be involved in binding to a variety of proteins including phosphorylated H2AX and MDC1 (Mediator of DNA-damage checkpoint 1) promoting both accumulation of repair proteins and a mechanism to control the cell cycle (Kobayashi et al., 2009; Wu, Luo, Lou, & Chen, 2008). RAD50 is involved in bridging the break site and promoting DNA end processing by Mre11 (Bhaskara et al., 2007). These proteins are all essential for DNA repair and mutations in each of them lead to chromosomal instabilities and impairments in DNA repair similar to that seen with mutations in ATM (Derheimer & Kastan, 2010). The MRN complex appears to bind DSBs independently of ATM however, accumulation of MRN is promoted by ATM physically binding to MRN (Uziel et al., 2003). This binding of ATM to the MRN complex can promote activation of ATM (Lee & Paull, 2004). As this is one of many ways ATM appears to be activated, the physical binding to the MRN complex may be a way to amplify the activation of ATM.

Phosphorylation of histone H2AX is an essential chromatin modification in DNA repair since mutation of serine 139 to a non-phosphorylatable amino acid results in a decrease in accumulation of DNA repair proteins and an overall reduction in repair efficiency (Bassing et al., 2002; Burma et al., 2001; Rogakou et al., 1998; I.M Ward & Chen, 2001). The phosphorylation of H2AX spreads up to 2 Mb either side of a break site, however, ChIP analysis revealed that there was little phosphorylated H2AX at the break

sites, possibly due to the removal of nucleosomes at break sites (Downs et al., 2004; Shroff et al., 2004; Ye Xu et al., 2010). Importantly, H2A which fulfils the role of H2AX in yeast, is capable of binding members of the NuA4 complex which is homologous to the mammalian TIP60 complex suggesting that the TIP60 complex is required for histone exchange at break sites (Downs et al., 2004).

TIP60 is involved in the activation of ATM through acetylation and is also required through the TIP60 complex. As mentioned above, TIP60 is part of a large chromatin remodeling complex known as the TIP60 complex. This complex contains TRRAP, a member of the PIKK family, the ATPase p400, the histone acetyl transferase TIP60 as well as a number of other proteins including helicases and actin-like proteins (T. Ikura et al., 2000). In *Saccharomyces cerevisiae* the NuA4 complex is able to bind to phosphorylated H2AX promoting acetylation of histone H4 (Figure 1.5 C) (Keogh et al., 2006; Kobor et al., 2004). This function is also conserved in the *Drosophila* homologue, dTIP60 in the Domino complex (Kusch et al., 2004). The acetylation of H4 promotes two functions. The first is the opening of the chromatin structure to promote an open chromatin state presumably for the accumulation of DNA repair proteins (R. Murr et al., 2006). Secondly, the acetylation of H4 is essential for the exchange of histone variants. This function is also completed through the TIP60 complex, with the chromatin remodeler p400 responsible for histone exchange (X. Jiang et al., 2010).

Finally, mammalian p400 has been shown to facilitate the exchange of histone H2A with the variant H2AZ (Figure 1.5 D). While this happens for transcriptional regulation, p400 has been shown to be important in DNA repair. In 2010, Xu et al highlighted the importance of p400 during DNA repair through the use of shRNA mediated knockdown of p400 and the use of an ATPase mutant. The absence of p400 resulted in an increase in nucleosome stability around break sites suggesting that p400 is involved in altering the nucleosome structure around the break site.

Figure 1.5: The DNA double-strand break repair response. A-B) In the presence of DNA damage, TIP60 acetylates ATM and promotes autophosphoryaltion of ATM. Phosphorylated ATM exists as a monomer in complex with TIP60. Active ATM rapidly phosphorylates H2AX around break sites in DNA. C) Additional repair proteins accumulate at the break sites. These include the MRN complex which, together with phosphorylated H2AX, acts as a docking site for DNA repair proteins. TIP60 is able to acetylate H4 of nucleosomes at break sites facilitating an opening of the chromatin structure allowing access of chromatin to remodeling complexes. DNA repair occurs at this step before, D) Chromatin remodeling complexes such as the TIP60 complex are recruited to the break site and facilitate the exchange of modified H2AX containing nucleosomes for unmodified H2AX containing nucleosomes to help return chromatin to its pre-break state. Blue spheres represent phosphorylation and yellow spheres represent acetylation.

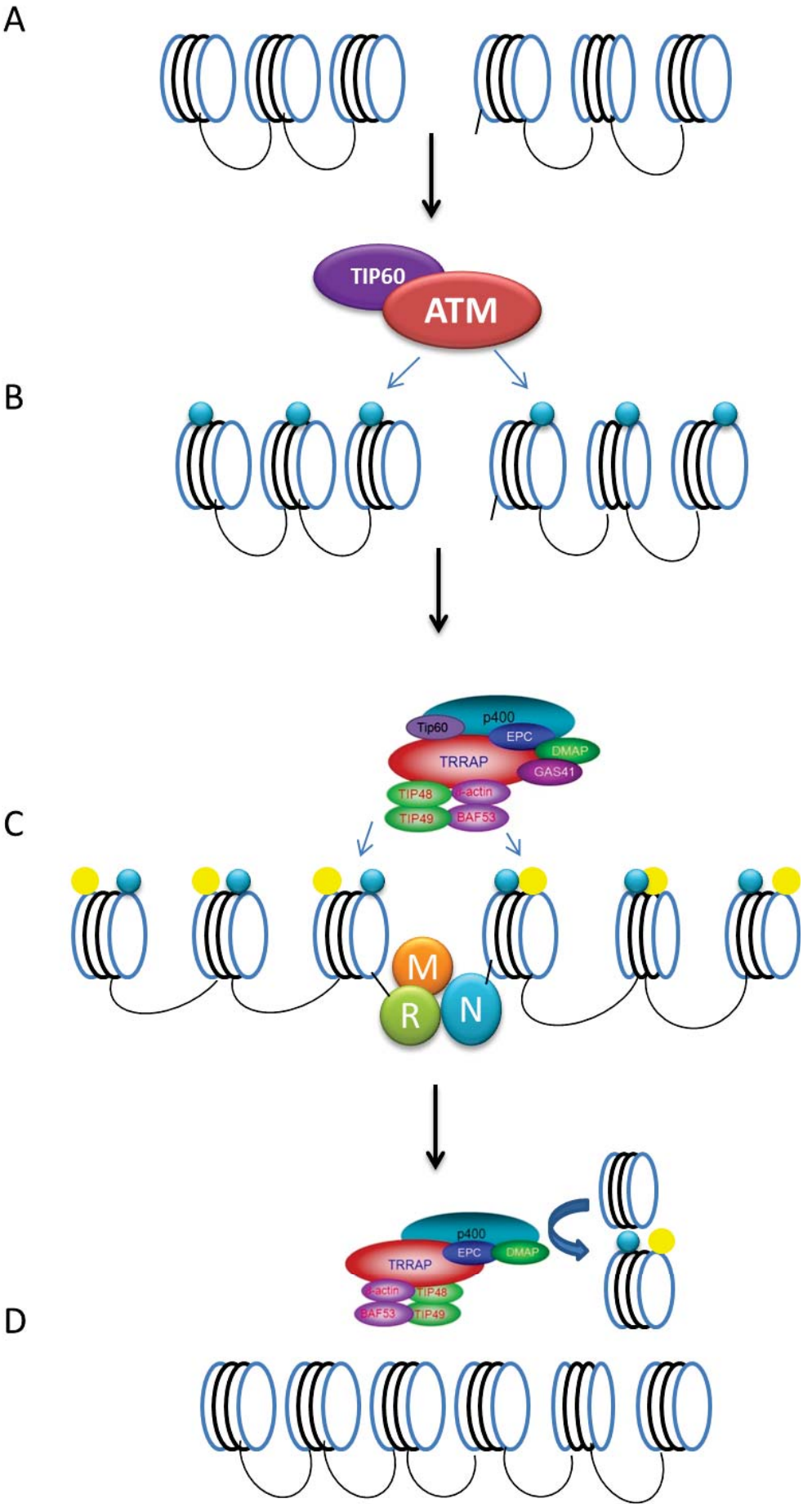
A
TIP60
ATM
B
p400
Tip60
EPC
DMAP
TRRAP
GAS41
TIP48
β-actin
TIP49
BAF53
C
M
R
N
p400
EPC
DMAP
TRRAP
β-actin
TIP48
BAF53
TIP49
D

1.8 TIP60, p400, ATM and cancer

Closely linked to the inability to repair DNA and thus the accumulation of mutations, is the development of cancers. Each of TIP60, p400 and ATM and their involvement in DNA repair has been described above. With an integral role in DNA repair played by each protein, it is reasonable to assume that alteration in their gene function or their possession of mutations affection function may play a role in the development of cancers.

ATM was originally described in its mutated form in the disease Ataxia Telangiectasia with patients showing an increase chromosomal breakages and sensitivity to DNA damaging agents (Lavin & Shiloh, 1997). More recently, mutated alleles of ATM have been seen in a number of breast and colorectal cancers (Gao et al., 2011; Goldgar et al., 2011; Prokopcova, Kleibl, Banwell, & Pohlreich, 2007). Additionally, loss of ATM has also been associated with an increase in cancer development in mice models (Barlow et al., 1996; Elson et al., 1996; Y. Xu et al., 1996). This finding goes hand in hand with the description of ATM as a haplioinsufficent tumour suppressor, where ATM heterozygous deficient mice showed an increase in the development of mammary carcinomas (Umesako et al., 2005).

TIP60 has been described in cancer development in several ways. Similar to ATM, TIP60 has been described as a haplioinsufficent tumour suppressor where monoallelic loss of TIP60 resulted in an increase in mammary carcinomas, lymphomas and head and neck carcinomas (Gorrini et al., 2007). In addition to this function, overexpressed TIP60 has been shown to promote prostate cancers through acetylating the androgen receptor, allowing translocation of the androgen receptor to the nucleus in the absence of any androgen (Shiota et al., 2010). Finally, the TIP60/p400 ratio has been shown to be important for colorectal cancer cell (HCT116) proliferation (L. Mattera et al., 2009). Knockdown or overexpression of TIP60 to correct the TIP60/p400 ratio has been shown to decrease proliferation of HCT116 colorectal cancer cells and promote apoptosis.

1.9 Thesis outline and Hypothesis

The integrity of DNA throughout the lifetime of an organism must be maintained to prevent the development of cancers and other chromosomal aberrations such as gene duplications and chromosomal translocations. As discussed, an organism contains numerous DNA repair pathways that work together to prevent the accumulation of mutations in a genome. The complexity and redundancy of these pathways means it is often difficult to elucidate all steps involved. A previous study showed an increase in the DNA damage response in the absence of a DNA damaging agent through overexpressed TIP60 or SANT domain of p400, possibly due to sequestration of a putative negative regulator (Smith, 2010). This study aims to investigate if a single domain of TIP60 or a mutated SANT domain of p400 is capable of inducing the DNA damage response in the absence of a DNA damaging agent.

Furthermore, the members of the PIKK family have been shown to have a modular domain, where if a domain within one member is replaced with the domain of another member the protein will retain function (Jiang, Sun, Chen, Roy, & Price, 2006). Keeping this in mind and the fact that one member of the PIKK family, TRRAP, has been shown to interact with p400 (Fuchs et al., 2001), an interaction between ATM and p400 was hypothesised.

1.9.1 Hypothesis

This study examines two hypotheses;

A) A single domain of TIP60 or a single helix within the SANT domain of p400 is capable of inducing H2AX phosphorylation in the absence of a DNA damaging agent.
B) An association between ATM and p400 plays a role in DNA repair.

1.9.2 Objectives

- Clone and express individual domains of TIP60 and examine H2AX phosphorylation.
- Clone and express SANT domain constructs carrying mutations in key helices and examine H2AX phosphorylation.

- Examine the interaction between ATM and p400 in a mammalian system through the use of coimmunoprecpitations.
- Examine the interaction between ATM and p400 in a non-mammalian system through the use of coimmunoprecipitation and examine the cellular localisation of ATM and p400 when expressed in SF9 cells.
- Functionally analyse the interaction between ATM and p400 by examining the kinase activity of ATM alone and when associated with p400.

2 Materials and Methods

2.1 Materials

Material	Supplier
3x FLAG peptide, ampicillin trihydrate, coomassie Brilliant blue R concentrate, Bromophenol blue sodium salt, 1Kb+ DNA Marker, ethidium bromide, formaldehyde solution, glycerol, glycine, Igapal CA-630 (NP-40), Imidazide, Kanamycin sulphate, LB broth, Phenol, potassium acetate, potassium chloride, potassium phosphate monobasic, puromycin dihydrochloride, sodium acetate anhydrous, sodium carbonate, sodium chloride, sodium deoxycholate, sodium dodecyl sulphate, sodium hydroxide, sodium phosphate monobasic, sodium phosphate dibasic, Tetramethylethylene diamie (TEMED), triton X-100, tween 20, α-FLAG M2 agarose, β-mercaptoethanol , Phenylmethanesulfonylfluorise solution (PMSF), paraformaldehyde, oligonucleotides, FLAG M2 monoclonal antibody (F3165), HA antibody (SAB4300603), B-actin antibody (A5316), α-rabbit Cy5 (A10524), α-mouse Cy3 (A10526)	Sigma chemical company, USA
Biomax general blue film, Biomax Maximum sensitivity film, Biomax MS intensifying screen cassette 8"x10", Biomax transcreen Low Energy intensifying screen	Eastman Kodak, USA
Chloroform, 40% Acrylamide-bis solution, Boric Acid, Absolute Ethanol, Methanol	Merck, Germany
60 mm Tissue culture plates, 24 well Tissue culture plate, 5 mL pipette, 10 mL pipette, 25 mL pipette, 15 mL centrifuge tubes, 50mL centrifuge tubes, 96 well Tissue culture plate	Greiner Bio-One, Germany
0.5% typsin-EDTA (10x), Charge SwitchPro PCR clean up kit, Dulbecco's Modified Eagle Medium (DMEM) + Glutamax, Foetal Bovine Serum , OPTI-MEM, Phusion Polymerase and HF buffer, Purelink Quick gel extraction kit, PureLink Quick plasmid Midiprep Kit, Prolong Gold with DAPI, penicillin/ streptomycin/ amphotericin B mix, H3 polyclonal antibody,	Life Technologies, USA
*BamH*I, *Kpn*I, Prestained protein marker broad range, *Cla*I, T4 Ligase, *Xho*I, *Dpn*I, *Nde*I, *Nco*I, *Eco*RI, *Fse*I	New England Biolabs, USA
Eppendorf Tubes, PCR Tubes, Pipette Tips	Axygen, USA
Pierce ECL western blotting substrate, Halt Protease	Thermo Scientific,

inhibitor cocktail, Super signal west femto maximum sensitivity substrate	USA
Agarose	Bioline, England
40% acrylamide-bis (29:1)	BioRad, USA
Agar Bacteriological	Oxoid, , UK
FastStart Taq, XtremeGeneHP	Roche, NZ
FuGENE® 6, FuGENE® HD	Promega Corporation, USA
H2AX polyclonal antibody (07-627) H2AX-P polyclonal antibody (07-164)	Millipore, USA
ATM polyclonal antibody (819844)	Calbiochem, Germany
goat anti-rabbit HRP conjugated antibody (SC2054), goat anti-mouse HRP conjugated antibody (SC2055)	Santa Cruz Biotechnology, USA

2.2 DNA methods

2.2.1 Polymerase Chain Reaction

The majority of PCR protocols were completed using Phusion polymerase from NEB. PCR reactions that did not use Phusion polymerase are specifically mentioned in chapter 3 and 4. Reactions were set up as follows according to manufacturer's instructions:

Component	Volume (µL)
5x High Fidelity Buffer	4
Forward Primer (10 µM)	0.5
Reverse Primer (10 µM)	0.5
dNTPs (10 mM)	2
Template DNA (10 ng/µL)	1
Phusion Polymerase (2 U/µL)	0.5
PCR Grade Water	11.5

Table 2.1 PCR reaction composition

PCR reactions using Phusion polymerase were carried out using the following protocol. Annealing temperatures for primer sets can be found in appendix A1.

Temperature	Time	Repeats
98^{0}C	30 sec	1
98^{0}C	20 sec	
55^{0}C	15 sec	30x
72^{0}C	2.5 min	
72^{0}C	10 min	1x
4^{0}C	Hold	

Table 2.2 PCR protocol

Amplification of products was examined using agarose gel electrophoresis (section 2.2.4) by loading 10% of each reaction on a 1% gel and visualised by staining with ethidium bromide.

Primers and annealing temperatures as well as additional PCR protocols that have been used in this study are included in appendix A1.

2.2.2 PCR purification

Products from PCR were purified using High Pure PCR Product Purification Kit according to the manufacturer's instructions. In this method, a chaotropic salt is added to DNA which allows it to bind to glass fleece. Contaminants, including proteins, salts and nucleotides, are washed away before purified DNA is eluted from the glass fleece using a low salt buffer.

2.2.3 Adenylation of PCR products

PCR products require a 3' A overhang for insertion into the pGEM-T easy vector. To adenylate blunt end PCR products produced by proofreading enzymes, 6 µL of purified PCR product (section 2.2.2) was incubated together with 1 µL ATP (10 mM), 2 µL High Fidelity (HF) buffer (Roche) and 1 µL *Taq* polymerase (1 U/µL) at 72°C for 15 min. Adenylated PCR products were used directly for ligation into the pGEM-T easy vector. *Taq* polymerase had been purified according to the method published by (Engelke, Krikos, Bruck, & Ginsburg, 1990).

2.2.4 Agarose Gel Electrophoresis

To separate DNA molecules, gel electrophoresis was generally carried out on 1% agarose (w/v) in 0.5x TBE (44.5 mM Tris-HCl, 44.5 mM boric acid, 10 mM EDTA). DNA samples , with the addition of 10% (v/v) DNA loading dye (30 % glycerol, 0.25% bromophenol blue), were loaded into wells and electrophoresis was generally carried out at 150 V for 1 hour. DNA was visualised by staining the gel with 0.5 µg/mL ethidium bromide in 0.5x TBE for 15 minutes before destaining in water for 5 min. A gel documentation system was used to visualise DNA under UV light. DNA sizes were estimated by comparing to a 1kb+ DNA standard marker.

2.2.5 DNA purification from agarose gel

After DNA fragments were separated as in section 2.2.4, DNA bands were visualised under long wavelength UV light and excised ensuring a minimal amount of excess agarose is removed. DNA was purified using the E.Z.N.A® gel extraction kit from Omega. This method allows DNA to bind to the HiBind® matrix while proteins and other contaminants to be washed away. DNA can be released from the matrix using deionized water or a low salt buffer.

2.2.6 Restriction enzyme digestion

Generally, 1 µg of DNA was digested with 1 µL of enzyme (5000 U/µL) in buffer conditions according to the manufacturer's instructions. Digestions were incubated at 37^{0}C for at least two hours to ensure complete digestion. Digestion products were examined by gel electrophoresis (section 2.2.4) and if appropriate, purified by gel purification (section 2.2.5)

2.2.7 Calf intestinal phosphatase digestion

Treatment of digested plasmid DNA with calf intestinal phosphatase (CIP) is to reduce religation of empty vector DNA by removing 5' phosphate groups. One µL of CIP was added to plasmid digest reactions. No additional buffer was needed as all digestions were completed using the NEB system and CIP is active in all NEB buffers. CIP treated digestions were incubated for a minimum of 2 hours and maximally overnight at 37^{0}C to ensure maximal removal of phosphate groups. CIP treatment was completed prior to purification via gel electrophoresis.

2.2.8 DNA ligation

DNA that had been digested and purified was used in ligation reactions. Between 50 – 100 ng DNA per ligation was used in a molar ratio of 3:1 insert to vector DNA. Reactions were made up to a total volume of 10 µL with buffer and ligase (1 µL at 1 U/µL) according to the manufacturer's instructions. Ligations were incubated overnight at 14^{0}C before being used for transformation of *E.coli*.

2.2.9 Preparation of competent *Escherichia coli (E.coli)*cells

Two strains of *E.coli* were used in this study, DH5α and DH10bac. Competent cell preparations of both strains were made in the following way:

E.coli was streaked on LB plates (20 g/L LB, 1.5% (w/v) agar) and grown overnight at 37^{0}C. A single colony was picked and used to inoculate 5 mL LB (20 g/L LB) which was grown overnight at 37^{0}C with shaking. A 100 mL LB broth was inoculated with 1 mL of the overnight culture and grown at 37^{0}C for two and a half hours. The culture was then split into two 50 mL tubes and centrifuged at 1500 g for 10 min at 4^{0}C. The supernatant was removed and the two pellets were resuspended in 5 mL ice cold 0.1 M $CaCl_2$. The pellets were pooled and centrifuged at 1500 g for 10 min at 4^{0}C. The supernatant was removed and the pellet was resuspended in 3.2 mL of 0.1 M $CaCl_2$ then incubated on ice overnight after which 0.8 mL of 50% glycerol (10% final concentration

(v/v)) was added to the cell suspension and gently mixed. Microfuge tubes were pre-chilled at -20^{0}C for 1 hour before cells were dispensed into 100 µL aliquots. Aliquots were placed at -80^{0}C for storage.

2.2.10 Transformation of DH5α *E.coli*

An aliquot of competent *E.coli* cells was thawed on ice. Once thawed, 0.5 µL of purified plasmid or 5 µL of a ligation reaction were added to the cells, gently mixed and incubated on ice for 30 min. Cells were heat-shocked at 42^{0}C for 1 min before being placed back on ice for 2 min. Generally, 400 µL of LB was added to the cell mixture before being incubated at 37^{0}C for 30 min with shaking. Approximately 150 µL of the reaction was spread onto an LB plate containing the appropriate selection antibiotic. Plates were incubated at room temperature until the reaction had been absorbed into the plate before being inverted and placed at 37^{0}C or 30^{0}C overnight.

2.2.11 Plasmid purification from *E.coli*

Several methods were used to purify plasmid DNA from *E.coli* depending on the application the DNA was required for.

2.2.11.1 Rapid boil

This method was used when screening more than 10 colonies when cloning. The buffer allows cells to be partially lysed, releasing plasmid DNA into the supernatant. The larger genomic DNA remains trapped in the cell debris and was separated from plasmid DNA by a simple centrifugation.

Colonies were picked from plates are used to inoculate 5 mL broths of LB with the appropriate selection antibiotic and grown overnight at 37^{0}C or 30^{0}C with shaking. One to two mL of culture is pelleted at 12000 g for 1 min at room temperature. The supernatant is removed before the pellet was resuspended in 350 µL of STET buffer (10 mM Tris-HCl, pH 8.0, 1 mM EDTA, 0.1 M NaCl, 5 % Triton x-100) supplemented with 25 µL freshly made lysozyme solution (10 mg/mL). The solution was boiled for 40 s before immediately being centrifuged at 12000 g for 10 min. The cell debris was removed using a sterile toothpick and 400 µL phenol: chloroform: Isoamyl alcohol (30:29:1) was added. Samples were inverted several times and centrifuged at 12000 g for 5 min. The upper aqueous phase was transferred to a new tube and 400 µL of isoproponal was added. Samples were mixed well before being incubated at -20^{0}C for 30 min before being centrifuged at 12000 g for 5 min. The remaining pellet was washed

once with ice-cold 96% EtOH followed by a final centrifugation at 12000 g for 2 min. The supernatant was removed and pellets were air dried before being resuspended in TE + RNase (10 mM Tris-HCl, pH 8.0, 1 mM EDTA, pH 8.0, 50 µg/mL RNase). Purified DNA was used for restriction endonuclease digestion (section 2.2.6) to allow conformation of plasmid identity.

2.2.11.2 High quality small scale plasmid isolation

Small scale plasmid isolations were performed using High Pure Plasmid Isolation Kit from Roche. Plasmid isolation was conducted according to the manufacturer's instructions using 3 mL of *E.coli* culture. This kit uses alkaline lysis to lyse cells, releasing DNA into the supernatant. The cell debris and genomic DNA are separated from plasmid DNA using centrifugation. The buffer contains a chaotropic salt, that when mixed with plasmid DNA allows the plasmid DNA to bind to glass fibres within the filter. This allows the DNA to be washed, removing contaminants such as proteins and salt, before DNA is released from the glass fibres using a low salt buffer. DNA can be quantified (section 2.2.14) and used for further applications.

2.2.11.3 High quality large scale plasmid isolation

Large scale plasmid isolations were performed using the QIAGEN Plasmid Midi Kit. Plasmid isolation was conducted according to the manufacturer's instructions using 200 mL of *E.coli* culture. This kit uses alkaline lysis to lyse cells, releasing DNA into the supernatant. The cell debris and genomic DNA is separated from plasmid DNA using centrifugation. The supernatant containing plasmid DNA is loaded on a column that used anion-exchange. DNA binds to the column in low-salt conditions, while impurities are removed using a medium-salt wash. DNA is eluted from the column using a high-salt buffer and precipitated using isoproponal. DNA pellets are washed with 70% EtOH and resuspended in TE buffer (10 mM Tris-HCl, pH 8.0, 1 mM EDTA). Plasmid DNA was quantified (section 2.2.13) and used in further applications such as mammalian cell transfection experiments (section 2.4.3).

2.2.12 Bacmid preparation

The Bac-to-Bac® baculovirus expression system is an efficient way of cloning genes of interest for protein expression in SF9 cells. cDNAs were cloned into the multiple cloning site of the pFastBac1 vector where the multiple cloning site is flanked by transposition sequences. When pFastBac1 plasmids are used to transform DH10Bac *E.coli*, there will be transposition of the cassette containing the gene of interest from the

pFastBac1 vector into a baculovirus shuttle vector (bacmid). The bacmid contains a LacZ gene that will be interrupted when the cassette from pFastBac1 is inserted into the bacmid. This allows for blue-white selection of colonies.

One hundred nanograms of pFastBac1 containing the gene of interest was added to an aliquot of DH10Bac *E.coli* that was been thawed on ice. Cells were incubated for 30 min on ice before being heat-shocked at 42^0C for 2 min. After the heat-shock, cells were placed on ice for 2 min before 900 µL of LB was added to the cells and placed at 37^0C with shaking for 4 hours. Before plating cells, a 1/10 dilution and a 1/100 dilution of cells were made. One hundred microliters of undiluted and diluted cells were plated onto LB agar plates containing 50 µg/mL kanamycin, 7 µg/mL gentamycin, 10 µg/mL tetracycline, 40 µg/mL IPTG and 100 µg/mL X-gal. Plates were incubated at 37^0C for 2 days for colonies to develop the blue colour indicative of bacmid that does not contain the gene of interest. White colonies were picked and grown in liquid LB containing 50 µg/mL kanamycin, 7 µg/mL gentamycin and 10 µg/mL tetracycline. Bacmid DNA is extracted as described in section 2.2.11.2.

2.2.13 DNA sequencing

Plasmid sequences were confirmed by Sanger sequencing. DNA was submitted to the Massey Genome Service for this purpose. DNA was supplied at 500 ng per 15 µL reaction with 4 pmol of primer.

2.2.14 DNA quantification

DNA was quantified by spectrophotometry using a Nanodrop® ND-1000 according to the manufacturer's instructions. The absorbance was quantified using the 260/280 nm to assess the quality of DNA.

2.2.15 *Dpn*I digestion

To remove template DNA from site-directed mutagenesis PCR reactions, NEB buffer 4 was added to a final concentration of 1X and 1 µL of enzyme was added (20000 U/µL). Samples were incubated overnight at 37^oC before PCR products were purified according to section 2.2.2.

2.3 Protein methods

2.3.1 Sodium dodecylsulphate polyacrylamide gel electrophoresis (SDS-PAGE)

All electrophoresis was carried out using the Miniprotean Tetra System (Biorad). Generally 10% polyacrylamide gels were prepared. 2.5 mL of resolving gel buffer (1.5 M Tris, pH 8.8, 0.4% SDS) was added to 2.5 mL of 40% acrylamide-bis (29:1) with water to 10 mL. One hundred micro litres of 10% ammonium persulphate (APS) and 20µL TEMED was added and the resolving gel was immediately poured into the glass plates, covered with 70% ethanol and allowed to set for 15 min. The ethanol was removed and a stacking gel consisting of 1 mL Tris/SDS (0.5 M Tris, pH 6.8, 0.4% SDS), 0.4mL 40% acrylamide, 2.6 mL water, 40 µL 10% APS and 8 µL TEMED was poured on top of the resolving gel and had a comb inserted. The stacking gel was allowed to solidify for 30 min before it was used. Gradient polyacrylamide gels (4-15%) were cast using the Hoefer SG30 gradient maker. A stacking gel was overlaid as described above.

Two step gradient gels were poured in two steps. First a 10% polyacrylamide gel was poured to fill the glass plates half way and allowed to solidify before a 5% polyacrylamide gel was poured to the top of the glass plate and allowed to solidify. A stacking gel was overlaid as described above.

Protein samples were prepared with 6X SDS sample buffer (60 mM Tris, 10% glycerol, 2% SDS, 0.01% bromophenol blue, 1.25% β-mercaptoethanol) and heated at 95˚C for 5 min before being loaded onto the gel. Gels were run at a constant amperage of 30 mA generally for 1 h 15 min in SDS electrophoresis buffer (25 mM Tris, 192 mM glycine, 0.1% SDS).

2.3.2 Western Blotting

Protein samples were resolved by SDS-PAGE as described in section 2.3.1 and left to equilibrate in chilled transfer buffer (25 mM Tris, 192 mM glycine, 20% methanol) for 20 min. PVDF membrane was charged by immersing it in methanol for 20 s, followed by washing with ddH_2O for 20 s and finally immersing it in chilled transfer buffer for at least 5 min. Protein was transferred to the membrane from the polyacrylamide gel at 150 mA for 4 h submerged in chilled transfer buffer using the Miniprotean Tetra System. When the blotting equipment was disassembled, the membrane was placed in

blocking buffer (10 mM Tris-HCl, pH 7.6, 150 mM NaCl, 0.2% Tween-20, 5% skim milk, 0.2% sodium azide) and shaken at room temperature for 1 h. The membrane was washed three times for 1 min with TBST (10 mM Tris-HCl, pH 7.6, 150 mM NaCl, 0.2% Tween-20). The membrane was then placed into primary antibody diluted in antibody dilution buffer (10 mM Tris-HCl, pH 7.6, 150 mM NaCl, 0.2% Tween-20, 1% skim milk, 0.05% sodium azide) and incubated overnight at 4°C with agitation. The primary antibody was removed and the membrane was washed three times for 10 min in TBST. The membrane was then incubated in secondary antibody diluted in antibody dilution buffer and incubated at room temperature for 30 min on a shaker. The secondary antibody was removed and the membrane was washed three times for 15 min in TBST. A chemiluminescent reagent together with X-ray film was used to detect the proteins of interest.

A list of antibody concentrations can be found in Appendix 2.

2.3.3 Immunoprecipitation

Approximately $9x10^6$ cells were lysed according to section 2.4.10 ensuring 30 µL of lysate was kept as an input sample. To the remaining 470 µL, generally 20 µL of antibody-agarose bead conjugates were added to the sample and incubated overnight on an orbital rotator at 4°C. The beads were pelleted by centrifuging sample for 4 min at 4000 g at 4°C. Beads were washed 4 times in 500 µL of cell lysis buffer (20 mM HEPES pH 7.4, 120 mM NaCl, 1.5 mM $MgCl_2$, 1 mM EGTA, 50 mM NaF, 0.2% Tween-20, 0.5 mM DTT, 1 mM PMSF) and pelleted by centrifugation (4 min at 4000 g at 4°C). The supernatant was removed and the beads were either used in a kinase assay (section 2.3.4) or examined by western blotting (section 2.3.2)

2.3.4 Kinase assay – antibody and p33

Approximately $9x10^6$ cells were lysed according to section 2.3.10 and subjected to immunoprecipitation as in section 2.3.3. After the 4 washes in lysis buffer, samples were washed twice in kinase wash buffer (50 mM HEPES, pH 7.4, 10 mM $MgCl_2$, 50 mM NaCl, 10 mM $MnCl_2$, 1 mM DTT, 1 mM PMSF) and the beads were pelleted by centrifugation at 4000 g for 4 min at 4°C. The supernatant was removed and all residual liquid was removed using a flattened gel loading tip. The beads were resuspended in 19 µL of kinase reaction buffer (50 mM HEPES, pH 7.4, 10 mM $MgCl_2$, 50 mM NaCl, 10 mM $MnCl_2$, 1 mM DTT, 1 mM PMSF, 10 µM acetylCoA, 0.5 mM okadiac acid) and 1

µL of 0.1 M ATP or 5 µCi of [P^{33}] ATP. Samples were mixed well and incubated on a vortex at 30°C for 60 min. Samples were resolved by SDS-PAGE and if membranes were to be examined by phosphospecific antibodies were subjected to western blotting according to section 2.3.3. For sample that contained [P^{33}] ATP, proteins were transferred to membrane according to section 2.3.3, however instead of being subjected to blocking buffer, the membrane was dried and exposed to X-ray film to measure radiation.

2.3.5 Coomassie Blue staining

Protein samples were resolved using SDS-PAGE (section 2.3.1) and were placed in Brilliant blue Coomassie stain (BioRad) for 15 min on a shaker. Coomassie stain was removed and placed in destain solution (20% methanol, 10% acetic acid) until bands were visible.

2.4 Cell Culture Methods

All cell culture work was carried out in an ESCO Class II Biohazard safety cabinet.

2.4.1 Cell passaging mammalian cells

Mammalian cells were grown in standard conditions of 5% CO_2 and 37°C in a humidified atmosphere. Growth media for mammalian cells consisted of Dulbecco's Modified Eagle Medium (DMEM), 5% Fetal Bovine Serum (FBS) and penicillin (5 U/mL), streptomycin (0.5 mg/mL), amphotericin B (0.125 µg/mL).

When cells were 90% confluent, medium was aspirated from the plate and cells were washed with PBS (137 mM NaCl, 2.7 mM KCl, 4.3 mM $Na_2H_2PO_4$, 1.47 mM KH_2PO_4) which was subsequently aspirated. For a 100 mm plate, 1 mL of 0.05% Trypsin/EDTA was added to the plate and after the cells were immersed, the trypsin/EDTA was removed by aspiration. The cells were released from the base of the plate by gentle tapping. Cells were resuspended in 10 mL fresh media. Cells were diluted by taking 1.5 mL of cell suspension and 8.5 mL fresh media before being plated and placed in a humidified incubator.

Cells can be used for transfection reactions up to passage 20. Cells that are older than this may not behave as expected.

2.4.2 Cell passaging SF9

SF9 cells were grown at 25°C in normal atmospheric conditions in supplemented Grace's Insect Media with 10 % FBS, 0.1 % Pluronic acid, 10 µg/mL gentamycin and penicillin (5 U/mL), streptomycin (0.5 mg/mL), amphotericin B (0.125 µg/mL). Cells are grown in suspension in a spinner flask until they reached a cell density of 1 $x10^6$ cells/mL. When 1 $x10^6$ cells/mL was reached, a volume of cell suspension was removed from the spinner flask and discarded. Fresh media is added to reduce the cell density to 2.5 $x10^5$ cells/mL and replaced in the 25°C incubator on a magnetic stirrer.

2.4.3 Transient Transfection of Mammalian cells

Cells were transfected 24 h after passaging or when they were 50-60% confluent. For transfecting 100 mm plates, 500 µL of OPTI-MEM was dispensed into a microfuge tube. DNA was added and mixed with gentle tapping before a transfection reagent, generally Fugene6 or XtremeGene9, was added and mixed with gentle tapping. For every 1 µg of DNA, 4 µL of transfection reagent was used. Reactions were left to incubate for 30 min before being added drop-wise to the cells. Transfected cells were generally incubated for 48 h before any downstream processing.

2.4.4 Transfection SF9 cells and generation of P1 baculovirus

Before transfection, 10 mL of SF9 cells at a density of 1 $x10^6$ cells/mL were plated in a 100 mm plate and left to adhere for 15 min. After cells had adhered to the plate, the media was aspirated and replaced with 10 mL of insect plating media (13.5% Grace's insect media supplemented, 85% unsupplemented Grace's insect media, 1.5% FBS). In a sterile microfuge tube, 32 µL of Cellfectin II was added to 400 µL of unsupplemented Grace's insect media and mixed well. In a separate microfuge tube, 4 µg of bacmid DNA was added to 400 µL of Grace's insect media unsupplemented and mixed well. The two solutions were combined and mixed well then left to incubate at room temperature for 15-30 min. The combined solution was added drop-wise onto the cells and the cells were incubated at 25°C for 3-5 h before the medium was removed and replaced with fresh growth media.

Cells were incubated at 25°C for 72 h before the media was collected and centrifuged at 100 g for 4 min to pellet cell debris. The supernatant was filter-sterilised and collected in a sterile 15 mL tube. The tube is wrapped in tin-foil to protect the virus from the light and stored at 4°C. This is the first generation of baculovirus (P1).

2.4.5 Baculovirus Propagation

For protein expression, later generations of virus (P2 or P3) are used as these later generations have a higher viral titre. Generations past P3 were not used to avoid recombination.

SF9 cells at a density of 1 x10^6 cells/mL were plated (10 mL per 100 mm plate) and allowed to adhere for 15 min at room temperature. To each plate, 1 mL of P1 virus is added drop-wise to the plate. Cells were incubated at 25°C for 72 h before the medium was collected, centrifuged at 100 g for 4 min and filter-sterilised. P2 virus was stored in a light-proof container and at 4°C.

This process was repeated using P2 virus to produce P3 virus.

2.4.6 SF9 infection with baculovirus

SF9 cells that are at a density of 1 x10^6 cells/mL were plated (10 mL per 100 mm plate) and allowed to adhere for 15 min at room temperature. An optimised amount of virus is added drop-wise to the plate and incubated at 25°C for 48 h before down-stream processing.

2.4.7 Cell freezing

Cells that are frozen in exponential growth provide the best opportunity for successful reanimation

2.4.7.1 Freezing mammalian cells

Four 100 mm plates that were 80% confluent were used. Basic growth medium was aspirated from the plates and the cells were washed with PBS (137 mM NaCl, 2.7 mM KCl, 4.3 mM $Na_2H_2PO_4$, 1.47 mM KH_2PO_4) which was subsequently aspirated. One mL of 0.05% Trypsin/EDTA was added to each plate and aspirated. The cells were dislodged from the plate by gentle tapping and each plate was resuspended in 5 mL of fresh basic media. The cell suspension was centrifuged at 1000 g for 5 min to pellet the cells and the supernatant was removed. Cells were resuspended in 4 mL of freezing media (10 % DMSO, 25% FBS, 65% DMEM) and 1 mL aliquots were transferred into cryovials and placed in a CoolCell® which was placed into a -80°C freezer to slowly freeze the cells. Cells were transferred to liquid nitrogen for long term storage.

2.4.7.2 Freezing SF9 cells

SF9 cells in suspension were frozen when they reached a cell density of 8 x10^5 cells/mL. For each vial that is to be frozen, 10 mL of culture was used. Cells were

pelleted by centrifugation at 1000 g for 5 min. The supernatant was removed and cells were resuspended in freezing media (10% DMSO, 25% FBS, 65% Grace's insect media supplemented). One mL aliquots were transferred into cryovials and placed in a CoolCell® which was placed into a -80°C freezer to slowly freeze the cells. Cells were transferred to liquid nitrogen storage for long term storage.

2.4.8 Cell reanimation

Vials of cells were thawed quickly at 37°C to ensure the damage to cells from thawing is kept to a minimum. Thawed cells were transferred to 5 mL of pre-warmed fresh media, mixed gently and then centrifuged at 1000 g for 5 min. The supernatant was removed and the cells were resuspended in fresh grown media, plated and placed in the appropriate incubator.

2.4.9 Confocal Microscopy

2.4.9.1 Preparing coverslips

For confocal microscopy, category #1 22 x 22 mm coverslips were used. Coverslips were washed with detergent in warm water and rinsed with ddH_2O. Coverslips were then rinsed in 95% ethanol before being allowed to air dry. Coverslips were sterilised by being placed under UV light for 30 min.

2.4.9.2 Preparation of immunofluroscent samples

In a 100 mm plate, several coverslips were added together with 10 mL of SF9 cells at a density of 8 x10^5 cells/mL. Cells were allowed to adhere for 15 min before being infected with the appropriate virus (section 2.4.6). Cells were incubated at 25°C for a specified time before each coverslip was transferred to one well of a 6-well plate. Cells were washed three times for 5 min with PBS with no shaking. Cells were then fixed with 2% paraformaldehyde in PBS for 15 min at room temperature with no shaking followed by two 10 min washes with PBS with no shaking. Cells were permeabilized with 0.2% Triton X-100 in PBS for 5 min with a gentle mix every few minutes. Cells were again washed twice for 10 min with PBS before being placed in blocking buffer (PBS, 5% BSA, 0.05% Tween-20). Cells were blocked for 60 min with gentle rocking. Coverslips were overlaid with primary antibody diluted in blocking buffer and incubated overnight at 4°C. In the morning, the primary antibody solution was removed and coverslips were washed three times for 5 min in PBS with 0.1% Triton X-100. From this point on, coverslips were be kept in the dark to prevent photo-bleaching. Coverslips were overlaid with secondary antibody diluted in blocking buffer and

incubated for 60 min at room temperature. Secondary antibody was removed and coverslips were washed three times for 5 min with 0.1% Triton X-100 in PBS and once with PBS for 5 min. Coverslips were then fixed in 2% paraformaldehyde in PBS for 15 min at room temperature. Coverslips were washed twice with PBS for 5 min before a final wash for 5 min in 0.1% Triton X-100 in PBS. Coverslips were rinsed in ddH_2O before being mounted on slides using 12 µL of ProLongGold®. Slides were left for 24 h before coverslips were fixed in place using nailpolish.

Antibody	Catalogue number	Initial Concentration	Final Concentration	Primary or secondary
M2 (FLAG) (mouse)	Sigma F3165	1 mg/mL	1 µg/mL	Primary
HA (rabbit)	SigmaSAB4300603	1 mg/mL	1 µg/mL	Primary
α-mouse Cy5	Life Technologies A10526	2 mg/mL	2 µg/mL	Secondary
α-rabbit Cy3	Life Technologies A10524	2 mg/mL	2 µg/mL	Secondary

Table 2.3 Antibodies used during confocal microscopy

Samples were examined by confocal microscopy using a Leica DM6000B confocal laser scanning microscope (CLSM). The Dyes used in this study and their excitation and absorption wavelengths are shown in table 2.4

Dye	Excitation (nm)	Absorption (nm)
DAPI	405	407-496
Cy3	514	571-616
Cy3	633	645-725

Table 2.4 Dyes used during confocal microscopy

2.4.10 Cell lysis

Media was aspirated from samples and 1 mL of PBS was added to each plate. Cells were released from the surface of the plate by scraping with a cell scraper. The cell solution was transferred to a microfuge tube and centrifuged at 1000 g for 5 min at 4°C. The supernatant was removed and the cell pellet was resuspended in 500 µL of lysis buffer (20 mM HEPES pH 7.4, 120 mM NaCl, 1.5 mM $MgCl_2$, 1 mM EGTA, 50 mM

NaF, 0.2% Tween-20, 0.5 mM DTT, 1 mM PMSF) and incubated on ice for 10 min. Samples were subjected to 20 s of vortexing followed by centrifugation at 16000 g for 10 min. The supernatant was transferred to a new microfuge tube while the pellet were used for histone extraction (section 2.4.11). An input sample of 30 µL of cell lysis was removed and the remaining lysate was subjected to immunoprecipitation (section 2.3.4).

2.4.11 Histone extraction

The pellet remaining after cell lysis (section 2.4.10) was resuspended in 1 mL ddH_2O then centrifuged at 16000 g for 10 min. The supernatant was removed and the pellet is recentrifuged at 16000 g for 1 min. The residual supernatant is removed to ensure there was no additional liquid with the pellet. The pellet was resuspended in 200 µL of 0.2N HCl and left on ice overnight. The sample was centrifuged at 16000 g for 10 min and the supernatant was transferred to a new microfuge tube. To neutralise the acid in the sample, 10 µL of 2 M Tris was added.

2.4.12 DNA damage induction

2.4.12.1 Doxorubicin induction

Doxorubicin was added directly to the cell culture media 4 h before harvesting. The final concentration was 1 µg/mL from an initial stock of 1 mg/mL in EtOH.

2.4.12.2 Bleomycin induction

Bleomycin was added directly to the cell culture media 4 h before harvesting. The final concentration was 1 µg/mL from an initial stock of 1 mg/mL in PBS.

2.4.12.3 UV induction

Cells were exposed to long wavelength ultraviolet light (UV) by being placed under an inverted Transilluminator UVP for 30 s. Plates were placed back in the incubator generally for a 1 h recovery period before harvesting.

3 Examination of TIP60 domains and p400 SANT domain helix deletion mutants in the DNA damage response

3.1 TIP60 as an activator of the DNA double-strand break response.

3.1.1 Introduction

TIP60 is a histone acetyl transferase that has several known functions within the cell, particularly during the DNA double-strand break (DSB) response. TIP60 is 60 kDa in size with multiple domains, one of which is the MYST domain named after the founding members of the family, MOZ, YBF2/SAS3, SAS2 and TIP60. The MYST domain contains a zinc finger domain that has been associated with protein-protein interactions and is essential for histone acetyl transferase (HAT) activity (Nordentoft & Jorgensen, 2003; Xiao et al., 2003). The MYST domain also contains an acetyl-coA binding site that is commonly referred to as the HAT domain. In addition to the MYST and zinc finger domains, TIP60 contains a chromo domain that has been shown to bind to methylated H3K9 enriched in heterochromatic regions (Sun et al., 2009). TIP60 is known to acetylate both histone and non-histone protein targets. During the DNA damage response, it is generally understood that TIP60 will acetylate ataxia telangiectasia mutated (ATM), an important kinase involved in DNA repair, on lysine 3016 which acts as a signal for ATM autophosphorylation on serine 1981 (shown in figure 3.1A) (Sun et al., 2005). This phosphorylation stimulates ATM to dissociate from an inactive dimer into an active monomer. This allows ATM to phosphorylate H2AX on serine 139 around break sites which provides a recognition signal for DNA repair proteins (Burma et al., 2001). Furthermore, TIP60 will acetylate histone H4 of the nucleosomes localised around the break site to help facilitate an open chromatin structure and allow repair proteins access to the break site (R. Murr et al., 2006). In addition to these well characterised functions of TIP60, a potentially novel function of TIP60 during DNA DSB repair has also been observed. Here, overexpressed TIP60 resulted in an increase in H2AX phosphorylation without induction of DNA damage (Smith, 2010). To explain this observation it was postulated that the overexpression of TIP60 would be responsible for sequestering a potential negative regulator from the ATM-TIP60 complex, stimulating ATM activation (figure 3.1B). In connection, this

artificial activation of ATM, through sequestering a negative regulator, could be attributed to a single domain within TIP60. Therefore, cDNAs representing the domains within TIP60 were individually cloned and expressed and their ability to induce H2AX phosphorylation was examined. If an individual domain could be attributed to H2AX phosphorylation induction, this information could aid in the identification of the negative regulator by suggesting a region of TIP60 to which it binds.

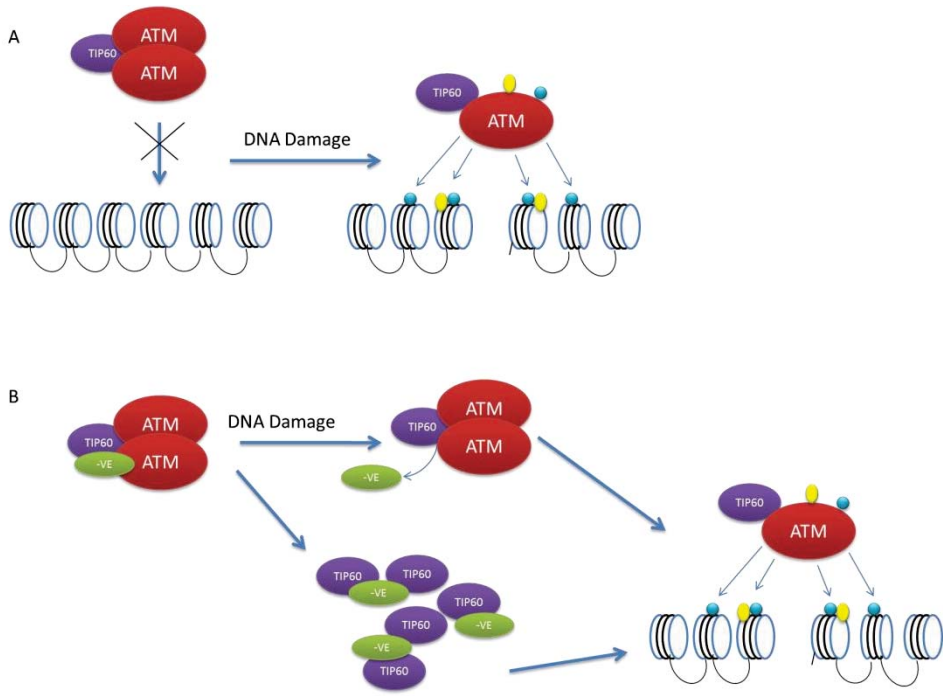

Figure 3.1 ATM activation by TIP60 and a hypothesised negative regulator. A. In an inactive state, two ATM proteins are in complex with TIP60. In the presence of DNA damage, TIP60 will acetylate ATM at lysine 3016 which will promote ATM monomerisation and subsequent autophosphorylation. ATM will then phosphorylate serine 139 sites on H2AX at sites of DNA damage while TIP60 will acetylate histone H4 around those break sites. B. It is hypothesised that a negative regulator is in complex with ATM and TIP60 preventing activation of the ATM-TIP60 complex. In the presence of DNA damage, the negative regulator (-VE) is removed and promotes ATM activation. Overexpressed TIP60 is hypothesised to sequester the negative regulator from the ATM-TIP60 complex and promote ATM activation in the absence of DNA damage. Yellow spheres represent acetylation while blue spheres represent phosphorylation.

3.1.2 Cloning and expression of TIP60 domains

The nucleotide and protein sequence for TIP60, accession numbers U74667.1, GI 1657981 respectively, were retrieved from the NCBI public database and were used to design primers with which to amplify individual domains or two adjacent domains. The domains found within TIP60 include the chromo domain, the zinc domain, and a histone

acetyltransferase (HAT) domain which are comprised of amino acids 25-76, 261-283, and 369-404 respectively (Figure 3.2). A previous study used the regions of residues 1-132, 134-301 and 281-421 to examine each domain (Park et al., 2010), therefore, these same regions were used in this study. The vector that was chosen for expression of the TIP60 domains was CBS-3HA. This vector contains a CMV promoter, which allows constitutive expression of the cDNA insert, a bovine 3' poly-adenylation recognition sequence and three hemagglutinin (HA) motifs at the 5' end of the construct. This vector also contained unique *EcoR*I and *Cla*I sites which allowed for directional cloning with the insert being in frame with the HA tag. The domain of interest was PCR-amplified using *Pfu* proof-reading polymerase (section 2.2.1) with an *EcoR*I site at the 5' end and a stop codon followed by a *Cla*I site at the 3' end of the amplicon. The amplified product was purified (Section 2.2) and the fragment was 3' A-tailed (section 2.2.3) to allow insertion into the pGEM-T vector. The pGEM-T easy™ kit uses blue-white selection for easy identification of potential clones. White colonies were grown and plasmids were screened by digestion with *EcoR*I and *Cla*I and potential positive clones were sequenced to ensure there were no PCR-induced errors. Correct clones were digested with *EcoR*I and *Cla*I and the insert purified using gel electrophoresis followed by agarose gel purification (section 2.2.5). The purified insert was used together in ligation reactions with gel purified and phosphatase treated CBS-3HA plasmid DNA which also had been digested with *EcoR*I and *Cla*I. Potential colonies were screened by digestion with *EcoR*I and *Cla*I. Clones were confirmed by DNA sequencing (section 2.2.13).

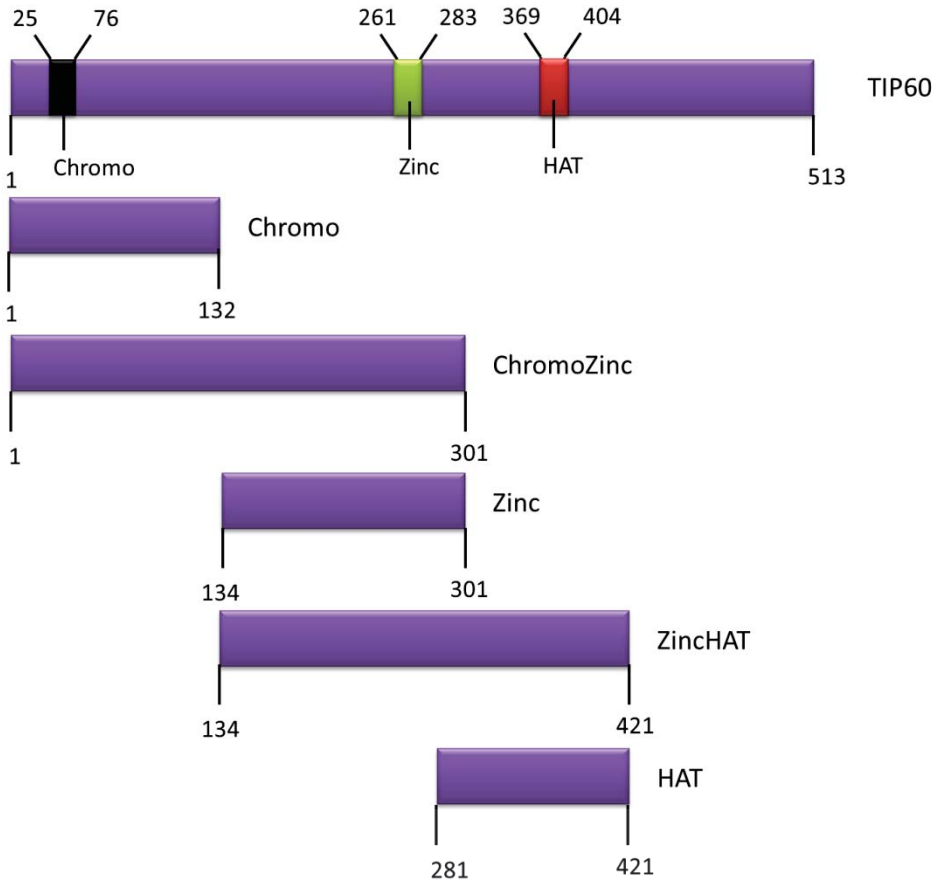

Figure 3.2 Schematic representation of full length TIP60 and domains. Full length TIP60 is 513 amino acids in length. It contains several functional domains including the chromo domain (amino acid 25-76), the zinc domain (amino acid 261-284) and the MYST HAT domain (amino acid 284-386). Five constructs were produced; The HA-chromo domain (amino acid 1-132), the HA-chromozinc domain (1-301), the HA-zinc domain (134-301), the HA-zincHAT domain (134-421) and the HA-HAT domain (281-421).

The forward primer was designed with an *EcoR*I site at the 5' end followed by the sequence for the region being amplified. The reverse primer was designed with a *Cla*I site at the 5' end followed by a stop codon and the 3' sequence of the region. PCR was carried out using the proofreading enzyme *Pfu* with results shown in Figure 3.3A. Lane 1 is a negative control and lane 2-6 show the amplification of the chromo (400 bp), chromozinc (chromo plus zinc) (900 bp), zinc (500 bp), zincHAT (zinc plus HAT) (920 bp) and the HAT (420 bp) domains respectively. The PCR amplification resulted in one major band for each amplicon (Figure 3.3A) with the negative control showing no amplification product. The zincHAT domain showed several non-specific amplification products, however, since the major band was the size of the predicted target sequence, the cloning process was carried out using this sample as well. Before the PCR product

could be used for cloning into the pGEM-T vector, 3' A tails were added using *Taq* polymerase as *Pfu* is a proofreading enzyme and will produce blunt ends which are incompatible with cloning into the pGEM-T easy vector (section 2.2.3). The adenylated PCR products were ligated into the pGEM-T vector according to the manufacturer's instructions and chemically competent DH5α *E.coli* were transformed with the ligation reaction before being grown on LB/agar plates with ampicillin, X-gal and IPTG (section 2.2.10).

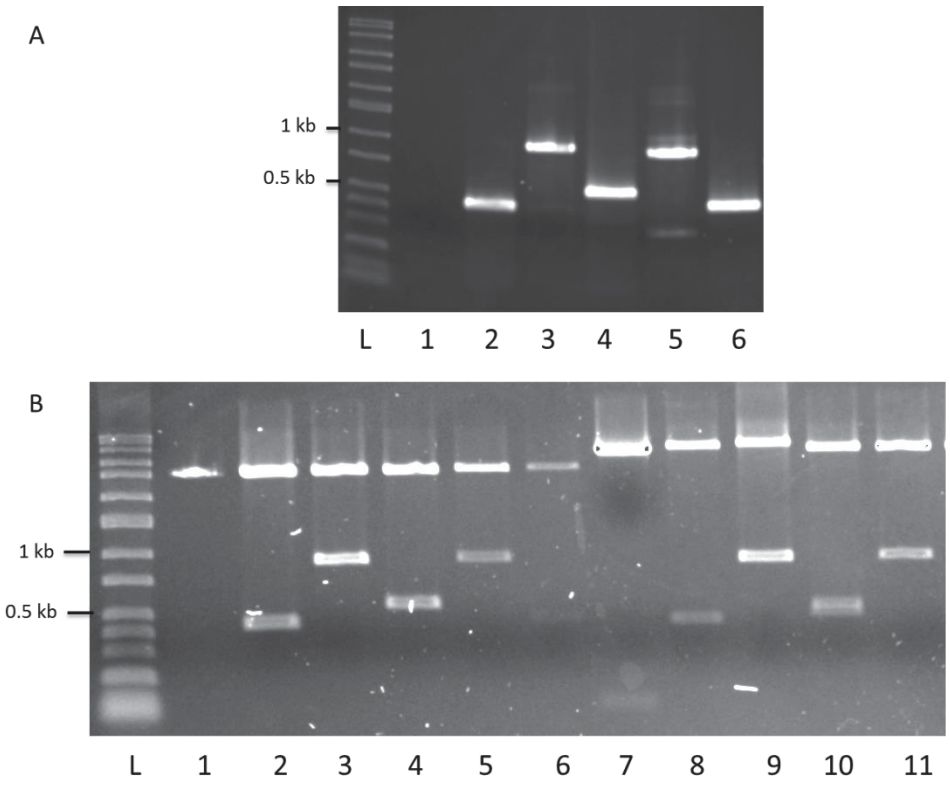

Figure 3.3 Cloning of CBS-HA-TIP60 domain constructs. A. PCR products for each of the domains of TIP60. L, DirectLoad™ wide range DNA marker from Sigma; Lane 1: Negative control, Lane 2: chromo domain, Lane 3: chromozinc domain, Lane 4: zinc domain, Lane 5: zincHAT domain, Lane 6: HAT domain. PCR products were amplified using *Pfu* polymerase and 5% of the reaction was analysed on a 1% agarose gel in 1x TBE for 1 h at 100 V. B. Colonies were screened for inclusion of the correct insert. DNA from pGEM-Insert colonies or CBS-Insert colonies (200 ng) were digested with *Cla*I and *Eco*RI enzyme to release the insert. Lane 1: pGEM-T empty, Lane 2: pGEM-chormo, Lane 3: pGEM-chromozinc, Lane 4: pGEM-zinc, Lane 5: pGEM-zincHAT, Lane 6: pGEM-HAT, Lane 7: empty CBS-3HA, Lane 8: CBS-chromo, Lane 9: CBS-chromozinc, Lane 10: CBS-zinc, Lane 11: CBS-zincHAT. Plasmid digests were analysed on a 1% agarose gel in 0.5x TBE for 1 h at 100 V before being stained with ethidium bromide (0.5 µg/mL in 0.5x TBE) and visualised under UV light.

Clones that contained the insert were first selected using blue-white selection, an intrinsic property of the pGEM-T system. Clones that showed the correct sized insert through *Cla*I and *Eco*RI digestion were confirmed using Sanger sequencing. Figure 3.3B lanes 1-6 show the pGEM-insert clones digested with *Cla*I and *Eco*RI. All clones showed the correct size insert and Sanger sequencing confirmed the presence of these without any PCR-induced errors. Prior to cloning into the CBS-3HA vector, the pGEM-insert clones were digested with *Cla*I and *Eco*RI and the inserts were resolved on a 1% agarose gel before being subjected to agarose gel purification (section 2.2.5). The CBS-3HA vector was also digested with *Cla*I and *Eco*RI to produce compatible sticky ends and the vector backbone was resolved on a 1% agarose gel before being purified using agarose gel purification (section 2.2.5). Linearised CBS-3HA vector and insert were ligated together using T4 ligase before *E.coli* DH5α were transformed with the ligation reaction (section 2.2.8). Potential colonies were screened using *Cla*I and *Eco*RI and positive clones are illustrated in Figure 3.3B lanes 7-11. Each plasmid when digested showed the correctly sized insert and Sanger sequencing (section 2.2.13) confirmed the production of error-free clones of TIP60 domains. Positive clones were identified for all inserts except for CBS-3HA-HAT. Since the HAT fragment (281-421) resides in the zincHAT fragment (134-421), construction of CBS-HAT was not further attempted.

While Sanger sequencing and restriction enzyme digestion confirmed that expression vectors had been constructed successfully, these constructs may fail to produce protein possibly due to protein instability. Therefore, HEK293T cells were transfected with each construct as described in section 2.4.3. The cells were incubated for 24 hours before whole cell extract was prepared (section 2.4.10) and expression of the cloned domains was examined by immunoblotting (section 2.3.2). Use of the CBS-3HA construct ensures that there is a HA tag at the N-terminus of the protein; therefore, antibodies raised against HA were used to examine expression. Figure 3.4 shows the expression of HA-TIP60 together with three domain constructs that were successfully prepared, HA-chromo, HA-zinc and HA-zincHAT in lane 2-5 respectively. Whole cell extracts of cells transfected with empty CBS-3HA vector was used as a negative control, which is included in lane 1. The chromozinc domain failed to express at detectable levels by immunoblotting which may have been unstable in the cell. Expression of TIP60 and the three domains were relatively equal and robust (using actin as a loading control). In summary, each separate domain of TIP60 was prepared as an

expression construct with the exception of the HAT domain alone. However, the HAT domain was included within the zincHAT domain.

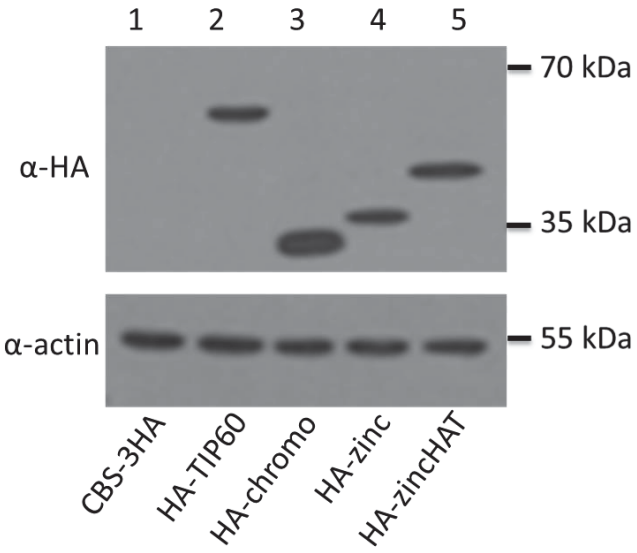

Figure 3.4 Expression of HA-TIP60 constructs. HEK-293T cells that were 60% confluent were transfected with 1 µg of DNA using FuGENE® HD as the transfection reagent. Whole cell extract was prepared after a 24 h incubation period and 10% (v/v) was resolved on a 10% polyacrylamide gel for 1 h at 30 mA. The proteins were transferred to a PVDF membrane for 3 h at 150 mA. The membrane was examined using antibodies raised against HA (α-HA) to visualise HA-TIP60 and domain derivatives. Equal loading was ensured by comparison to α-actin. Lane 1: CBS-3HA empty vector, Lane 2: CBS-HA-TIP60, Lane 3: CBS-HA-chromo, Lane 4: CBS-HA-zinc, Lane 5: CBS-HA-zincHAT.

3.1.3 H2AX phosphorylation by TIP60 domains

A previous study showed that overexpressed TIP60 was able to induce H2AX phosphorylation in the absence of a DNA damaging agent (Smith, 2010). To examine the ability of individual domains to induce histone H2AX phosphorylation, HEK293T cells were transfected with CBS-3HA vector, CBS-HA-TIP60, CBS-HA-chromo, CBS-HA-zinc or CBS-HA-zincHAT according to section 2.4.3 and were incubated for 24 h. Prior to harvest, one plate of cells transfected with CBS-3HA was treated with doxorubicin (section 2.4.12) and incubated for 4 h before being harvested for whole cell and histone extract (section 2.3.10 and 2.3.11). Whole cell extract (10% v/v) and histone extract (10% v/v) were examined by western blotting (section 2.3.2) using an antibody raised against HA to visualise TIP60 and TIP60 domain expression with α-actin used as a loading control to show equal loading while phosphorylation levels of

histone H2AX were examined using a phosphospecific antibody against S139 phosphorylation (α-H2AX-P) and a regular α-H2AX antibody as a loading control.

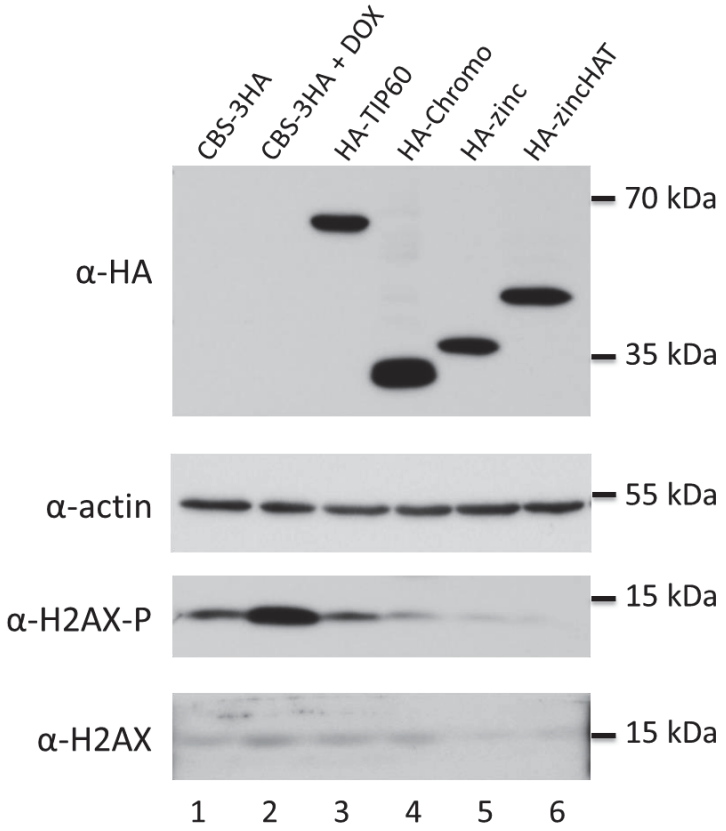

Figure 3.5 H2AX phosphorylation assay of TIP60 domains. Whole cell extract (10% v/v) was loaded onto a 10% polyacrylamide gel and resolved by electrophoresis. Histones were extracted using HCl (section 2.4.11) and histone samples (10% v/v) were loaded onto a 12% polyacrylamide gel and resolved by electrophoresis. Samples were separated at 30 mA for 1 h before being transferred to a PVDF membrane at 150 mA for 2 h. The membrane was examined with α-HA antibody for TIP60 derivatives expression and α-actin antibody as a loading control. Histones were examined on an immunoblot using H2AX-P antibody for phosphorylation induction and H2AX as a loading control. Lane 1: CBS-3HA empty vector, Lane 2: CBS-3HA empty vector +DOX, Lane 3: CBS-HA-TIP60, Lane 4: CBS-HA-chromo, Lane 5: CBS-HA-zinc, Lane 6: CBS-HA-zincHAT.

Figure 3.5 shows the result of the H2AX phosphorylation assay. Lane 1 and 2 show cells transfected with empty CBS-3HA DNA in the absence (lane 1) and presence (lane 2) of a DNA double-strand break inducer, doxorubicin. As expected, there is no signal seen in the α-HA panel as no HA tagged proteins were expressed. Lane 1 and 2 show the desired H2AX phosphorylation response in the absence and presence of DNA damage. In the absence of doxorubicin (lane 1) there is a basal level of histone H2AX

phosphorylation which is usually present due to replication stress (I.M Ward & Chen, 2001). Lane 2 shows an increase in histone H2AX phosphorylation in response to doxorubicin. The α-HA panel shows expression of HA-TIP60, HA-Chromo, HA-Zinc and HA-ZincHAT in lanes 3-6 respectively. These proteins appear to express at relatively equal levels. Equal amounts of actin suggest that equal amounts of protein were loaded in each sample. When the H2AX phosphorylation levels were examined, there appeared to be no significant increase in phosphorylation in any samples, including TIP60 which had previously shown to increase H2AX phosphorylation levels (Smith, 2010). The H2AX panel showed that relatively equal amounts of histone were loaded in each sample. Figure 3.5 is a one example figure of the experiment repeated upwards of 15 times. The phosphorylation level of H2AX failed to show any consistencies when TIP60 domains were overexpressed. However, each experiment resulted in a variation in H2AX phosphorylation levels. While the doxorubicin induction remained consistent in each experiment, the level of H2AX phosphorylation seen. In addition, various different cell lines including HEK293, HeLa and U2OS were also used in an attempt to show reproducible results. Again, these cell lines failed to show consistent H2AX phosphorylation induction with TIP60 or TIP60 domain overexpression. Therefore, no conclusions can be drawn about the ability of individual domains of TIP60 to induce H2AX phosphorylation in the absence of a DNA damaging agent.

3.2 The SANT domain of p400 as an activator of the DNA double-strand break response.

3.2.1 Introduction

p400 is an ATP-dependent chromatin remodeling protein that is responsible for exchanging H2A:H2B dimers for H2AZ:H2B dimers throughout the genome, particularly in promoter regions (Fuchs et al., 2001; Kobor et al., 2004; Kusch et al., 2004). Additionally, p400 has been shown to have a functional role during DNA repair (Ye Xu et al., 2010). It is a multidomain protein comprising a HSA (Helicase and SANT Associated) domain, a SWI2/SNF2 homology domain, a polyQ domain and a SANT domain. While the ATPase function of p400 has been associated with histone exchange, little information is available about the function of the other domains within p400. p400 is found in two main complexes in a cell, the p400 complex and the TIP60

complex (Fuchs et al., 2001; T. Ikura et al., 2000). These two complexes are essentially the same in composition including proteins such as TRRAP, BAF53 (53 kDa BRG1/human BRG1-associated factor), TIP60 associated proteins TAP53α and β, as well as TIP49 (TATA binding protein (TBP)- interacting protein) with the exception that the the p400 complex does not contain TIP60.

The SANT domains are commonly found within chromatin remodeling proteins and are postulated to have one of two roles. The first is a DNA binding activity. The SANT domain structure is similar to the helix-turn-helix motif of MYB and MYB-like domains which have known roles in DNA binding (Boyer et al., 2004; Mohrmann et al., 2002). The SANT domain has also been suggested to play a role in protein-protein interactions (Humphrey et al., 2001; Sterner et al., 2002). In 2010, Park et al. showed that the SANT domain of p400 was able to interact with TIP60 (a histone acetyl transferase found within the larger TIP60 complex) and subsequently, cause a robust inhibition of TIP60 HAT activity. Additionally, a previous study also showed that overexpression of the SANT domain caused an increase in histone H2AX phosphorylation in the absence of a DNA damaging agent (Smith, 2010). Two speculations were suggested to explain these observations. Firstly, as overexpression of TIP60 (discussed in section 3.1) may be able to sequester a negative regulator from the ATM-TIP60 complex, the overexpression of the SANT domain may be able to sequester the same negative regulator from the ATM-TIP60 complex which would result in activation of this complex and a consequent increase in H2AX phosphorylation (Figure 3.6A). The second speculation was that the SANT domain of p400 was able to bind independently to regions of DNA through a DNA-binding activity and imitate DNA damage, thus promoting H2AX phosphorylation (Figure 3.6B).

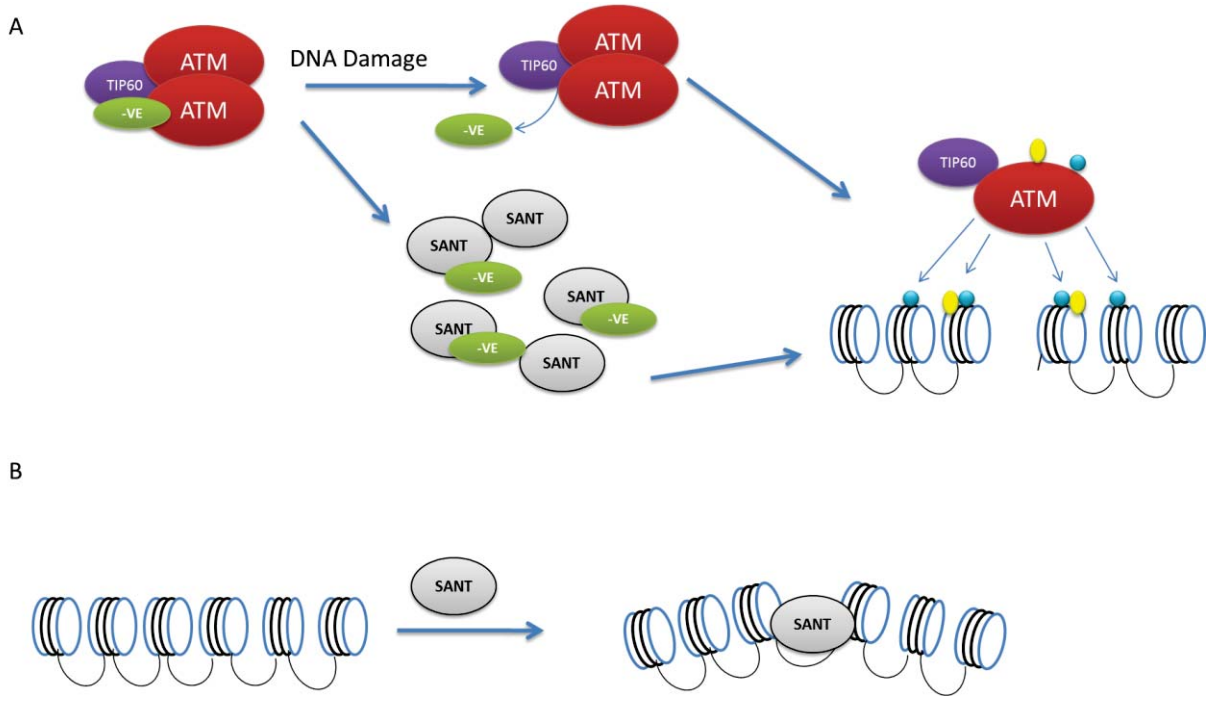

Figure 3.6 SANT domain activates ATM through sequestering a negative regulator or perturbing chromatin structure A. It is hypothesised that a negative regulator is in complex with ATM and TIP60 preventing activation of the ATM-TIP60 complex. In the presence of DNA damage, the negative regulator (-VE) is removed and promotes ATM activation. Overexpressed SANT domain is hypothesised to sequester the negative regulator from the ATM-TIP60 complex and promote ATM activation in the absence of DNA damage. Yellow spheres represent acetylation while blue spheres represent phosphorylation. B. Binding of the SANT domain to chromatin will perturb the chromatin structure, imitating DNA double-strand breaks and facilitate activation of the DNA double-strand break response.

While the SANT domain structure of p400 has not yet been determined by X-ray crystallographic analysis, the SANT domain from the chromatin remodeler ISWI from Xenopus has been resolved and shows the expected helix-turn-helix motif that forms three α-helices. Additionally, closely related helix-turn-helix motifs, the MYB domain and the MYB-like domain share the same triple α-helical structure. While the MYB domain and the MYB-like domains are commonly described as DNA binding motifs, with the third helix forming the recognition helix, the function of the SANT domain remains ambiguous. Interestingly, in 2002, Sterner et al showed that the SANT domain of ADA2, a subunit of the SAGA complex, was able to interact with GCN5, a histone acetyl transferase, which is reminiscent of the interaction seen between the SANT domain of p400 and TIP60. The study also suggested that the SANT domain allows ADA2 to interact with nucleosomes, tempting to suggest that p400 may have a similiar ability (Sterner et al., 2002). Studies investigating the role of different helices in the

SANT domain-containing proteins such as the chromatin remodlers SWI3, RSC8 and ADA2 have shown that the third helix is responsible for the majority of function associated with the SANT domain (Barbaric et al., 2003; Boyer et al., 2002; Sterner et al., 2002).

The functionality of these SANT domains appears to be conserved, therefore it is likely that a single helix within the SANT domain of p400 is responsible for the ability to increase H2AX phosphorylation in the absence of DNA damage. Accordingly, three helix deletion constructs, with small deletions within a helix or deletion of an entire helix, within the SANT domain of p400 were produced and used to examine SANT domain function.

3.2.2 Identification of p400 SANT domain helices and selection of deletions

To identify the position of the three helices within the SANT domain of p400, a ClustalW alignment of homologous sequences from 110 sources was obtained from prosite.expasy.org, a public database for protein domains, families and functional sites. Figure 3.7 shows the alignment of 110 SANT domains found in a variety of species ranging from yeast, drosophila, arabidopsis, mouse and human. Residues that are highlighted in dark grey are highly conserved through the aligned sequences while the residues highlighted in light grey show amino acids with conserved properties.

The ability to predict the beginning and end of α-helices represents a significant challenge for secondary structure prediction programs. Here the helices have been defined through the alignment and presence of conserved amino acids. Human p400, residues 2360-2429, is indicated by the blue arrow in Figure 3.7. Helix 1, shown in the first red box, is defined by the conserved tryptophan highlighted in dark grey and the conserved leucine also shown in dark grey (WLISEDWAL). Helix 2, shown in the second red box, is defined by the highly conserved tryptophan highlighted in dark grey and ends with a valine highlighted in light grey (WDLVSDVV). The final helix is defined by an arginine highlighted in dark grey and ends with a tyrosine residue (RSSKQCRNRY), shown in the third red box.

Figure 3.7 Alignment of SANT domain/MYB-like domain containing proteins. ClustalW has been used to align 110 sequences of SANT/MYB-like domains from a variety of species. Residues highlighted in dark grey show highly conserved residues while those highlighted in light grey show residues with conserved properties, eg, residues highlighted at this region are all basic residues. The human p400 SANT domain is highlighted by a blue arrow with predicted helices highlighted in a red boxes. Alignment was retrived from http://prosite.expasy.org/cgi-bin/aligner?psa=PS50090&color=1&maxinsert=10&linelen=0

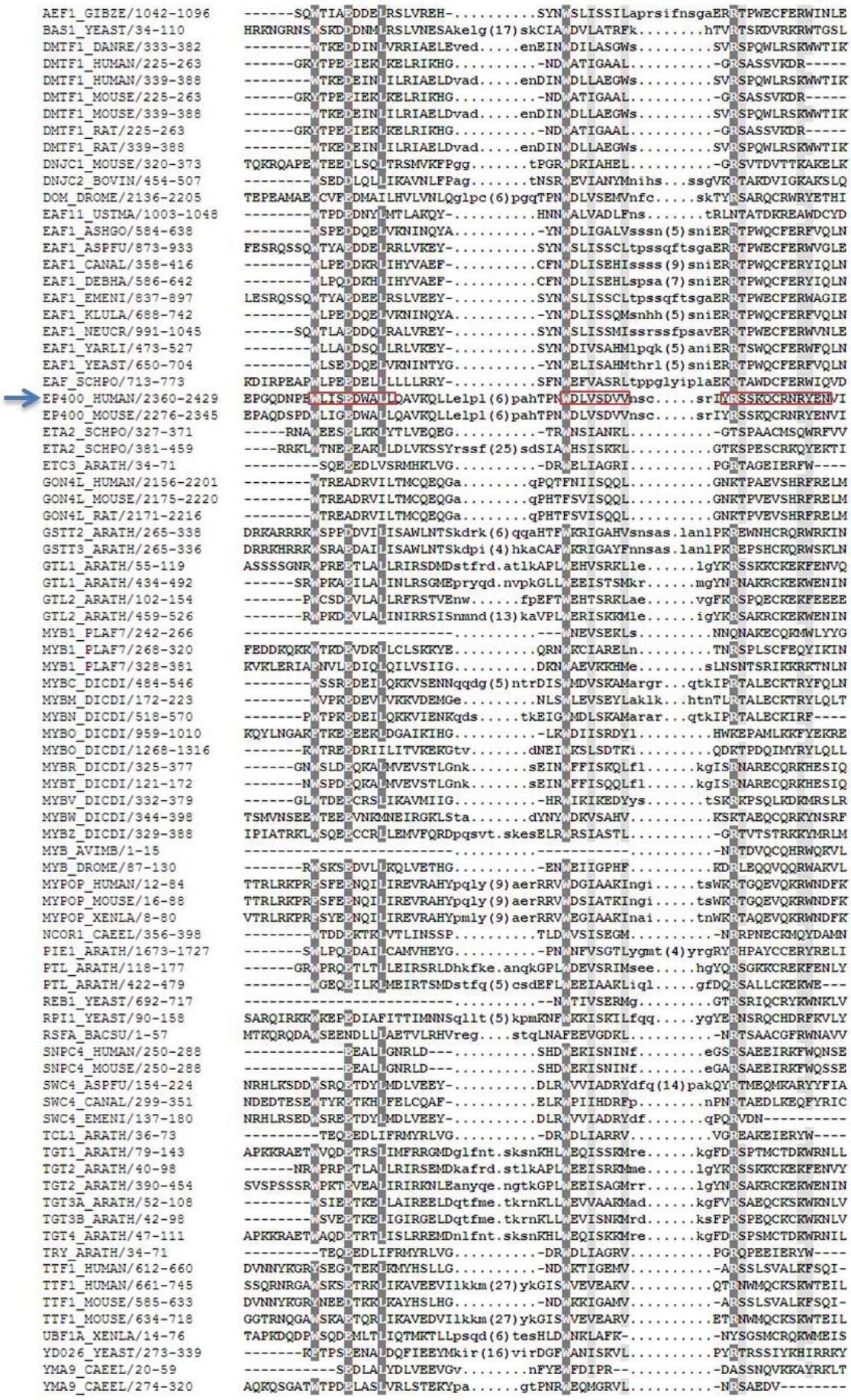

To investigate the importance of each individual helix to induce H2AX phosphorylation, three helix deletion mutants were designed using the FLAG-SANT (2249-2472) construct. This construct had been used previously and was shown to increase H2AX phosphorylation in the absence of DNA damage (Smith, 2010). Other studies investigating the role of each helix within SANT domains have deleted regions from the beginning or middle of the domains, or deleted entire helices. In the current study, the first construct SANT-ΔH1 contained a three amino acid deletion in the middle of the first predicted helix (residues 2372-2374, EDW). This includes a highly conserved glutamate (E) residue. The second helix deletion, SANT-ΔH2 deleted three amino acids from the beginning of the second predicted helix (2402-2404, WDL). This includes a highly conserved tryptophan residue (W). The final helix deletion, SANT-ΔH3 deletes an entire helix, including an amino acid either side of the two most conserved residues (2415-2427, YRSSKQCRNRYEN). The third helix is predicted to be the recognition helix and studies examining the function of this helix within SANT domains usually delete the entire helix. Therefore, to allow comparison with previous studies, Helix 3 was deleted.

The sequence of the WT SANT domain and the helix deletions were examined using Phyre2 (**P**rotein **H**omology/analog**Y** **R**ecognition **E**ngine V **2**.0), a resource available online, to determine the potential effect of deletion these regions may have on the secondary and tertiary structure of the SANT domain. This program used PSI-Blast to search for homologues with known 3D structure to the target amino acid sequence. An alignment based on homologies and evolutionary changes is produced showing the predicted secondary and tertiary structure for the target amino acid sequence.

Initially, the structure of the WT SANT domain of p400 (amino acids 2249-2472) was predicted based on the structure without deletions. The secondary structure read out (Figure 3.8A) shows several different types of analysis. First, the primary sequence that was used is shown on the first line of the read out. Below this is the predicted secondary structure and then below that, a coloured line indicating the confidence of the prediction. The key is included at the bottom of the readout with the highest confidence shown in red and the lowest confidence shown in blue. Below these two lines are the predicted Disorder and the Disorder confidence. Again red indicates the most confidence and blue for least confidence. Of the several alpha helices that are predicted throughout the secondary structure readout from Phyre2, the three predicted between

amino acids 84-150 represent the SANT domain of p400. This region corresponds with residues 2372-2434 of p400. The helices between 90-100, 117-125 and 134-143 are predicted with high confidence (shown by the red colour in the 'SS confidence' row). These predicted helices show extended regions; however these are predicted with low confidence and it is likely that each helix is only approximately 10 amino acids long. Figure 3.8B shows the predicted tertiary structure for amino acids 84-149 of the target sequence, which is shown in Figure 3.8A between the two black triangles. The tertiary structure in Figure 3.8B shows a helix-turn-helix motif as three α-helices with the N terminus shown in red and following the rainbow colours to violet at the C terminus. The program models the tertiary structure with 97.9% confidence against the known structure of the DNA-binding domain of the human cell division cycle 5 like protein.

The SANT_ΔH1 amino sequence has a three amino acid deletion (EDW) in the predicted first helix, as indicated by the red arrow in Figure 3.9A. This small deletion does not appear to change the predicted secondary structure except to perhaps shorten the first predicted helix within the sequence between the two black triangles. The predicted tertiary structure (Figure 3.9B) shows amino acids 84-146 of the target sequence. The tertiary structure in Figure 3.9B shows a helix-turn-helix motif as three α-helices with the N terminus shown in red and following the rainbow colours to violet at the C terminus. The third helix, shown in blue, appears to have a reduced helix motif and increased unstructured sequence. Again, the program models the tertiary structure with 97.1% confidence against the DNA-binding domain of the human cell division cycle 5 like protein. It is possible that the three amino acid deletion which has been shown to be highly conserved may contribute to the overall stability and structure of the motif. With the changes observed, it is possible that this three amino acid deletion could cause dysfunction of the SANT domain; alternatively, as two helices appear unchanged, the three amino acid deletion have little effect on function.

The SANT_ΔH2 amino sequence has a three amino acid deletion (WDL) in the predicted second helix, as indicated by the red arrow in Figure 3.10A. This small deletion results in the prediction of a significant change in secondary structure. This change can be seen in the first alpha helix between the black arrows where the alpha helix shows a change to a transmembrane helix and an additional small beta sheet. The predicted tertiary structure (figure 3B) does not show much change to the first and third helices, with both showing near identical positioning when compared to the WT SANT

domain. The second helix however, shows a large change with a much smaller helical structure and an increase in disordered sequence. This suggests that the three amino acid deletion may have a large effect on the second helix and its function while leaving the functionality of helix one and three intact. The tertiary structure for the SANT_ ΔH2 mutant is also modelled with 97.1% confidence against the DNA-binding domain of the human cell division cycle 5 like protein.

The SANT_ ΔH3 construct has a more severe deletion with the entire third helix removed in addition to one amino acid on the N terminal end and two additional amino acids on the C terminal end. The deleted amino acids, YRSSKQCRNRYEN, have been removed from the sequence as indicated by the red arrow on Figure 3.11A. This deletion results in a significant change in secondary structure compared to the WT SANT domain. The first two helices, seen between the two black triangles, do not show any difference compared to WT, however the third helix is missing and has been replaced with a short beta sheet. The predicted tertiary structure is illustrated in Figure 3.11B and is modelled with 81.4% confidence against the DNA binding protein RDA2 from *Antirrhinium majus.* This model uses amino acids 81-128 of the target sequence for the predicted structure which is significantly different when compared to the WT SANT domain. As the sequence used to produce the prediction is shorter than the previous sequences, the two helices shown are comparable to helix 1 and 2 of WT SANT domain. Additionally the two helices show a marked difference in length with the first helix being shorter and the second being much longer. This particular model is produced with a lower confidence than any other deletion and reflects the severity of the deletion.

Overall, the WT SANT domain shows the same tertiary structure predicted from Phyre2 which is predicted by current literature of a helix-turn-helix motif consisting of a three helix bundle. Additionally, the small deletions from helix 1 and 2 show a slight change in the predicted tertiary structure of the SANT domain but the overall orientation of the helices remains the same. The larger deletion of helix three shows the most significant change in tertiary structure and is likely to produce a different phenotype compared to the WT SANT domain.

Figure 3.8 Predicted secondary and tertiary structure for the SANT domain of p400 using Phyre2. The amino acid sequence for the SANT domain (2249-2472) of p400 was used for modelling the secondary structure using the intensive mode. The predicted secondary structure is shown in panel A. The input sequence is shown on the top line (with numbers indicating the amino acid number). Underneath this is the predicted secondary structure followed by a colour indicator of the confidence of the prediction (high to low confidence is represented by the colours of the rainbow as shown at the bottom of panel A). The lower two lines show disorder and confidence for the disorder. B shows the tertiary structure that is predicted for amino acids 84-149, the residues between the two black triangles. The N terminus of the structure is shown in red and follows the rainbow colours to the C terminus in violet.

A

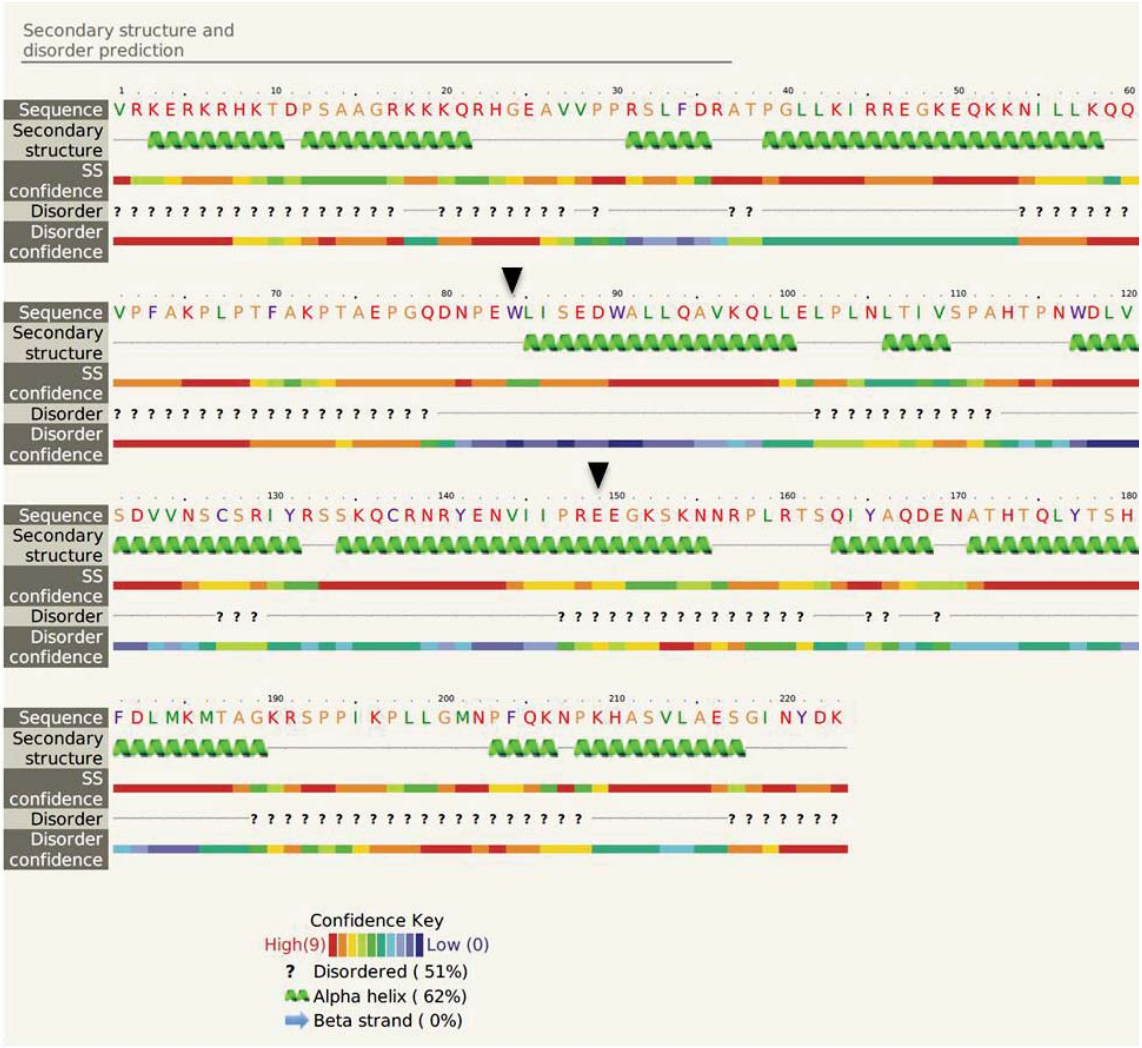
Secondary structure and disorder prediction
Sequence
Secondary structure
SS confidence
Disorder
Disorder confidence
VRKERKRHKTDPSAAGRKKKQRHGEAVVPPRSLFDRATPGLLKIRREGKEQKKNILLKQQ
VPFAKPLPTFAKPTAEPGQDNPEWLISEDWALLQAVKQLLELPLNLTIVSPAHTPNWDLV
SDVVNSCSRIYRSSKQCRNRYENVIIPREEGKSKNNRPLRTSQIYAQDENATHTQLYTSH
FDLMKMTAGKRSPPIKPLLGMNPFQKNPKHASVLAESGINYDK
Confidence Key
High(9) Low (0)
? Disordered (51%)
Alpha helix (62%)
Beta strand (0%)

B

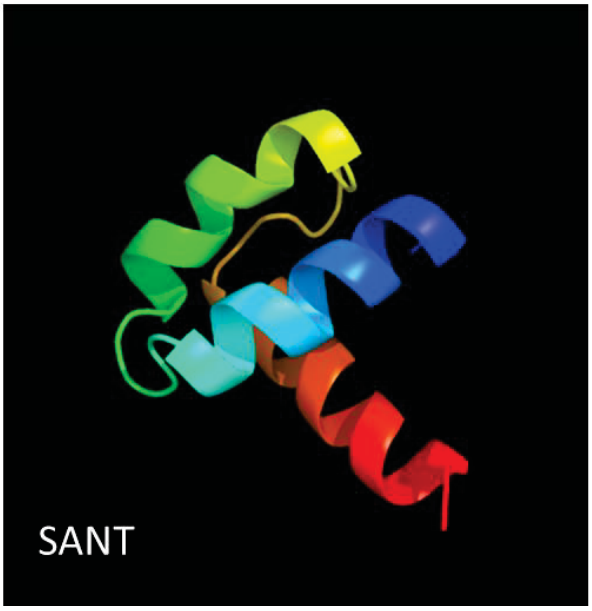
SANT

Figure 3.9 Predicted secondary and tertiary structure for the SANT-ΔH1 domain of p400 using Phyre2. The amino acid sequence for the SANT domain (2249-2472) of p400 was used for modelling the secondary structure using the intensive mode. The predicted secondary structure is shown in panel A. The input sequence is shown on the top line (with numbers indicating the amino acid number). Underneath this is the predicted secondary structure followed by a colour indicator of the confidence of the prediction (high to low confidence is represented by the colours of the rainbow as shown at the bottom of panel A). The lower two lines show disorder and confidence for the disorder. B shows the tertiary structure that is predicted for amino acids 84-146, the residues between the two black triangles. The three amino acid deletion of EDW is indicated by the red triangle. The N terminus of the structure is shown in red and follows the rainbow colours to the C terminus in violet.

A

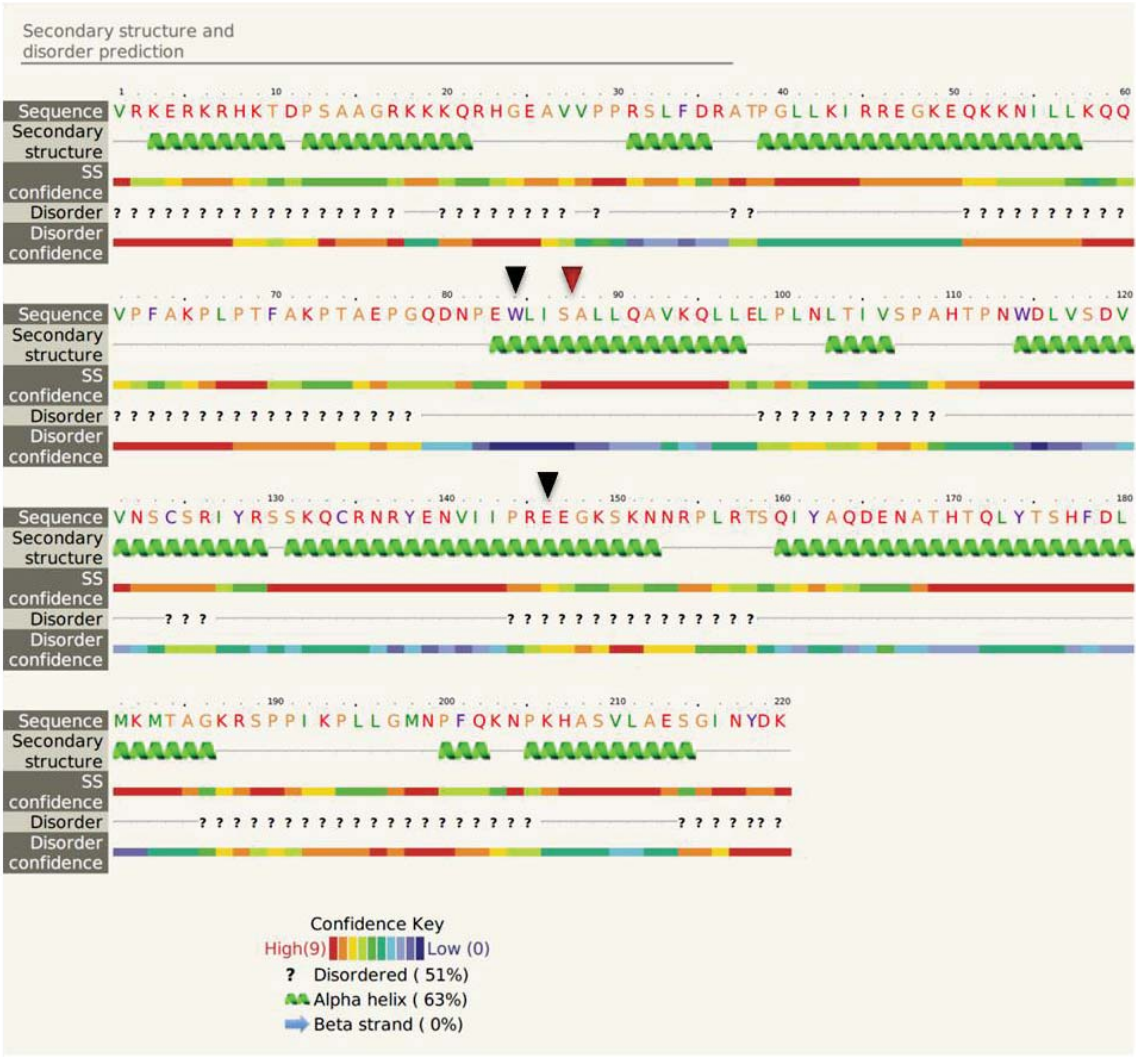
Secondary structure and disorder prediction
Sequence
Secondary structure
SS confidence
Disorder
Disorder confidence
VRKERKRHKTDPSAAGRKKKQRHGEAVVPPRSLFDRATPGLLKIRREGKEQKKNILLKQQ
VPFAKPLPTFAKPTAEPGQDNPEWLISALLQAVKQLLELPLNLTIVSPAHTPNWDLVSDV
VNSCSRIYRSSKQCRNRYENVIIPREEGKSKNNRPLRTSQIYAQDENATHTQLYTSHFDL
MKMTAGKRSPPIKPLLGMNPFQKNPKHASVLAESGINYDK
Confidence Key
High(9) Low (0)
? Disordered (51%)
Alpha helix (63%)
Beta strand (0%)

B

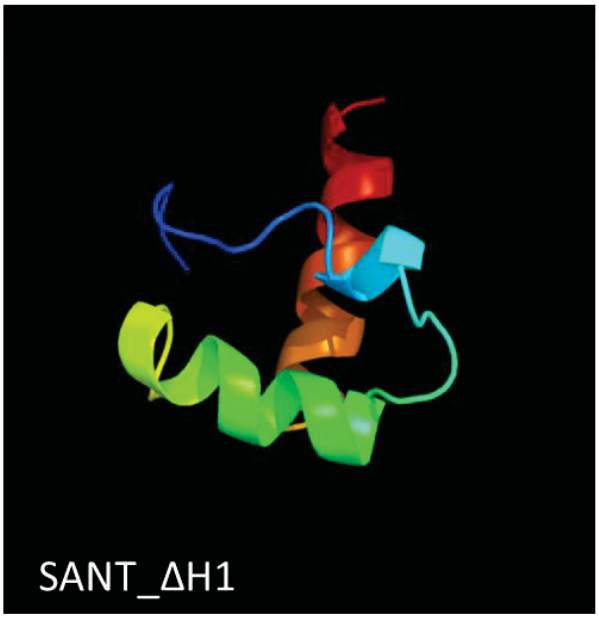
SANT_ΔH1

Figure 3.10 Predicted secondary and tertiary structure for the SANT-ΔH2 domain of p400 using Phyre2. The amino acid sequence for the SANT domain (2249-2472) of p400 was used for modelling the secondary structure using the intensive mode. The predicted secondary structure is shown in panel A. The input sequence is shown on the top line (with numbers indicating the amino acid number). Underneath this is the predicted secondary structure followed by a colour indicator of the confidence of the prediction (high to low confidence is represented by the colours of the rainbow as shown at the bottom of panel A). The lower two lines show disorder and confidence for the disorder. B shows the tertiary structure that is predicted for amino acids 84-146, the residues between the two black triangles. The three amino acid deletion of WDL is indicated by the red triangle. The N terminus of the structure is shown in red and follows the rainbow colours to the C terminus in violet.

A

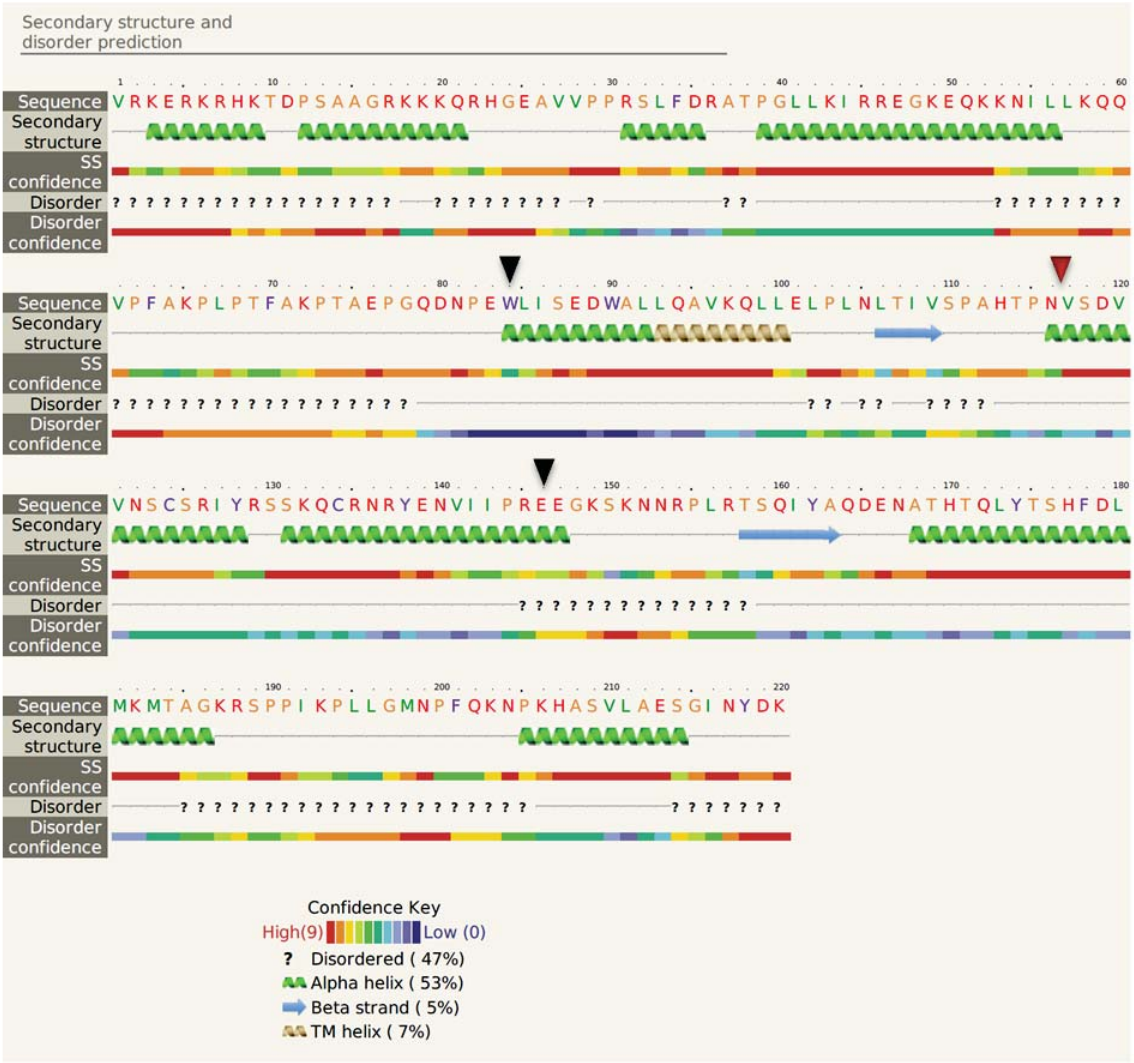
Secondary structure and disorder prediction
Sequence
Secondary structure
SS confidence
Disorder
Disorder confidence
VRKERKRHKTDPSAAGRKKKQRHGEAVVPPRSLFDRATPGLLKIRREGKEQKKNILLKQQ
VPFAKPLPTFAKPTAEPGQDNPEWLISEDWALLQAVKQLLELPLNLTIVSPAHTPNVSDV
VNSCSRIYRSSKQCRNRYENVIIPREEGKSKNNRPLRTSQIYAQDENATHTQLYTSHFDL
MKMTAGKRSPPIKPLLGMNPFQKNPKHASVLAESGINYDK
Confidence Key
High(9) Low (0)
? Disordered (47%)
Alpha helix (53%)
Beta strand (5%)
TM helix (7%)

B

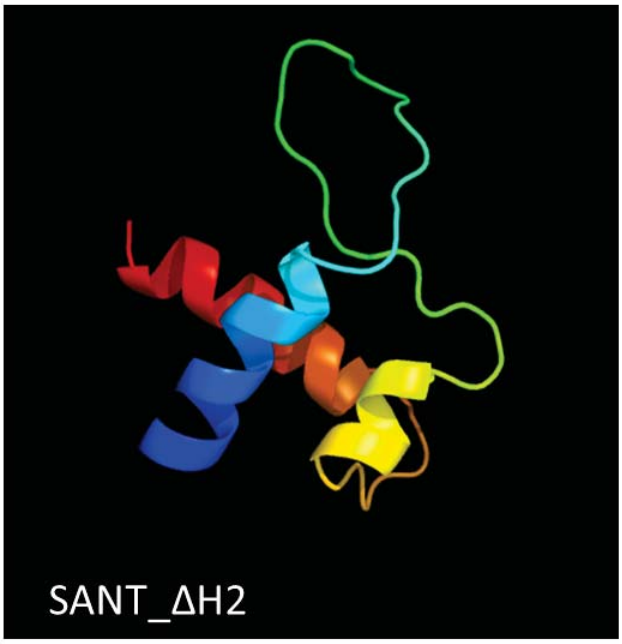
SANT_ΔH2

Figure 3.11 Predicted secondary and tertiary structure for the SANT-ΔH3 domain of p400 using Phyre2. The amino acid sequence for the SANT domain (2249-2472) of p400 was used for modelling the secondary structure using the intensive mode. The predicted secondary structure is shown in panel A. The input sequence is shown on the top line (with numbers indicating the amino acid number). Underneath this is the predicted secondary structure followed by a colour indicator of the confidence of the prediction (high to low confidence is represented by the colours of the rainbow as shown at the bottom of panel A). The lower two lines show disorder and confidence for the disorder. B shows the tertiary structure that is predicted for amino acids 81-128, the residues between the two black triangles. The 10 amino acid deletion of YRSSKQCRNRYE is indicated by the red triangle. The N terminus of the structure is shown in red and follows the rainbow colours to the C terminus in violet.

A

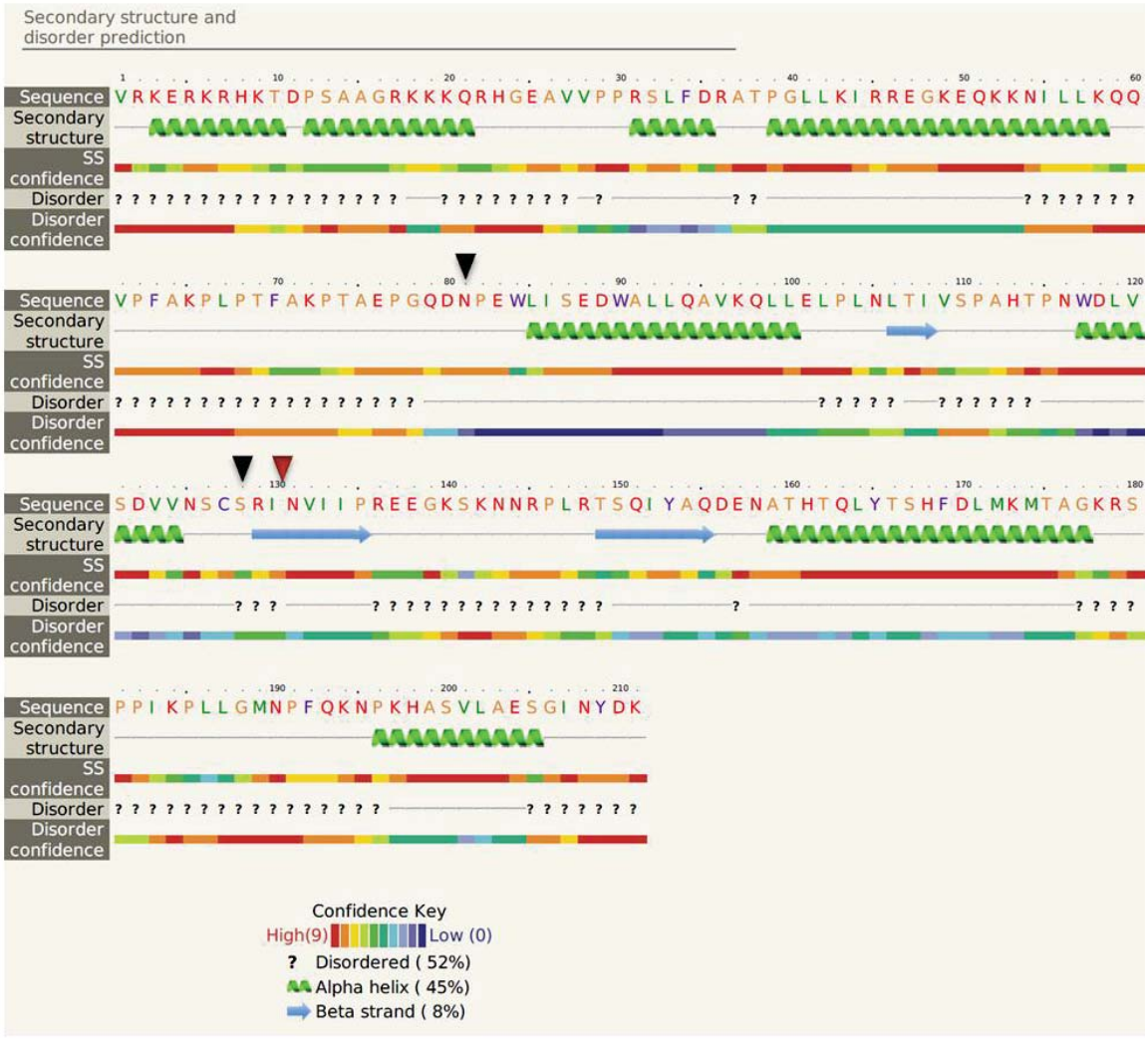
Secondary structure and
disorder prediction
Sequence
Secondary structure
SS confidence
Disorder
Disorder confidence
Confidence Key
High(9) Low (0)
? Disordered (52%)
Alpha helix (45%)
Beta strand (8%)

B

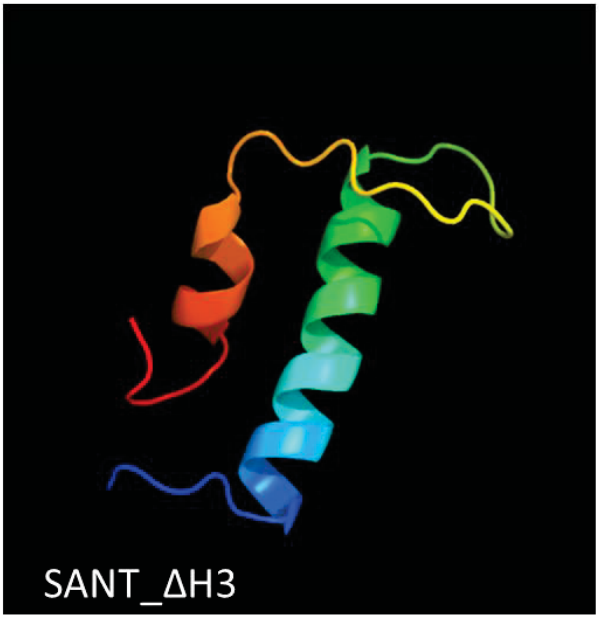
SANT_ΔH3

3.2.3 Production and expression of SANT domain deletion mutants.

Site-directed mutagenesis based on the QuikChange® method was used to produce the helix deletions. Primers were designed to flank the deleted sequence (looping out the deleted sequence) with the addition of a 5' phosphate group on the end of the primers so that when the *E.coli* were transformed with the PCR product, the endogenous ligase could religate the long PCR product to make a circular plasmid. Primers for Helix deletion 1 were designed to delete residues 2372-2374 of the SANT domain while primers for Helix deletion 2 were designed to delete residues 2402-2404 of the SANT domain. Primers for the Helix 3 deletion were designed to delete 12 amino acids (residues 2415-2426) of the SANT domain. Additionally, the asparagine immediately after the helix deletion in the Helix 3 (residue 2427) was mutated to produce an aspartic acid by substituting an adenine for a guanine. This essentially changes a basic amine to a carboxylate group. While this may seem like a significant change it is less significant than the deletion of the entire helix. This single nucleotide substitution allowed for the introduction of a *Cla*I site for the easy identification of deletion clones. Restriction sites were not included in helix deletion 1 or 2 as this would have been a far more significant change. Instead, clones were to be screened by sequencing to identify positive clones. A full list of primers can be found in appendix 1. A schematic diagram showing the constructs used in this chapter can be seen in in figure 3.12.

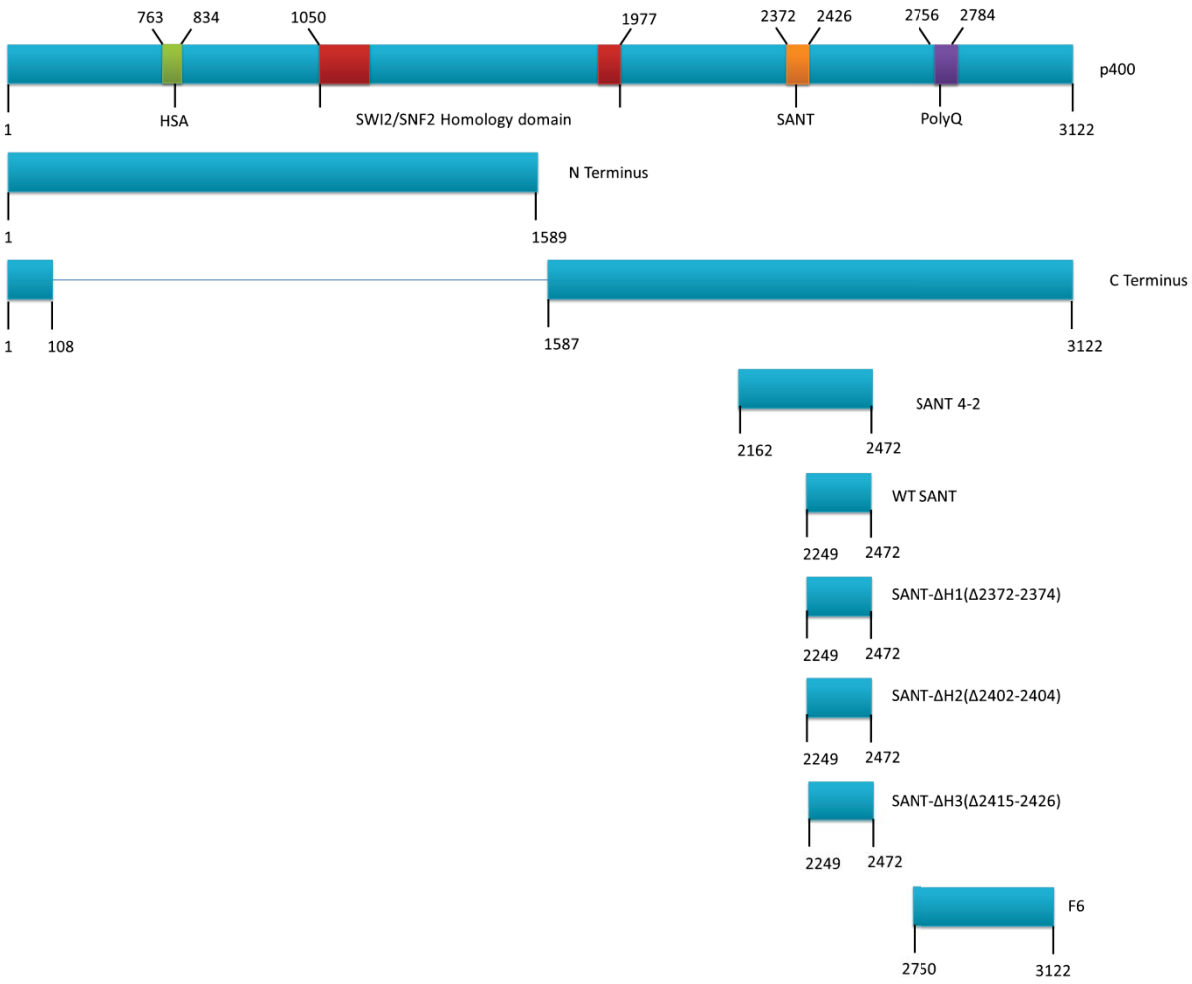

Figure 3.12 Schematic representation of full length p400 and derivatives used in this study. Full length p400 is 3122 amino acids in length. It contains several functional domains including the HSA domain (amino acid 763-834), the SWI2/SNF2 homology domain (amino acid 1050-1977) the SANT domain (amino acid 2372-2426) and the PolyQ domain (amino acid 2756-2784). Several constructs were provided from a previous study including the N-Terminus (amino acid 1-1589), the C-terminus (amino acid 1587-3122 with the first 101 amino acids at the N terminus), SANT 4-2 (amino acid 2162-2472 of p400), WT SANT (amino acid 2249-2472) and F6 (amino acid 2750-3122). Three constructs were produced in this study; SANT-ΔH1(Δ2372-2374), SANT-ΔH2(Δ2402-2404) and SANT-ΔH3(Δ2415-2426)

PCR reactions were carried out with the Elongase® from Life Technologies, which is a proofreading enzyme designed to amplify long regions of DNA with high fidelity. The programs used for PCR amplification are included in appendix 1. PCR products were subjected to *Dpn*I digestion (section 2.2.15) to remove any template DNA before being purified according to section 2. *E.coli* DH5α cells were transformed with the purified *Dpn*I treated PCR product and grown on LB agar plates with ampicillin (50 µg/mL) (section 2.2.10). Clones for helix 3 were screened using *Cla*I digestion which should

result in the release of a 250 bp fragment if mutagenesis was successful (section 2.2.6). Potential clones for helix 1 and 2 deletions were screened using Sanger sequencing. Clones of helix 3 deletion showing the expected digestion pattern were verified by Sanger sequencing (section 2.2.13).

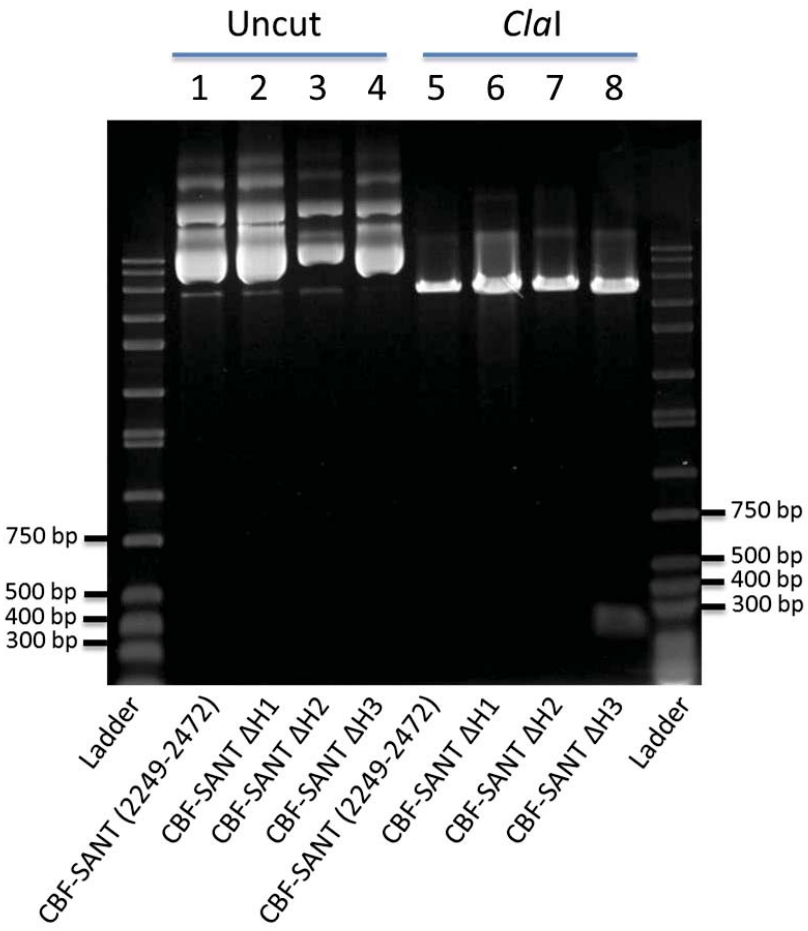

Figure 3.13 Digestion of FLAG-SANT WT and deletion mutants with *Cla*I. Plasmid DNA for WT FLAG-SANT, FLAG-SANT-ΔH1, FLAG-SANT-ΔH2 and FLAG-SANT-ΔH3 (200 ng) were digested with *Cla*I according to section 2.2.6. The samples were resolved on a 1% agarose gel in 0.5x TBE for 1 h at 180 V (section 2.2.5). The gel was stained with ethidium bromide (0.5 µg/mL in 0.5x TBE) before being examined using the BioRad Gel Doc™. The ladder used is the DirectLoad ™ wide range marker from Sigma. Lanes are labeled with the name of the plasmid used in each sample. ™

Plasmid DNA of FLAG-SANT, FLAG-SANT-ΔH1, FLAG-SANT-ΔH2 and FLAG-SANT-ΔH3 were purified according to section 2.2.11.2 before being subjected to restriction enzyme digestion with *Cla*I according to section 2.26. The samples, along with an undigested control, were resolved on an agarose gel according to section 2.2.5. Figure 3.13 shows the digestion of plasmid DNA with *Cla*I. Lanes 1-4 show undigested

plasmid from FLAG-SANT, FLAG-SANT-ΔH1, FLAG-SANT-ΔH2 and FLAG-SANT-ΔH3 respectively while lanes 5-8 show FLAG-SANT, FLAG-SANT-ΔH1, FLAG-SANT-ΔH2 and FLAG-SANT-ΔH3 respectively digested with *Cla*I. The WT SANT, ΔH1 and ΔH2 have one *Cla*I restriction site and therefore show one band in the digested samples. FLAG-SANT-ΔH3 has an additional *Cla*I restriction site and results in a 250 bp band being released. This can be seen in lane 8. The release of this band suggests that the ΔH3 mutation has been successfully incorporated into this construct. Sanger sequencing was required to confirm both these results and those for ΔH1 and ΔH2.

To confirm the production of FLAG-SANT-ΔH1, FLAG-SANT-ΔH2 as well as confirm the deletion of FLAG-SANT-ΔH3, the plasmid DNA was sequenced by the Massey Genome Service using Sanger sequencing as described in section 2.2.13 in both the forward and reverse directions. The primers used for sequencing in the CBS vector are listed in appendix 1. The sequences were then aligned against the sequence for WT SANT using Vector NTI® from Life Technologies. This alignment program uses ClustalW for pairwise alignment. Figure 3.14 shows the alignments that were produced. Figure 3.14A confirms the production of FLAG-SANT-ΔH1. The alignment shows that a 9 nucleotide gap in the forward and reverse sequence, corresponding to the deletion. Figure 3.14B confirms the production of FLAG-SANT-ΔH2 with the alignment showing the 9 nucleotide gap in the forward and reverse sequence corresponding to the deletion. Figure 3.14C shows the alignment for FLAG-SANT-ΔH3 and confirms the production of the plasmid as expected. The alignment shows a 36 nucleotide gap which corresponds with the deletion. Additionally, the alignment also shows the A to G mutation which produces the *Cla*I restriction site. Overall, the production of all three deletion mutants was confirmed and no additional variants were found. This means that any difference observed when the protein is expressed should be due to the introduced deletions and not any additional PCR-induced errors.

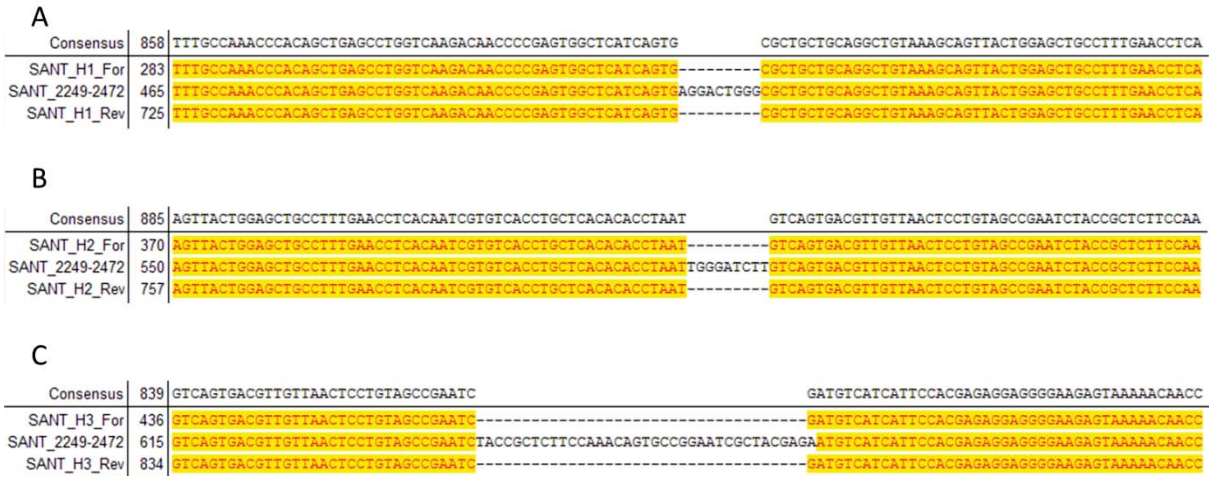

Figure 3.14 Sequence alignments of the SANT domain and helix deletion mutants. Constructs were sequenced in both the forward and reverse directions and aligned against the sequence for WT SANT using Vector NTI with ClustalW as the alignment algorithm. The top panel shows the alignment for the ΔH1 mutant. The sequence from the forward primer is shown in the top yellow line (SANT_H1_For) and the sequence from the reverse primer is shown in the bottom yellow line (SANT_H1_Rev). The WT SANT domain sequence is shown in the middle yellow line (SANT_2249-2472). The nucleotides highlighted in yellow show the nucleotides in common between all three aligned sequences. The '-' indicate missing sequence and thus the region that has been deleted. The nomenclature is the same for the ΔH2 mutant (middle panel) and the ΔH3 mutant (bottom panel).

It is important that the SANT domain and the three helix deletion constructs are expressed to approximately the same amounts. To examine this, HEK293T cells were transfected with 1 µg of plasmid DNA (section 2.4.3). Whole cell extract was produced after a 24h incubation according to section 2.4.10 and extracts were by western blotting (section 2.3.1 and 2.3.2). As the SANT domain and the deletion mutants are all FLAG tagged, the membranes were probed with an antibody against FLAG (α-FLAG) to examine the expression of the SANT domain derivatives and β actin was used as a loading control (Fig 3.16). The immunoblot analysis shows that the SANT domain (Lane 2) and the three helix deletions, ΔH1-3 respectively (Lanes 3-5) all express, however, ΔH2 and ΔH3 appear to express at a lower level. While only a few amino acids were deleted in each deletion mutant, there is a visible difference if migration on a SDS-PAGE between the WT SANT domain and Helix 1 and 3 deletions. The Helix 2 deletion does not show much difference in size compared to WT SANT. The robust expression of all helix deletion constructs suggests that they have stable protein folding and are not being targeted for proteosomal degradation.

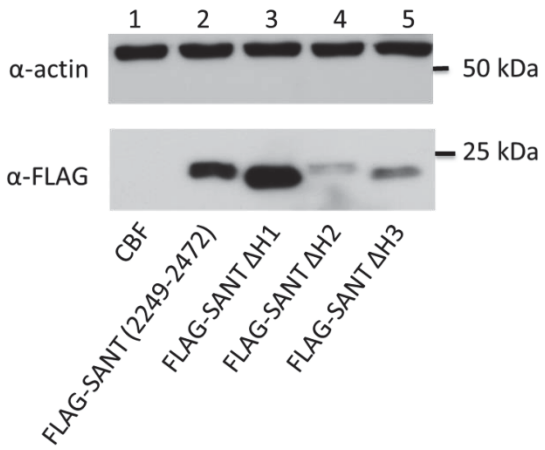

Figure 3.15 Expression of SANT and Helix deletion mutants. HEK293T cells were transfected with empty CBF vector (lane 1) or CBF-SANT, CBF-SANT-ΔH1, CBF-SANT-ΔH2, CBF-SANT-ΔH3 (lanes 2-5 respectively). Cells were incubated for 24 h before whole cell extract was produced (section 2.4.10). Ten percent (v/v) of the prepared extract was loaded onto a 10% SDS polyacrylamide gel and resolved by electrophoresis. Samples were separated at 30 mA for 1 h before being transferred to a PVDF membrane at 150 mA for 2 h. The membrane was examined with α-FLAG antibody for SANT domain expression and α-actin as a loading control.

3.3.4 H2AX phosphorylation by p400 derivatives

In a previous study, overexpression of the SANT domain of p400 led to an increase in H2AX phosphorylation in the absence of a DNA damaging agent (Smith, 2010). Here, the ability of the SANT domain with deletions in each of the three predicted SANT domain helices was examined for the ability to induce H2AX phosphorylation in the absence of DNA damage. HEK293T cells were transfected with 1 µg of empty CBF vector, CBF-SANT 4-2, CBF-SANT, CBF-SANT-ΔH1, CBF-SANT-ΔH2, CBF-SANT-ΔH3 or CBF-F6 (section 2.4.3). Whole cell and histone extract was prepared after 24 h incubation (section 2.4.10 and 2.4.11). Prior to harvest, one plate of cells transfected with empty CBF was treated with doxorubicin (section 2.4.12). Whole cell and histone extracts were examined by western blotting using an antibody raised against FLAG (α-FLAG) to visualise the expression of FLAG tagged p400 SANT domains and F6 with α-actin used as a loading control to show equal loading. Fragment 6 was used as a negative control as this region had previously shown not to interact with TIP60 and does not contain and known domain structures (Park et al., 2010). Phosphorylation

levels of H2AX were examined using α-H2AX-P with α-H2AX used as a loading control.

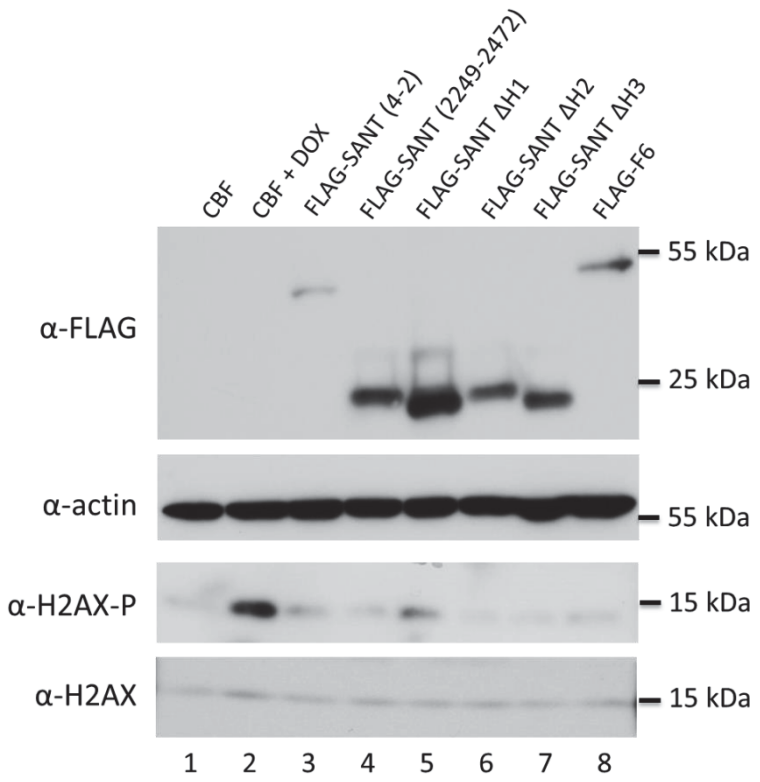

Figure 3.16 H2AX phosphorylation assay of SANT domain derivatives. HEK293T cells were transfected with CBF vector (lane 1 and 2) or CBF-SANT 4-2, CBF-SANT, CBF-SANT-ΔH1, CBF-SANT-ΔH2, CBF-SANT-ΔH3 or CBF-F6 (lane 3-8 respectively). Cells were incubated for 24 h before whole cell extract was produced (section 2.4.10). Cells in lane 2 were treated with doxorubicin (1 µg/mL) for 4 h before being harvested. Whole cell extract (10% v/v) was loaded onto a 10% polyacrylamide gel and resolved by electrophoresis. Histones were extracted using HCl (section 2.4.12) and histone samples (10% v/v) were loaded onto a 12% polyacrylamide gel and resolved by electrophoresis. Samples were separated at 30 mA for 1 h before being transferred to a PVDF membrane at 150 mA for 2 h. The membrane was examined with α-FLAG antibody for p400 derivative expression and α-actin as a loading control. Histones were examined using H2AX-P antibody for phosphorylation induction and H2AX as a loading control.

Figure 3.16 shows an example image of the H2AX phosphorylation assay with SANT domain derivatives. Lane 1 and 2 contains empty CBF vector and therefore show no protein expression in the FLAG panel. These two lanes show the response of H2AX phosphorylation in the absence (lane 1) and presence (lane 2) of DNA damage in the α-H2AX-P panel in Figure 3.16. Basal levels of H2AX phosphorylation, presumably from replication, can be seen in lane 1 with a large increase in H2AX phosphorylation in lane

2 which has been treated with the DNA double-strand break inducer doxorubicin. The FLAG panel shows that the p400 derivatives expressed at relatively equal levels except for SANT 4-2 and F6 which show reduced expression. There is no increase in H2AX phosphorylation seen in lanes 3-8 suggesting that the overexpression of SANT domain derivatives do not promote activation of the ATM pathway. This figure is an example image of the assay repeated upwards of 15 times. On different occasions, the SANT domain and SANT domain derivatives have not been consistent and reproducible in regards to the increase of H2AX phosphorylation. In addition to HEK293T cells, the experiment was repeated in several additional cell lines including HeLa cells and U2OS cells (data not shown). These additional cell types also failed to produce reproducible results.

If the SANT domain of p400 was acting to sequester a negative regulator from the ATM-TIP60 complex, full length p400 or half-length p400 containing the SANT domain should have the same effect. To examine this, HEK293T cells were transfected with 1 µg of empty CBF vector, 2 µg of CBF-p400, CBF-p400 ATPase mutant, CBF-N Terminus, CBF-C Terminus, 1 µg of CBF-SANT, CBF-F6 or CBF-TIP49. The N-terminal half of p400 does not include the SANT domain and should therefore not induce H2AX phosphorylation if the hypothesis is correct. Additionally, F6 of p400 and TIP49 (a member of the TIP60 complex) were used as additional negative controls. Whole cell and histone extract was prepared from cells that had in transfected for 24 h and examined by western blotting (section 2.4.3, 2.4.10 and 2.3.2). Membranes were examined using an antibody raised against FLAG (α-FLAG) to visualise the expression of FLAG tagged p400 domains, TIP49 and F6 and α-actin antibody as a loading control to show equal loading. Phosphorylation levels of histone H2AX were examined using α-H2AX-P antibody which were compared to total histone H2AX levels as a loading control.

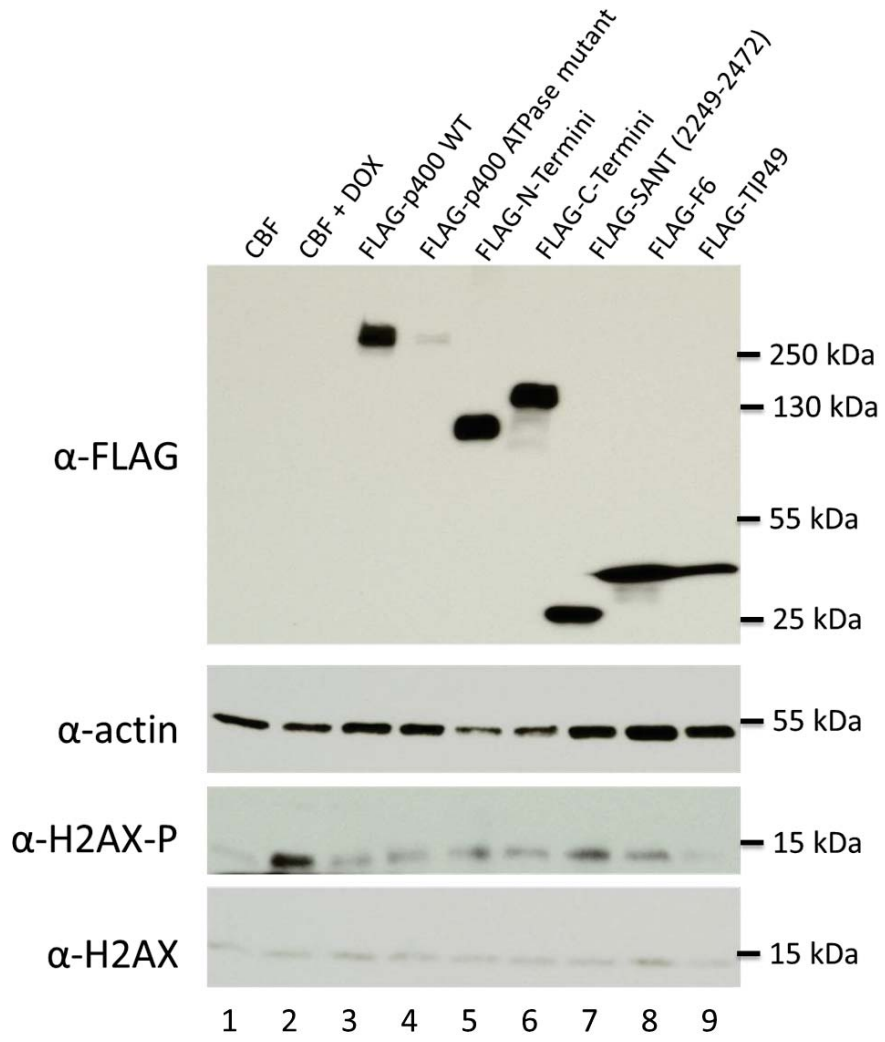

Figure 3.17 H2AX phosphorylation assay of p400 derivatives. HEK293T cells were transfected with CBF vector (lane 1-2) or CBF-p400, CBf-p400 ATPase mutant, CBF-N terminal, CBF-C terminal, CBF-SANT, CBF-F6 or CBF-TIP49 (lanes 3-9 respectively). Cells were incubated for 24 h before whole cell extract was produced (section 2.4.10). Cells in lane 2 were treated with doxorubicin (1 µg/mL) for 4 h before being harvested. Whole cell extract (10% v/v) was loaded onto a 4-12% polyacrylamide gel and resolved by electrophoresis. Histones were extracted using HCl (section 2.4.11) and histone samples (10% v/v) were loaded onto a 12% polyacrylamide gel and resolved by electrophoresis. Samples were separated at 30 mA for 1 h before being transferred to a PVDF membrane at 150 mA for 2 h. The membrane was examined with α-FLAG antibody for p400 derivative expression and α-actin antibody as a loading control. Histones were examined using H2AX-P antibody for phosphorylation induction and total H2AX levels as a loading control.

Figure 3.17 shows the H2AX phosphorylation assay with larger p400 constructs. H2AX phosphorylation shows a DNA damage-dependent response with an increase in H2AX-P seen with doxorubicin treatment (compare lane 1 to 2). Of the proteins expressed, only the p400 ATPase mutant did not express well. This sample was included to show

that if p400 induced H2AX phosphorylation, it was an effect either dependent or independent of the ATPase activity of p400. However, as full length p400 failed to induce any H2AX phosphorylation (compare H2AX-P in lane 2 and 3) and as p400 ATPase mutant failed to express to acceptable levels, no conclusions can be drawn about the ATPase activity of p400 being involved in promoting H2AX phosphorylation. The N and C terminal fragments of p400 expressed robustly (lane 5 and 6 respectively in the α-FLAG panel) but also did not show any significant increase in H2AX phosphorylation upon their expression compared to the control in lane 1. The final three samples, SANT, F6 and TIP49 (lanes 7-9 respectively) all expressed well (see α-FLAG panel) but all failed to induce H2AX phosphorylation to any level above the control (lane 1). This is a representative figure from three repeats. In these repeats, the consistency and reproducibility of each sample to induce H2AX phosphorylation were variable.

3.3 Discussion

Cellular systems rely on a coordinated effort between a large number of factors in a number of pathways, often with crosstalk between the different pathways. DNA repair is one such system that requires effective recognition and signalling, often with proteins having more than one function within a pathway. This study focused on the activation of the ATM-TIP60 complex, particularly the ability of overexpressed TIP60 or the SANT domain of p400 to induce the double-strand break response in the absence of a DNA damaging agent. A previous study had suggested that overexpression of these two proteins caused an increase in H2AX phosphorylation in the absence of a DNA damaging agent (Smith, 2010), possibly due to sequestration of a negative regulator associated with the ATM/TIP60 complex.

TIP60 is intricately involved in the double-strand break response. A major role of TIP60 is acetylation of histone H2AX and H4 around break sites as well as acetylation of ATM which promotes ATM activation (Tsuyoshi Ikura et al., 2007; Rabih Murr et al., 2006; Sun et al., 2005). Additionally, TIP60 has been described as a haploinsufficient tumour suppressor where reduction in TIP60 levels are frequently seen in human head-and-neck and mammary carcinomas as well as in lymphomas (Gorrini et al., 2007). This decrease in TIP60 may result in inadequate activation of ATM and other TIP60-related functions. Consistent with a role as a haploinsufficient tumour suppressor,

overexpression of TIP60 leads to a preemptive activation of the double-strand break response with H2AX phosphorylation in the absence of a DNA damaging agent (Smith, 2010).

This study hypothesised that overexpression of TIP60 or a single domain of TIP60 could activate the ATM-TIP60 complex and promote activation of the DNA double-strand break response. Previous studies have shown that the zinc finger domain of TIP60 was responsible for facilitating protein-protein interactions (J.-W. Kim et al., 2008; M.-Y. Kim et al., 2007) while the chromodomain was responsible for facilitating the interaction between TIP60 and methylated histone H3K9 (Sun et al., 2009). Individual or two consecutive domains were cloned into a mammalian expression vector and their ability upon overexpression to induce H2AX phosphorylation was examined. Multiple attempts to examine the induction of H2AX phosphorylation upon overexpression of full length TIP60 or the TIP60 domains failed to produce any consistent results. The experiments were repeated upwards of 15 times and the H2AX phosphorylation level varied from experiment to experiment with the exception of doxorubicin induction which consistently showed an increase in H2AX phosphorylation. While this study and the one completed in 2010 were completed in HEK293T cells, the cells varied considerably in age and passage number and this may have resulted in different composition of proteins for the two experiments (Smith, 2010). It is possible that the induction observed in the previous study may have been an artefact of the cell type or the state the cell was in, therefore a number of different cell lines, including HeLa and U2OS were used in addition to HEK293T cells in an attempt to determine if the response may be cell type specific (data not shown). Again, the induction of H2AX phosphorylation varied upon repeats.

The previous study that showed TIP60 induced H2AX phosphorylation also showed an increase in H2AX phosphorylation with the overexpression of the SANT domain of p400 (Smith, 2010). Two hypotheses regarding how this was stimulated by the SANT domain were conceived. Firstly, the SANT domain may sequester or displace the putative negative regulator associated with the ATM-TIP60 complex and promote activation of this complex. The SANT domain of p400 has been shown to interact with TIP60 (Park et al., 2010) and when overexpressed may displace the putative negative regulator associated with the complex. Secondly, the SANT domain of p400 may bind to chromatin and induce a conformational change similar to that found in double-strand

breaks thus inducing ATM activation similar to an effect shown by chloroquine and HDAC inhibitors, methods known to alter the structure of chromatin (Bakkenist & Kastan, 2003). Interestingly, a study completed in 2009 described an increase in ATM phosphorylation and the induction of the DNA double-strand break response with the knockdown of p400 (L. Mattera et al., 2009). A follow up study in 2010 suggested the induction of the DNA damage response upon p400 knockdown was due to an increase in reactive oxygen species (C. Courilleau et al., 2010; Lise Mattera et al., 2010). In this study, the knockdown of p400 was repeated and no activation of the DNA damage response was seen (data not shown). A subsequent study illustrated the involvement of p400 in the stability of nucleosomes in response to DNA damage resulting in increased radiosensitivity and chromosome aberrations (Ye Xu et al., 2010). These two studies suggest that changes to chromatin structure through the loss of nucleosome stability may play a role in inducing the DNA double-strand break response supporting the hypothesis that SANT domain induced alterations in chromatin structure may induce the DNA double-strand break response.

The SANT domain structure is related to the Myb and Myb-like domains (Grune et al., 2003). These domains share a common helix-turn-helix motif which manifests as a three helix bundle. The third helix in these structures has been identified as the recognition helix, and mutations within this helix result in a decrease or loss of function of the motif (Barbaric et al., 2003; Boyer et al., 2002; Ogata et al., 1994; Sterner et al., 2002). In this study, mutations were introduced into each of the three helices of the SANT domain of p400 and used to examine the induction of H2AX phosphorylation upon overexpression. While all three helix deletion mutants were constructed and expressed, the ability to induce H2AX phosphorylation was inconsistent and not reproducible. Additionally, WT SANT domain overexpression also failed to induce H2AX phosphorylation. These experiments were completed upwards of 15 times in a number of cell lines including U2OS and HeLa cells to exclude the possibility that the effect from overexpression was a cell type specific effect. As mentioned previously, the two experiments were conducted over a year apart and even though the same cell line was used in both experiments, the age and passage number of the cells varied and this may have changed the composition of proteins within the cell lines. It is also possible that the H2AX phosphorylation seen in the previous study was simply an artefact.

While the overexpression of TIP60 or the SANT domain of p400 failed to induce the DNA double-strand break response in this study, the importance of these two proteins in DNA repair cannot be ignored. Alterations in the TIP60:p400 ratio have been implicated in the transformation of colorectal cells and a key factor in the expression of the cell cycle regulator p21. When the ratio was altered to increase TIP60 compared to p400, an increase in p21 expression was observed, and conversely a TIP60 knockdown resulted in decreased p21 expression (L. Mattera et al., 2009). Additionally, the SANT domain of p400 has previously been implicated in inhibiting TIP60 HAT activity (Park et al., 2010). The effect these two proteins have on each other during DNA repair may be a valuable area of research as they provide a potential target for novel cancer therapies. The inhibition of the HAT activity of TIP60 by the SANT domain may have an effect on histone H4 and H2AX acetylation and ATM acetylation, all of which are essential for effective DNA repair (T. Ikura et al., 2000; Tsuyoshi Ikura et al., 2007; R. Murr et al., 2006; Sun et al., 2005). The effect of altering the TIP60:p400 ratio subsequently affecting DNA repair may be due to this interaction between TIP60 and the SANT domain of p400. Investigation into this area may assist in understanding the regulation of DNA repair and may act as a platform for manipulation in cancer therapies.

4 A novel interaction between ATM and p400

4.1 An interaction between ATM and p400 in a mammalian system

4.1.1 Introduction

ATM (ataxia-telangiectasia mutated) is a member of the PIKK (phosphatidyl inositol 3' kinase-related kinase) family of proteins that include other members such as ATR (ataxia- and Rad3-related) and TRRAP (transformation/transcription domain-associated protein) (Shiloh, 2003). These proteins are implicated in cellular signalling and DNA repair. ATM and ATR have essential roles in DNA repair by phosphorylating H2AX around DNA break sites, by which H2AX acts as a marker molecule to assemble other repair proteins (Burma et al., 2001; Kinner, Wu, Staudt, & Iliakis, 2008; Stiff et al., 2004). TRRAP is the only member of the PIKK family that lacks a kinase activity. It is however, integral in DNA repair systems and cells lacking TRRAP show remarkably compromised DNA repair (R. Murr et al., 2006). The PIKK proteins generally require interactions with other proteins for activity. For instance, latent dimeric ATM is known to interact with the histone acetyl transferase, TIP60 (Sun et al., 2005). When DNA damage is detected by a yet undefined mechanism, TIP60 is known to acetylate ATM and promote monomerisation, in which monomerised ATM subsequently phosphorylations histone H2AX (Bakkenist & Kastan, 2003). TRRAP is a subunit of the multi-subunit complex known as the TIP60 complex which contains a number of proteins with different functions including helicases and acetylases (T. Ikura et al., 2000). TRRAP has previously been shown to immunoprecipitate with p400 (Fuchs et al., 2001). Interestingly, the members of the PIKK family have been shown to have modular domains, where if a domain within one member is swapped with the domain of another member, the chimeric protein retains its function (Jiang et al., 2006). TIP60 has been shown to interact with p400 in addition to its interaction with ATM. The TIP60-p400 interaction has shown to be facilitated primarily by the SANT domain of p400 and cause a robust inhibition of TIP60 histone acetylase activity (Park et al., 2010). The commonality of binding partners (TIP60) between ATM and p400, and the modular domain structure of PIKK proteins suggests that there may be an interaction between ATM and p400.

Co-immunoprecipitation is a useful tool to examine the interaction between proteins or within a larger protein complex. In this study, epitope tagged ATM and p400 were used to investigate the interation. FLAG-tagged full-length constructs of both ATM and p400 were provided by Dr Armin Gamper and Dr Jeong Park respectively. In order to facilitate examination of the interaction between the two proteins, HA epitope tagged variants of both ATM and p400 were also prepared in addition to the FLAG tagged constructs.

4.1.2 Cloning and expression of HA-ATM

ATM has a large cDNA of 9.1 kb which would increase the chance of PCR-induced errors when it is amplified as one large product. Therefore a small 1300 bp fragment that includes a FLAG tag was exchanged for one containing a HA tag to reduce the chance of PCR induced errors. Figure 4.1 shows the strategy employed for the production of the pcDNA-HA-ATM construct. The mammalian expression vector for FLAG-ATM that was provided at the beginning of this study was pcDNA-FLAG-ATM. This particular construct has several features that were utilised during the production of a HA tagged version. Firstly, there are two *Eco*RV sites found within the construct. The first is immediately 5' of the transcriptional start site and the second is 1300 bp within the ATM sequence. Secondly, this construct contains two *Kpn*I sites. The first is also immediately 5' of the transcriptional start site and the second is 4000 bp into the ATM sequence. A forward primer was designed that contained an *Eco*RV site followed immediately by a *Kpn*I site, the sequence for HA and finally the first 20 nt of the ATM sequence to produce a primer 70 nt in length. The reverse primer was designed with the *Eco*RV site 1300 bp into the sequence with an additional 20 nt of ATM 3' of the restriction site. These primers were designed to amplify the first 1300 nt of ATM with the inclusion of the new HA tag at the N terminus of the protein and an additional *Kpn*I site that will allow easy identification of correct clones. The PCR product was amplified using Roche FastStart Taq polymerase which is a high fidelity polymerase, minimising the possible errors introduced during PCR amplification. This polymerase is also a hot start polymerase which requires an initial heating step to become activated which allows the long forward primer to bind to the correct sequence and thus prevent secondary products from forming. The specific primer sequences and amplification program can be found in found in appendix 1.

Figure 4.1 Cloning strategy for HA-ATM. A 1300 bp insert (including 2 *Eco*RV sites, a *Kpn*I site and a HA sequence) was amplified and 3'A tailed. The insert was ligated into pGEM-T easy and the insert was released by *Eco*RV digestion. The pcDNA-FLAG-ATM plasmid was digested with *Eco*RV and the vector backbone was incubated together with the HA-insert from pGEM-T to create the full length pcDNA-HA-ATM construct. The vector backbone is represented by a single solid line while the open reading frame is represented by the open boxes.

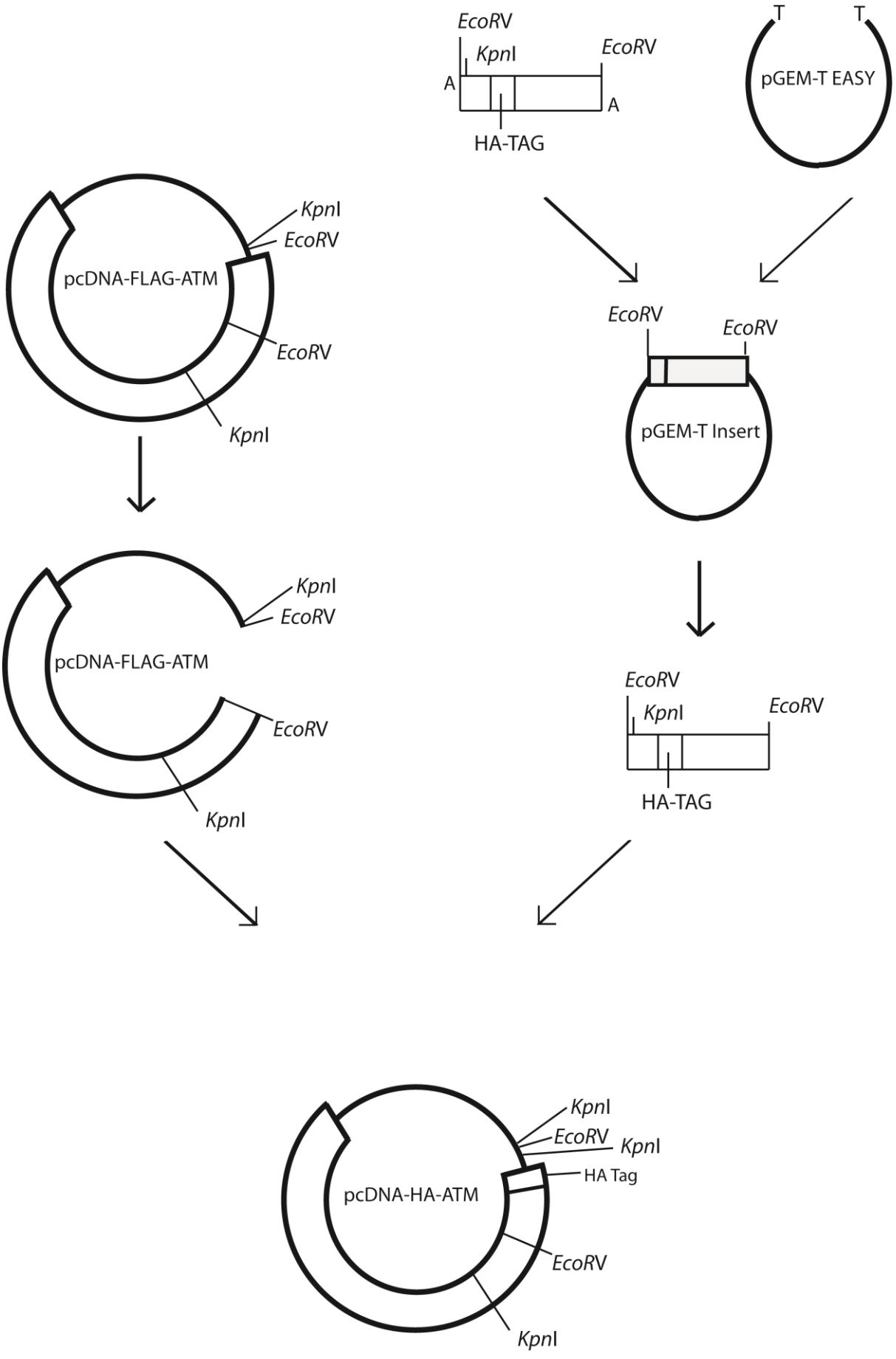
EcoRV
KpnI
EcoRV
A
A
HA-TAG
T
T
pGEM-T EASY
KpnI
EcoRV
pcDNA-FLAG-ATM
EcoRV
KpnI
EcoRV
EcoRV
pGEM-T Insert
KpnI
EcoRV
pcDNA-FLAG-ATM
EcoRV
KpnI
EcoRV
KpnI
EcoRV
HA-TAG
KpnI
EcoRV
KpnI
HA Tag
pcDNA-HA-ATM
EcoRV
KpnI

FastStart Taq polymerase was used to amplify the PCR product. This polymerase produces blunt-ended products which would be incompatible with cloning into the pGEM-T vector. Therefore the 1300 bp amplicon was adenylated (section 2.2.3) to allow ligation into the pGEM-T™ vector. Ligation of the insert and pGEM-T vector was carried out according to the manufacturer's instructions and *E.coli* DH5α were transformed according to section 2.2.10 then plated onto LB/Agar plates with ampicillin (50 µg/mL), X-gal (80 µg/mL) and IPTG (0.5 mM). Colonies were screened by blue-white selection and purified plasmid DNA was screened by digestion with *Eco*RV (section 2.2.10.2 and 2.2.6). Clones that showed the expected banding pattern were confirmed by Sanger sequencing (section 2.2.13). Figure 4.2 shows the digestion of 200 ng of empty pGEM-T (lane 1 and 3, undigested and digested respectively) and pGEM-ATM-insert (lane 2 and 4 undigested and digested respectively) with *Eco*RV. Lane 4 shows the presence of the 1.3 kb insert that is consistent with the production of the pGEM-ATM-insert clone. Sequencing of this construct confirmed the production of the pGEM-ATM-insert clone with no PCR induced errors.

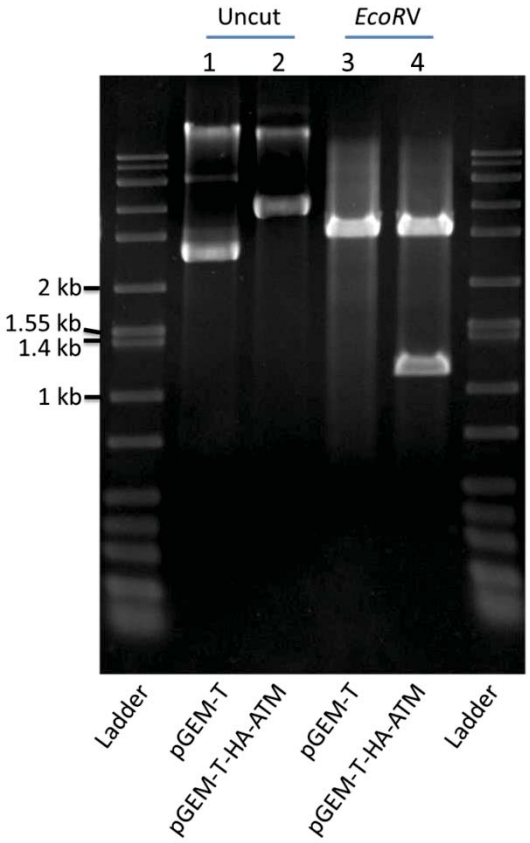

Figure 4.2 Identification of pGEM-HA-ATM. 200 ng of empty pGEM-T clones and pGEM-T-ATM-insert were digested with *Eco*RV. DNA was analysed on a 1% agarose gel in 1x TBE for 1 h at 150 V. L shows the DirectLoad™ ladder from Sigma while lane 1 and 2 show undigested empty pGEM-T and pGEM-HA-ATM, respectively. Lane 3 and 4 show empty pGEM-T and pGEM-HA-ATM, respectively digested with *Eco*RV. The gel was stained with ethidium bromide before being visualised under UV light.

Plasmid DNA from pGEM-ATM-insert and the pcDNA-FLAG-ATM vector were digested with *Eco*RV and the insert and backbone respectively were purified using agarose gel purification (section 2.25). The purified HA-tagged insert and the pcDNA backbone were used in a ligation reaction according to section 2.2.8 before *E.coli* DH5α were transformed with the ligation reaction (section 2.2.9). Potential clones were screened using *Kpn*I digestion. Clones that have the insert in the correct orientation should show two large bands of 11000 bp and 4000 bp and one small band of 40 bp while clones with the insert in the incorrect orientation will show a large 11000 bp band and two medium sized bands of 2855 bp and 1320 bp, upon *Kpn*I digestion. Clones that showed the expected banding pattern were also verified by Sanger sequencing (section 2.2.13).

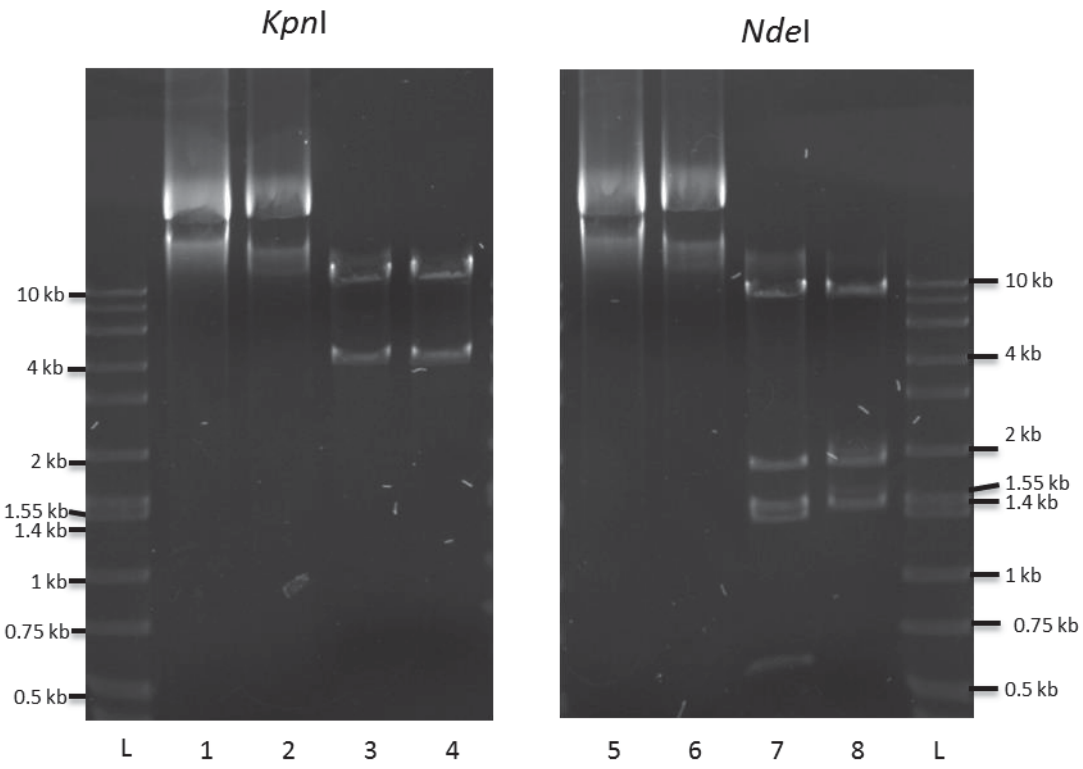

Figure 4.3 Restriction endonuclease digestion of pcDNA-FLAG-ATM and pcDNA-HA-ATM. Full length pcDNA-FLAG-ATM (200 ng) and pcDNA-HA-ATM (300 ng) were digested with *Kpn*I or *Nde*I, respectively. L shows the DirectLoad™ ladder from Sigma while lane 1 and 2 show undigested pcDNA-FLAG-ATM and pcDNA-HA-ATM respectively. Lane 3 and 4 show pcDNA-FLAG-ATM and pcDNA-HA-ATM respectively digested with *Kpn*I. Lane 5 and 6 show undigested pcDNA-FLAG-ATM and pcDNA-HA-ATM respectively while land 7 and 8 show pcDNA-FLAG-ATM and pcDNA-HA-ATM respectively digested with *Nco*I. DNA was resolved on a 1% agarose gel in TBE for 1 h at 150 V. The gel was stained with ethidium bromide before being visualised under UV light.

Figure 4.3 shows the digestion of full length pcDNA-FLAG-ATM and pcDNA-HA-ATM with *Kpn*I and *Nde*I to confirm the production of pcDNA-HA-ATM. Lane 1 and 2 shows undigested pcDNA-FLAG-ATM and pcDNA-HA-ATM respectively while lane 3 and 4 show pcDNA-FLAG-ATM and pcDNA-HA-ATM respectively digested with *Kpn*I. Both samples show the larger 11 kb fragment and the smaller 4 kb fragment. This suggests that the insert has been inserted in the correct orientation in the HA-ATM construct. An additional means of confirming production of pcDNA-HA-ATM is digestion with *Nde*I. Here, the FLAG-ATM construct will produce a unique 500 bp band that is absent from the HA-ATM construct. Lane 5 and 6 show undigested pcDNA-FLAG-ATM and pcDNA-HA-ATM respectively while lane 7 and 8 show pcDNA-FLAG-ATM and pcDNA-HA-ATM respectively digested with *Nde*I. The

presence of the 500 bp fragment in lane 7 that is absent in lane 8 confirms the production of pcDNA-HA-ATM.

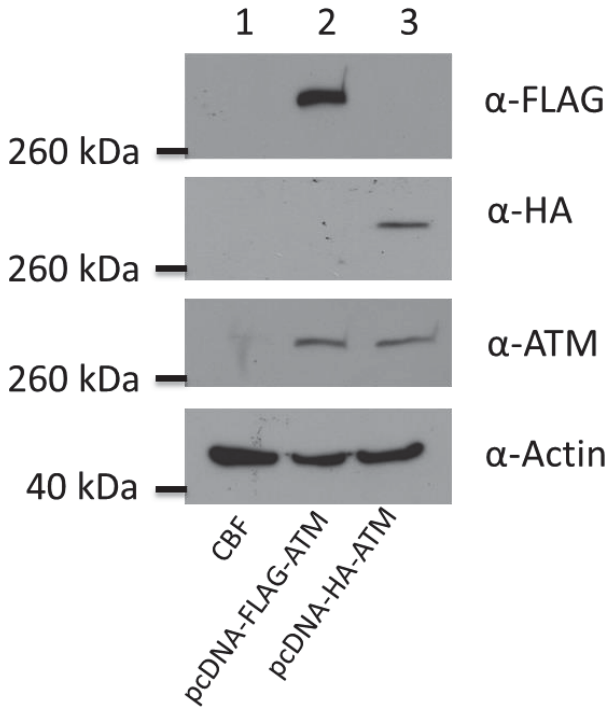

Figure 4.4 Expression of HA-ATM and FLAG-ATM. HEK293T cells that were 60% confluent were transfected with 1 µg of DNA with 4 µL of FuGENE™ HD. Cells were incubated for 48 hours and harvested for whole cell extract. 10% of the extracts were separated on a 5% polyacrylamide gel by SDS-PAGE for 1 h at 30 mA. Proteins were transferred to PVDF membrane by immunoblotting at 150 mA for 4 h. Samples were examined with α-HA, α-FLAG, α-ATM and α-actin antibodies. Lane 1: CBF empty vector, Lane 2: pcDNA-FLAG-ATM, Lane 3: pcDNA-HA-ATM.

The expression of HA-ATM from pcDNA-HA-ATM was examined in HEK293T cells. HEK293T cells were transfected with 1 µg of either pcDNA-HA-ATM or control pcDNA-FLAG-ATM. The cells were incubated for 48 h before being harvested for the preparation of whole cell extract in a volume of 200 µL. The whole cell extract (10 % v/v) was resolved by SDS-PAGE and examined by western blotting using antibodies raised against HA, FLAG, ATM and β-actin (Figure 4.4). Examination with α-FLAG and α-HA antibodies showed that both constructs were able to express the correct epitope tagged protein (see lane 2 α-FLAG panel and lane 3 α-HA panel). Examination with α-ATM antibody showed that there was approximately the same expression from both constructs and the amount of ATM produced was significantly more than endogenous levels (lane 1 compared to 2 and 3 in the α-ATM panel). The loading

control of α-actin showed approximately the same amount of protein had been loaded in each lane. Overall, the construction of pcDNA-HA-ATM was successful with the construct having approximately equal expression to the original expression vector pcDNA-FLAG-ATM.

4.1.3 Cloning and expression of HA-p400

Figure 4.5 shows the strategy employed for the production of the HA-p400 construct. The FLAG-tagged p400 construct that was provided at the beginning of this study was CBS-FLAG-p400. This has FLAG-p400 under the control of a constitutively active CMV promoter. Several features of this construct were exploited to generate the HA-tagged p400 construct. There is a single *Eco*RI site immediately 5' of the transcriptional start site as well as a single *Kpn*I site that is found at the 3' end of the coding sequence, after the transcription termination site. Additionally, there is a single *Fse*I site 700 bp downstream of the 5' end of the gene. The forward primer was designed to containe an *Eco*RI site followed immediately by a *Kpn*I site then the HA sequence and the initial 20 nt of the p400 coding sequence. The reverse primer contained a *Fse*I site and the 20 nt 5' of the *Fse*I site in the p400 sequence. The *Kpn*I site that was included in the forward primer should allow easy identification of positive clones. It also provided the Kozac sequence that promotes binding of the ribosome. The PCR product using these primers is 770 bp in length which will reduce the possibility of introducing PCR-induced errors. The PCR product was amplified using Roche FastStart polymerase (Appendix 1). The specific primer sequences and amplification program for HA-p400 can be found in appendix 1.

Figure 4.5 Cloning strategy for HA-p400. A 770 bp insert (including an *Eco*RI site, a *Kpn*I site and a HA sequence and a *Fse*I site) was amplified and adenylated to produce 3' A overhangs. The insert was ligated into pGEM-T easy and then released by *Eco*RI and *Fse*I digestion. The CBS-FLAG-p400 construct was digested with *Eco*RI and *Fse*I and the vector backbone was ligated to the HA-insert from pGEM-T to create the full length CBS-HA-p400 construct. The vector backbone is represented by a single solid line while the open reading frame is represented by the open boxes.

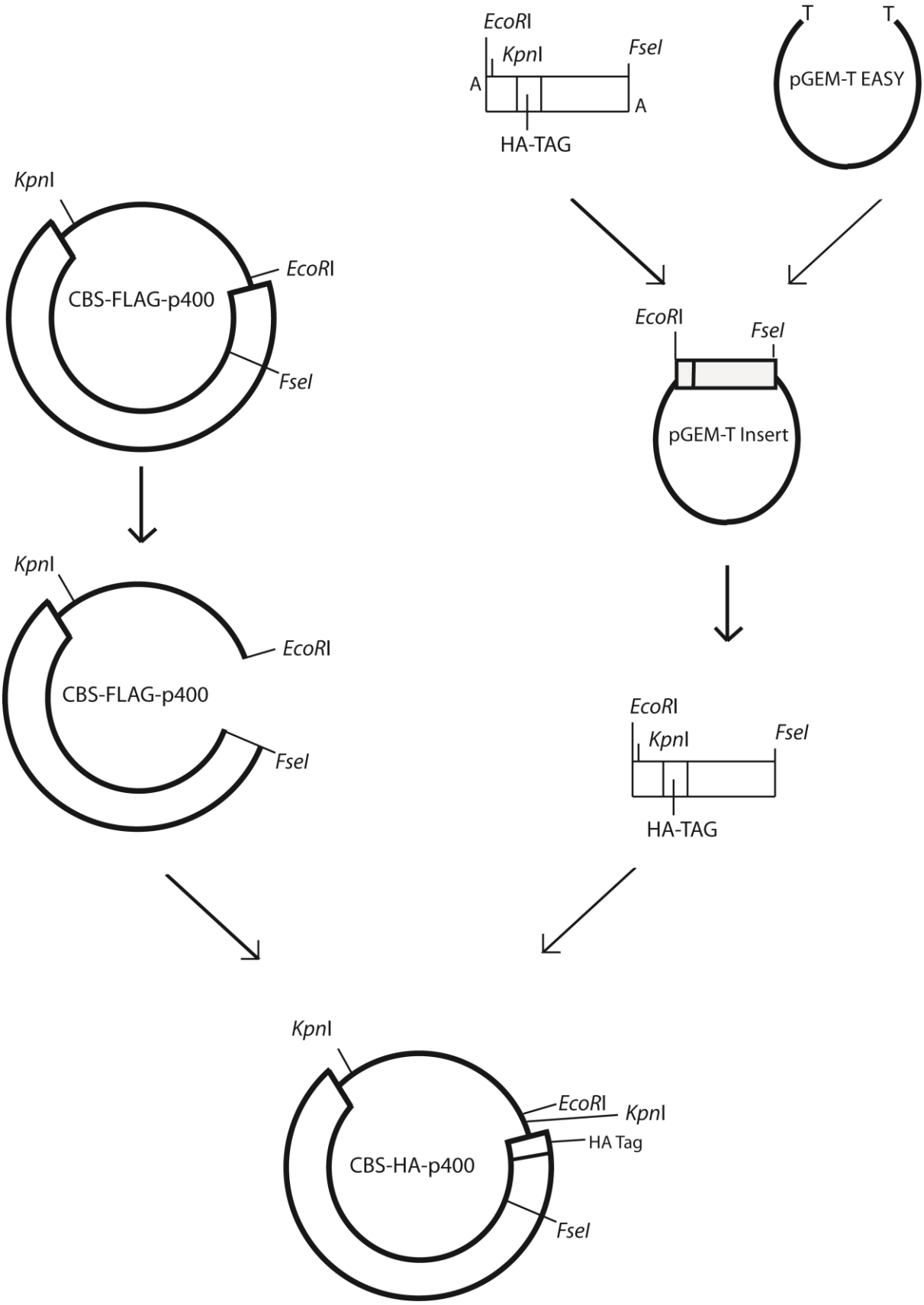
EcoRI
KpnI
FseI
A
A
HA-TAG
T
T
pGEM-T EASY
KpnI
EcoRI
CBS-FLAG-p400
FseI
EcoRI
FseI
pGEM-T Insert
KpnI
EcoRI
CBS-FLAG-p400
FseI
EcoRI
KpnI
FseI
HA-TAG
KpnI
EcoRI
KpnI
HA Tag
CBS-HA-p400
FseI

Amplified PCR products were adenylated using *Taq* polymerase (section 2.2.3) before being used for ligations into the pGEM-T easy vector. This is a linear vector with 5' T overhangs that adenylated PCR products can be ligated into. Ligations were carried out according to the manufacturer's instructions and used to transform *E.coli* DH5α. Cells were plated on LB/Agar plates with ampicillin (50 µg/mL), X-gal (80 µg/mL) and IPTG (0.5 mM) to allow for blue/white selection. Plasmids from white colonies were purified being examined by digestion with *Eco*RI and *Fse*I. Clones that showed the expected banding pattern were verified by Sanger sequencing (2.2.13). Of the 5 clones that were screened, all showed the correct digestion pattern with *Eco*RI and *Fse*I and Sanger sequencing confirmed all were the correct amplicon with no PCR-induced errors. Figure 4.6 shows the digestion of 200 ng of pGEM-T and pGEM-HA-p400 undigested (lane 1 and 2) and digested with *Eco*RI and *Fse*I (lane 3 and 4). The pGEM-HA-p400 plasmid shows the release of a 770 bp fragment with *Eco*RI and *Fse*I digestion (lane 4) while the empty vector does not (lane 3).

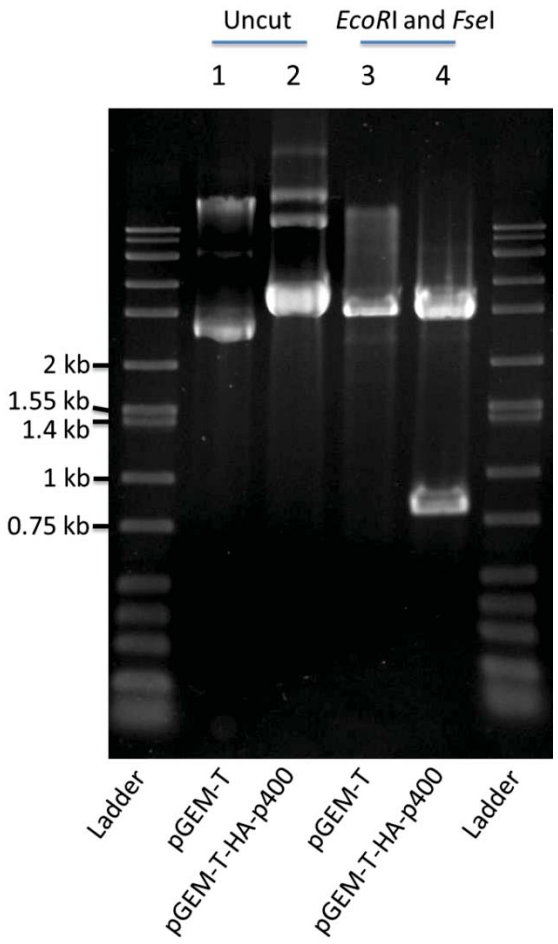

Figure 4.6 Identification of pGEM-HA-p400. 200 ng of empty pGEM-T clones (blue colony) and pGEM-HA-p400 (white colony) were digested with *Eco*RI and *Fse*I. Plasmid DNA was analysed on a 1% agarose gel in 1x TBE for 1 h at 150 V. L shows 1 kb+ ladder while lane 1 and 2 show undigested empty pGEM-T and pGEM-HA-p400 respectively. Lane 3 and 4 show empty pGEM-T and pGEM-HA-p400 respectively digested with *Eco*RI and *Fse*I. The gel was stained with ethidium bromide before being visualised under UV light.

pGEM-HA-p400 and CBS-FLAG-p400 were digested with *Eco*RI and *Fse*I to release the insert and prepare the backbone respectively (section 2.2.6) before being resolves on a 1% agarose gel in 0.5X TBE (2.2.4). The insert and backbone were purified by agarose gel purification (2.2.5) before being ligated together (section 2.2.8) to produce CBS-HA-p400. Potential clones were screened using *Kpn*I digestion. Clones that have the HA insert should show two large bands of 9597 bp and 4609 bp while CBS-FLAG-p400 will show one large band of 14206 bp. Additionally, digestion with *Nco*I should show bands of 5199 bp, 3662 bp, 1881 bp, 1558 bp, 815 bp, 435 bp and 54 bp in common between the FLAG and HA tagged constructs. In addition to these, each

construct had a unique band. CBS-HA-p400 had a unique band of 602 bp while CBS-FLAG-p400 construct has 562 bp and 31 bp bands unique to it upon *Nco*I digestion. Figure 4.7 shows the digestion of 200 ng of full length CBS-FLAG-p400 and CBS-HA-p400. Lane 1 and 2 show undigested CBS-FLAG-p400 and CBS-HA-p400 while lane 3 and 4 show CBS-FLAG-p400 and CBS-HA-p400 respectively digested with *Kpn*I. The double bands that are distinctive of CBS-HA-p400 can be clearly seen in lane 4 while the single band of CBS-FLAG-p400 can be seen in lane 3. Lane 5 and 6 again show undigested CBS-FLAG-p400 and CBS-HA-p400 respectively and lane 7 and 8 shows CBS-FLAG-p400 and CBS-HA-p400 respectively digested with *Nco*I. The CBS-HA-p400 was verified by Sanger sequencing (2.2.13) which confirmed the construct had been correctly made.

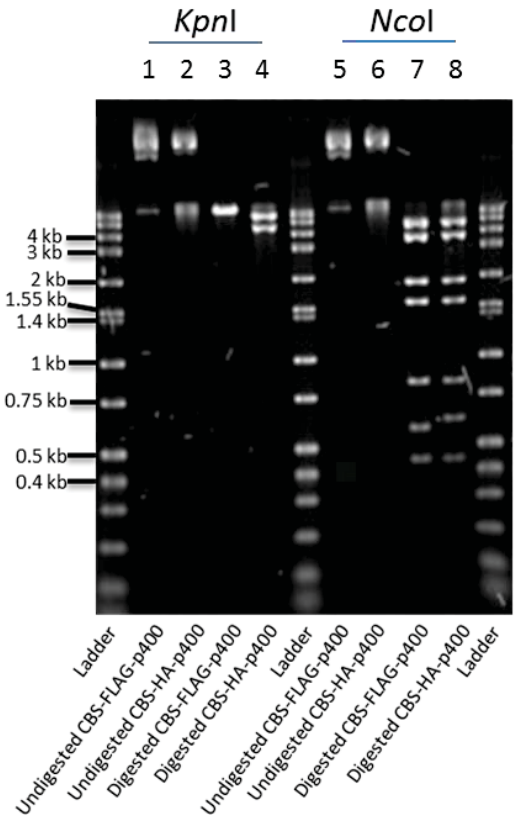

Figure 4.7 Digestion of FLAG-p400 and HA-p400. CBS-FLAG-p400 (200 ng) and CBS-HA-p400 (200 ng) was digested with *Nco*I or *Kpn*I. Undigested and digested plasmids were subjected to electrophoresis on a 1% agarose, 0.5x TBE gel at 100 V for 1 h. Samples were visualised using ethidium bromide under UV light. L: Ladder, 1: CBS-bsk-FLAG-p400 undigested, 2: CBS-HA-p400 undigested, 3: CBS-bsk-FLAG-p400 digested with *Kpn*I, 4: CBS -HA-p400 digested with *Kpn*I, 5: CBS-bsk-FLAG-p400 undigested, 6: CBS-HA-p400 undigested, 7: CBS-FLAG-p400 digested with *Nco*I, 8: CBS-HA-p400 digested with *Nco*I.

Expression of HA-p400 was confirmed by transfection of HEK293T cells with 1 µg of CBS-HA-p400 DNA or 1 µg control CBS-FLAG-p400 DNA. The cells were incubated for 48 h before being harvested for whole cell extract. Ten percent (v/v) of the prepared whole cell extract was examined by western blotting (section 2.3.2) using antibodies raised against HA, FLAG, p400 and α-Ku86 which was used as a loading control (Figure 4.8). Examination with α-FLAG and α-HA showed that both constructs were able to express the correct epitope tagged protein (see lane 2 α-FLAG for FLAG-ATM expression and lane 3 α-HA for HA-ATM expression). Examination with α-p400 showed that there was approximately the same expression from both constructs and the amount of p400 produced was significantly more than endogenous levels (lane 1 compared to 2 and 3). The loading control with α-Ku86 showed approximately the same amount of protein had been loaded in each lane. Overall, the construction of CBS-HA-p400 was successful with the construct having approximately equal expression to the original expression vector CBS-FLAG-p400.

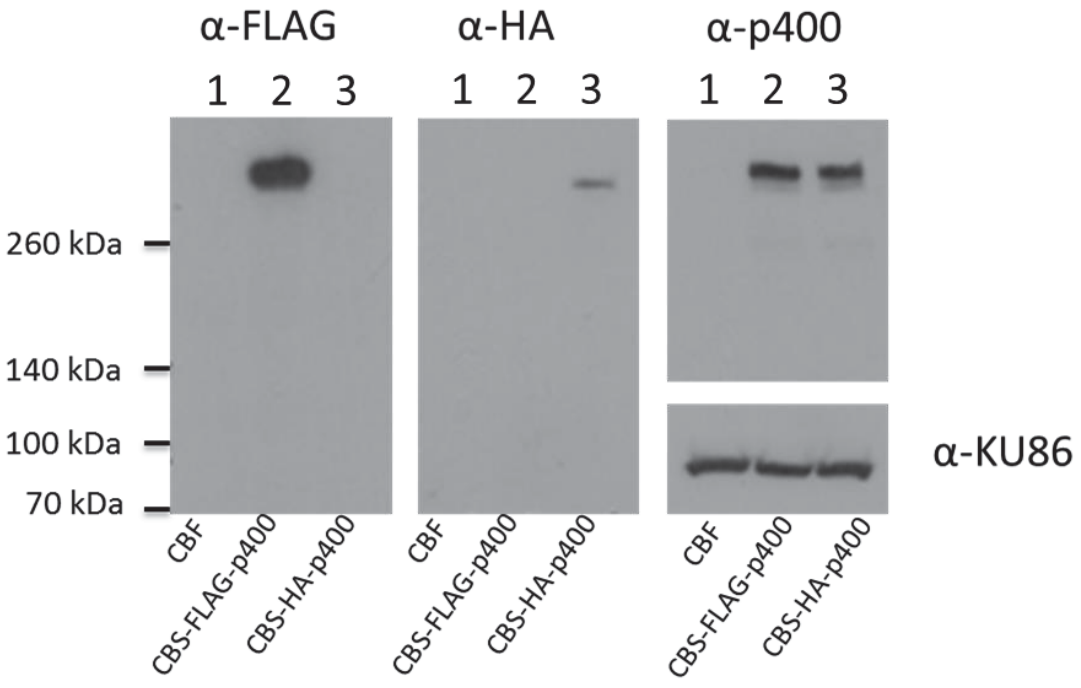

Figure 4.8 Expression of HA-p400 and FLAG-p400. HEK293T cells were transfected with 1 µg of DNA with 4 µL of FuGENE™ HD. Cells were incubated for 48 hours and harvested for whole cell extract. 10% (v/v) of the samples were separated on a 5% polyacrylamide gel by SDS-PAGE for 1 h at 30 mA. Proteins were transferred to PVDF membrane at 150 mA for 4 h. Samples were examined on an immunoblot with α-HA, α-FLAG, α-p400 and α-Ku86 antibodies. Lane 1: CBF empty vector, Lane 2: CBS-FLAG-p400, Lane 3: CBS-HA-p400.

4.1.4 Association between ATM and p400.

With the production of a HA-p400 expression construct, the interaction between ATM and p400 *in vivo* could be investigated through a co-immunoprecipitation assay. As interactions between ATM and TIP60 and TIP60 and p400 have previously been established, these were used as positive controls. HEK293T were transfected with pcDNA-FLAG-ATM (4 µg), CBS-HA-TIP60 (1 µg), CBF-TIP60 (1 µg), CBS-HA-p400 (4 µg) in various combinations and were incubated for 48 h before being lysed in 500 µL of whole cell extract (section 2.4.10) with 30 µL being kept as an input sample. The whole cell extract was subjected to immunoprecipitation using 15 µL of EziView HA-conjugated beads according to section 2.3.3. Input and immunoprecipitates were resolved on 5-10% two-step gradient polyacrylamide gels before being immunoblotted (section 2.3.1 and 2.3.2). As seen in Figure 4.9, the single FLAG-tagged proteins (FLAG-TIP60, lane 2 and FLAG-ATM, lane 4) were unable to be pulled down by the HA beads. The HA-tagged constructs (HA-TIP60, lane 3 and HA-p400, lane 5) were pulled down by the HA beads. This was expected and shows the specificity of the beads to pull down only HA-tagged proteins. In lane 6, HA-p400 was able to successfully pull down FLAG-TIP60, an interaction that has previously been confirmed. Additionally, in lane 7, HA-TIP60 was able to pull down FLAG-ATM, another previously characterised interaction. Interestingly, lane 8 shows that HA-p400 was able to pull down FLAG-ATM, an as yet uncharacterised interaction. The antibody that was conjugated to the beads used for the pull down can be seen in the two TIP60 panels in the immunoprecipitation blots.

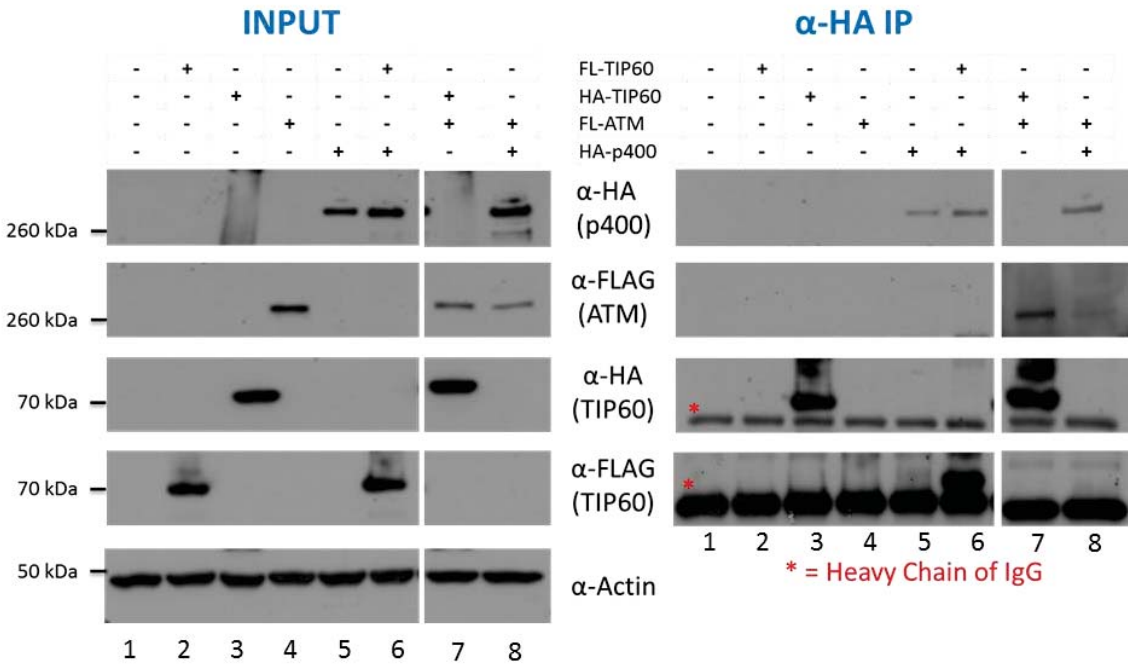

Figure 4.9 Co-immunoprecipitation between ATM and p400. HEK293T cells were transfected with pcDNA-FLAG-ATM (4 µg), CBS-HA-TIP60 (1 µg), CBF-TIP60 (1 µg), CBS-HA-p400 (4 µg) or with various combinations using FuGENE™ HD with a DNA: FuGENE ratio of 1:4. Both input and immunoprecipitation samples were separated on a 5-10% two step gradient SDS polyacrylamide gel that was electrophoresised at 30 mA for 1 h 15 min. The samples were transferred to a PVDF membrane at 150 mA for four hours. Both input and immunoprecipitation membranes were examined on an immunoblot using α-HA and α-FLAG antibodies while the input samples were also examined with α-actin antibody as a loading control to show relative loading. Lane 1: empty vector, Lane 2: FLAG-TIP60, Lane 3: HA-TIP60, Lane 4: FLAG-ATM, Lane 5: HA-p400, Lane 6: FLAG-TIP60 and HA-p400, Lane 7: HA-TIP60 and FLAG-ATM, Lane 8: FLAG-ATM and HA-p400.

The reciprocal interaction was attempted with ATM being used to pull down p400 however was unable to show the interaction (data not shown). It was speculated that it was due to the apparent weak interaction between p400 and ATM. Only a small amount of ATM was able to be pulled down with a significant amount of ATM (figure 4.9, lane 8). Therefore, the amount of p400 that could be pulled down with ATM may not be detectable by western blot. However, the reciprocal interaction is addressed later in the study (see figure 4.19).

The interaction observed between ATM and p400 in Figure 4.9 may be direct or indirect as p400 is a subunit of the larger TIP60 complex and ATM may be interacting with any other member of the TIP60 complex. Therefore, co-immunoprecipitation experiments between ATM and other subunits of the TIP60 complex were carried out in order to

show that the interaction between ATM and p400 is distinct. It is important to note that the proteins that were used for this co-immunoprecipitation experiment, BAF53 and GAS41, are integral members of the TIP60 complex and if pulled down, should co-purify the entire TIP60 complex along with them. HEK293T cells were transfected with pcDNA-FLAG-ATM (4 µg), CBS-HA-TIP60 (1 µg), CBS-HA-GAS41 (1 µg), CBS-HA-BAF53 (1 µg) in various combinations and incubated for 48 h before being subjected to whole cell extract preperation in a total volume of 500 µL with 30 µL being kept as an input sample. The whole cell extract was subjected to immunoprecipitation using 15 µL of α-HA antibody conjugated beads described in section 2.3.3. The input and immunoprecipitation samples were resolved on a 5-10% two step gradient gel and examined by western blotting (section 2.3.1 and 2.3.2) using α-HA and α-FLAG antibodies. Equal loading was confirmed using α-actin antibody.

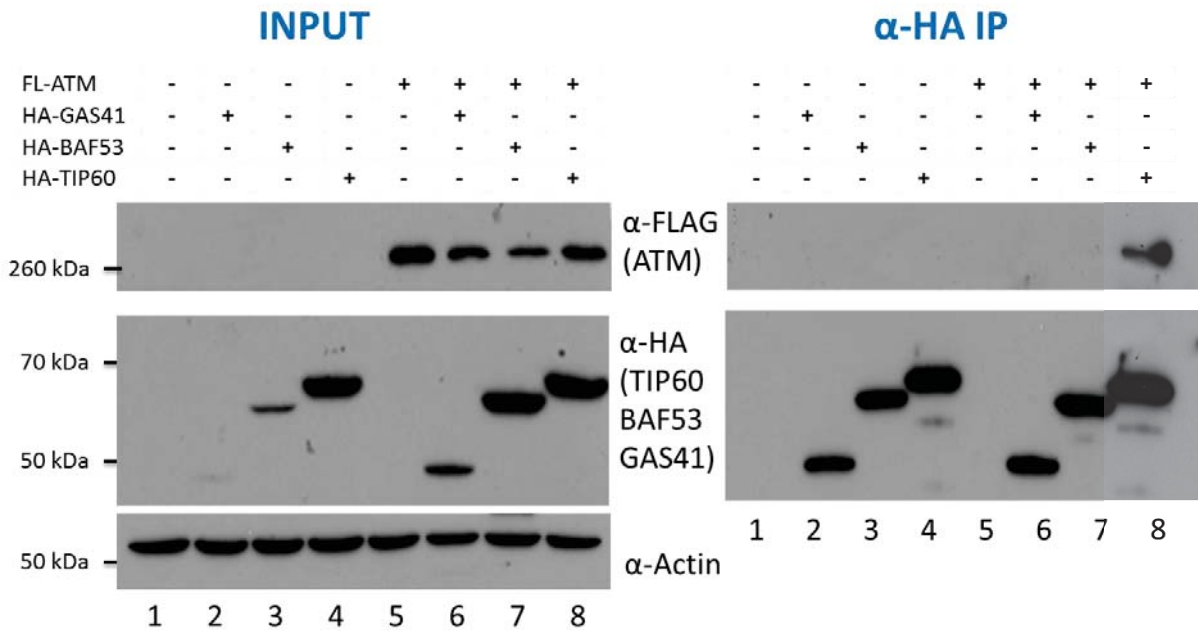

Figure 4.10 Interaction between ATM and members of the TIP60 complex. HEK293T cells were transfected with pcDNA-FLAG-ATM (4 µg), CBS-HA-TIP60 (1 µg), CBS-HA-GAS41 (1 µg), CBS-HA-BAF53 (1 µg) individually of with various combinations using FuGENE™ HD with a DNA: FuGENE ratio of 1:4. Both input and immunoprecipitation samples were separated on a 5-10% two step gradient SDS polyacrylamide gel that was electrophoresised at 30 mA for 1 h 15 min. The samples were transferred to a PVDF membrane at 150 mA for four hours. Both input and immunoprecipitation membranes were examined using α-HA and α-FLAG antibodies while the input samples were also examined with α-actin antibody to show relative loading. Lane 1: empty vector, Lane 2: HA-GAS41, Lane 3: HA-BAF53, Lane 4: HA-TIP60, Lane 5: FLAG-ATM, Lane 6: FLAG-ATM and HA-GAS41, Lane 7: FLAG-ATM and HA-BAF53, Lane 8: FLAG-ATM and HA-TIP60.

Each of the individually expressed HA-tagged constructs (TIP60, GAS41 and BAF53) show equal amount of pull down (Figure 4.10, α-HA IP panel, lanes 2-5) even though GAS41 and BAF53 appear to have slightly lower expression levels compared to TIP60 (see input lanes 2 and 3). This suggests that when incubated with the beads, the binding capacity of the beads becomes fully saturated. Again, FLAG-ATM is unable to bind to the HA beads by itself (IP panel lane 5). The control immunoprecipitation between ATM and TIP60 shows an interaction (IP panel lane 8) while the other two members of the TIP60 complex do not show the ability to pull down ATM (IP panel lane 6 and 7). This suggests that the interaction seen between ATM and p400 is not due to an interaction of ATM with the TIP60 complex but instead, a distinct interaction between ATM and p400. The absence of ATM association with TIP60 complex members is not due to low ATM expression levels as there are relatively equal amounts of ATM seen in each input sample (see lane 6-8 input panel α-ATM)

ATM and p400 have both been associated with DNA repair (Berkovich, Monnat, & Kastan, 2007; Burma et al., 2001; Doyon & Cote, 2004). It is possible that the interaction may be dependent on DNA damage. To investigate this possibility, the interaction between ATM and p400 was examined in the presence of bleomycin, an inducer of DNA double-strand breaks. HEK293T cells that were 50% confluent were transfected in duplicate with pcDNA-FLAG-ATM (4 μg) alone or with CBS-HA-TIP60 (1 μg) or CBS-HA-p400 (4 μg) as above. Before harvesting, one plate of ATM alone, one of TIP60 together with ATM and one of p400 together with ATM were treated with bleomycin for 4 h. The cells were harvested for whole cell extract and subjected to immunoprecipitation with α-HA antibody conjugated beads. A 6% input sample was saved and the insoluble chromatin fraction was subjected to histone extraction (section 2.4.11). Immunoprecipitation was carried out according to section 2.3.3 before being resolved on a 5-10% two-step gradient gel (section 2.3.1) and transferred to a PVDF membrane (section 2.3.2). Histone samples were resolved on a 12% polyacrylamide gel and transferred to a PVDF membrane (section 2.3.1 and 2.3.2). Figure 4.11 shows the results of the immunoprecipitation. Input and immunoprecipitates were examined using α-HA and α-FLAG antibodies while the input sample was also examined with α-actin antibody as a loading control. The histone samples were also examined with α-H2AX-S139P antibody to investigate the induction of the DNA damage response total histone H2AX levels as a loading control.

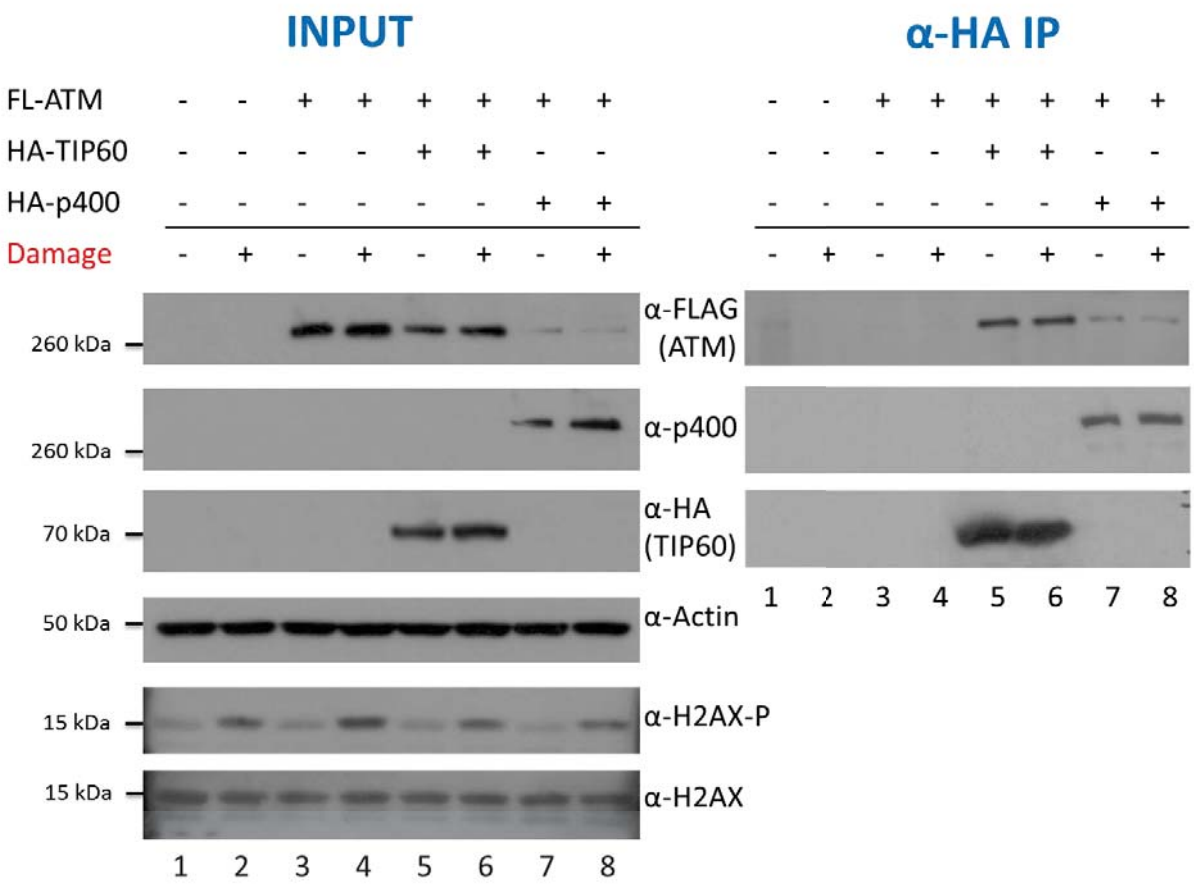

Figure 4.11 Co-immunoprecipitation between ATM and p400 in the presence and absence of DNA damage. HEK293T cells were transfected with pcDNA-FLAG-ATM (4 µg) alone or with CBS-HA-TIP60 (1 µg) or CBS-HA-p400 (4 µg) and incubated for 48 h. Cells were treated with bleomycin for 4 h before being harvested and whole cell extract subjected to immunoprecipitation. Samples were resolved on a 5-10% two step gradient gel for 1 h 15 min before being transferred to a PVDF membrane for four hours at 150 mA. Membranes were examined with α-HA and α-FLAG antibodies while the input samples were also examined with α-actin antibody to see equal loading. To examine the activity of bleomycin, histone samples were resolved on a 12 % acrylamide gel for 50 min at 30 mA before being transferred to a PVDF membrane for 2 h at 150 mA. The membranes were examined with α-H2AX and α-H2AX-S139P. Lane 1: empty vector, Lane 2: empty vector and bleomycin, Lane 3: FLAG-ATM, Lane 4: FLAG-ATM and bleomycin, Lane 5: FLAG-ATM and HA-TIP60, Lane 6: FLAG-ATM and HA-TIP60 and bleomycin, Lane 7: FLAG-ATM and HA-p400, Lane 8: FLAG-ATM and HA-p400 and bleomycin.

Each pair of samples shows an increase in H2AX phosphorylation in the presence of bleomycin, indicating that DNA double-strand breaks were induced and repair pathways were activated in bleomycin treated cells (Figure 4.11 compare lane 1 to 2, 3 to 4, 5 to 6 and 7 to 8). Additionally, each pair of samples ± bleomycin showed equal amounts of ATM and either p400 or TIP60 which allowed direct comparison between the two samples. The pull down of ATM together with TIP60 in the presence and absence of

DNA damage remained the same (compare lane 5 and 6). This is consistent with previously literature (Sun, Xu, Roy, & Price, 2007). Similarly, the pull down of ATM together with p400 remained equal in the presence and absence of DNA damage. As the interaction between ATM and p400 does not change in the presence of DNA damage, it suggests that the interaction is not affected by the activation of ATM or any potential posttranslational modifications that p400 may experience in the presence of DNA damage. This experiment used over expressed ATM and p400 and therefore it is possible that the system would not function in the same manner as an endogenous system. It remains to be determined whether the interaction between endogenous ATM and p400 occurs in a DNA damage-independent manner.

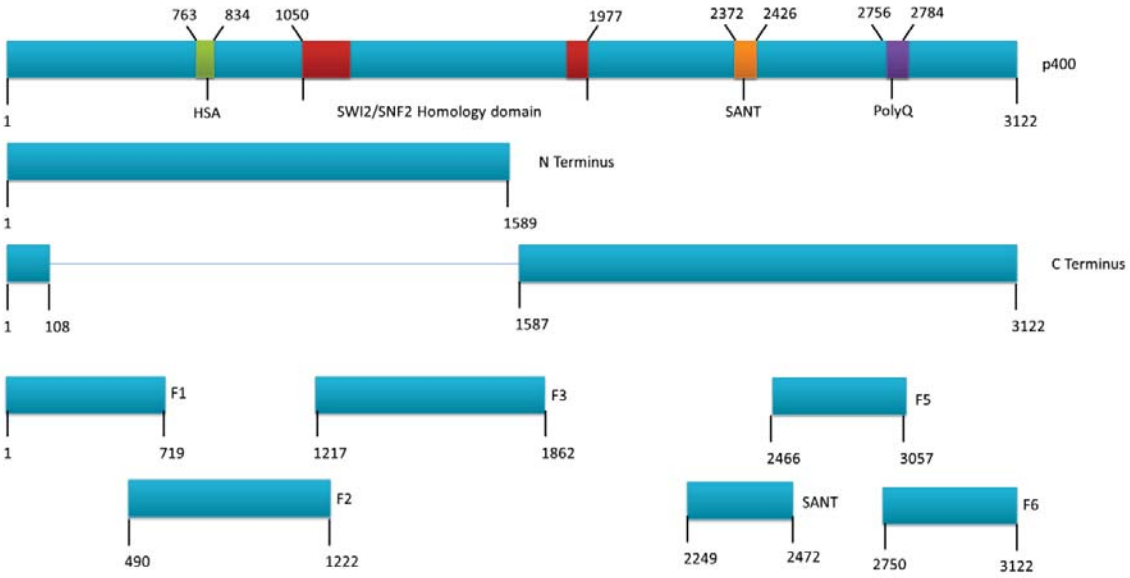

Figure 4.12 Schematic representation of full length p400 and derivatives used in this study. Full length p400 is 3122 amino acids in length. It contains several functional domains including the HSA domain (amino acid 763-834), the SWI2/SNF2 homology domain (amino acid 1050-1977) the SANT domain (amino acid 2372-2426) and the PolyQ domain (amino acid 2756-2784). Several constructs were provided from a previous study including the N-Terminus (amino acid 1-1589), the C-terminus (amino acid 1587-3122 with the first 101 amino acids at the N terminus), Fragment 1 (amino acid 1-719 of p400), Fragment 2 (amino acid 490-1222) and Fragment 3 (amino acid 1217-1862), Fragment 4 (SANT) (amino acid 2249-2472), Fragment 5 (amino acid 2466-3057) and Fragment 6 (amino acid 2750-3122). All p400 derivatives are FLAG-tagged in the mammalian expression vector CBF.

The interaction between ATM and p400 was investigated in further detail. Two constructs were provided by Dr Jeong Park which express FLAG tagged N terminus of p400, residues 1-1589, or FLAG tagged C terminus of p400, residue 1587-3122 containing a short N-terminal p400 fragment. A schematic representation of the p400

derivatives used in this study can be seen in Figure 4.12. HEK293T cells were transfected with pcDNA-HA-ATM (4 μg) and either CBS-FLAG-p400 (4 μg), CBS-FLAG-N-terminus (1.5 μg) or CBS-FLAG-C-terminus (1.5 μg) as described in section 2.4.3. Cells were incubated for 48 h before they were used to produce whole cell extract (section 2.4.10). Immunoprecipitation was carried out according to section 2.3.3 using 15 μL of α-FLAG antibody conjugated beads before samples were resolved on a 5-10% two-step gradient SDS polyacrylamide gel and immunoblotting (section 2.3.1 and 2.3.2). The blots were examined with antibodies raised against ATM and FLAG with β-actin used as a loading control and the results are shown in Figure 4.13. From the α-ATM panel, overexpressed ATM can be seen in lane 2, 4 and 5 with endogenous levels of ATM in lane 1 and 3. The expression of HA-ATM in lane 3 is not obvious since the level of total ATM is comparable to the endogenous level of ATM in lane 1. The FLAG tagged p400 (lane 3), and N and C termini of p400 (lane 4 and 5) all expressed to relatively similar amount. In the immunoprecipitation panel, the positive control of ATM being pulled down by p400 can be seen in lane 3. The amount of ATM that is pulled down is low, but this relates to the amount of ATM in the input. It is possible that HA-ATM did not express in this sample and the ATM that is pulled down would likely be endogenously expressed ATM. Interestingly, both N and C terminal fragments of p400 were able to pull down ATM, with the N terminus fragment (lane 4) precipitating a greater amount of ATM than the C terminus (lane 5). It is possible that ATM interacts with several regions of p400, or that the interaction between ATM and p400 is facilitated between residues 1-108 of p400 that were present in both N and C terminal constructs. The interaction of ATM with p400 was attempted to map using 6 fragments of p400.

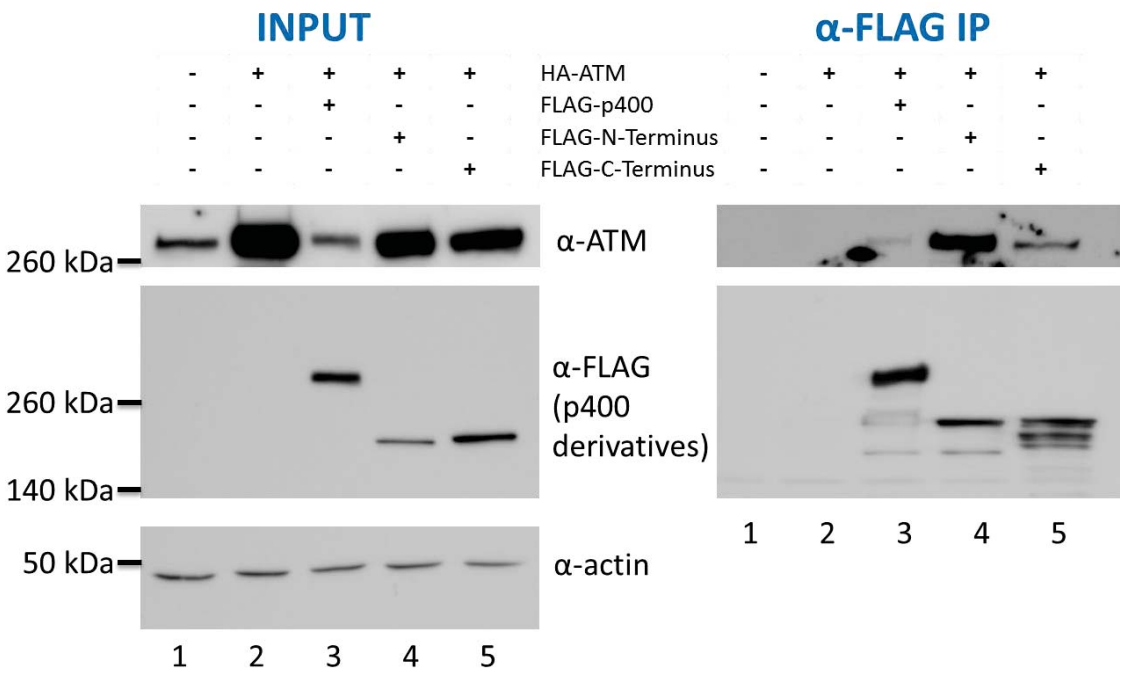

Figure 4.13 Co-immunoprecipitation between ATM and N and C terminus of p400. HEK293T cells were transfected with pcDNA-HA-ATM (4 µg) alone or with CBF-FLAG-p400 (4 µg) or CBF-N-Terminus (1.5 µg) or CBF-C Terminus (1.5 µg) with a DNA to FuGENE ratio of 1:4 and incubated for 48 h before being harvested and whole cell extract subjected to immunoprecipitation. Samples were resolved on a 5-10% two step gradient gel for 1 h 15 min before being transferred to a PVDF membrane for four hours at 150 mA. Membranes were examined with α-HA and α-FLAG antibodies while the input samples were also examined with α-actin antibody to see equal loading. Lane 1: empty vector, Lane 2: HA-ATM, Lane 3: HA-ATM and FLAG-p400, Lane 4: HA-ATM and FLAG-N-Terminus, Lane 5: HA-ATM and FLAG-C-Terminus.

To map the interaction of ATM to a region within p400, six FLAG-tagged fragments of p400 were provided by Dr Jeong Park (Figure 4.12) and were used in co-immunoprecipitation experiments with HA-ATM. HEK293T cells were transfected with pcDNA-HA-ATM (4 µg) alone or with CBS-FLAG-p400 (4 µg), CBS-FLAG-F1 (1 µg), CBS-FLAG-F2 (1 µg), CBS-FLAG-F3 (1 µg), CBS-FLAG-SANT (2249-2472) (2 µg), CBS-FLAG-F5 (2 µg) or CBS-FLAG-F6 (1 µg). Cells were incubated for 48 h before they were used to produce whole cell extract (section 2.4.10). Immunoprecipitation was carried out according to section 2.3.3 before samples were resolved on a 5-10% two-step gradient SDS polyacrylamide gel and immunoblotting (section 2.3.1 and 2.3.2). The blots were examined with antibodies raised against HA and FLAG and with β-actin antibody as a loading control.

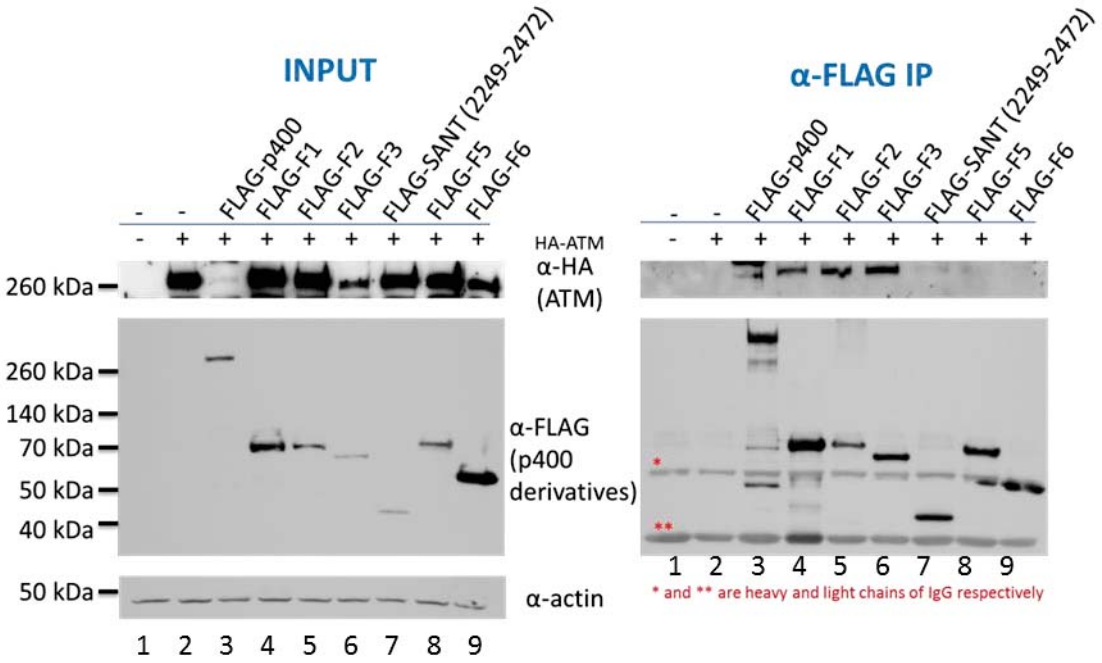

Figure 4.14 Co-immunoprecipitation between ATM and Fragment 1-6 of p400. A 100 mm plate of HEK293T cells were transfected with pcDNA-HA-ATM (4 µg) alone or with CBF-FLAG-p400 (4 µg) or CBF-F1 (1 µg), CBF-F2 (1 µg), CBF-F3 (1.5 µg), CBF-SANT (2249-2472) (1.5 µg), CBF-F5 (1 µg), CBF-F6 (1 µg) using a DNA to FuGENE ratio of 1:4 and incubated for 48 h before being harvested and whole cell extract subjected to immunoprecipitation. Samples were resolved on a 5-10% two step gradient gel for 1 h 15 min before being transferred to a PVDF membrane for four hours at 150 mA. Membranes were examined with α-HA and α-FLAG antibodies while the input samples were also examined with α-actin antibody to check equal loading. Lane 1: empty vector, Lane 2: HA-ATM, Lane 3: HA-ATM and FLAG-p400, Lane 4: HA-ATM and FLAG-F1, Lane 5: HA-ATM and FLAG-F2, Lane 6: HA-ATM and FLAG-F3, Lane 7: HA-ATM and FLAG-SANT (2249-2472), Lane 8: HA-ATM and FLAG-F5, Lane 9: HA-ATM and FLAG-F6.

Figure 4.14 shows the co-immunoprecipitation between HA-ATM and the FLAG tagged fragments of p400. The input shows that all FLAG-tagged p400 constructs expressed (see α-FLAG panel, lanes 3-9) and HA-ATM expressed in samples 2-9 (see input α-FLAG panel). The level of ATM in sample 3 was significantly lower than in the other samples as well and lane 5 also showed a slight reduction in ATM expression. When the immunoprecipitates were examined, the positive control of ATM and full length p400 (lane 3) showed ATM co-immunoprecipitating with p400. The amount of ATM pulled down is low but this reflects the poor expression of ATM seen in the input sample. Interestingly, ATM was able to co-immunoprecipitate with several fragments of p400 as seen in the α-FLAG IP panel lanes 4-8. There is a significant co-

immunoprecipitation of ATM with fragments 1, 2 and 3 of p400 which reflects the strong association of ATM with the N terminus of p400 in Figure 4.13. ATM was also able to co-immunoprecipitate with the SANT domain (2249-2472) which is fragment 4 of p400. This co-immunoprecpitation appears to be not as strong as fragments 1, 2 and 3 as only a small amount of ATM was pulled down. Fragment 5 showed an even lower amount of ATM co-immunoprecipitating and may not be a true interacting domain.

4.2 An interaction between ATM and p400 in a non-mammalian system.

4.2.1 Introduction

The interaction between ATM and p400 has been identified in HEK293T cells using overexpressed ATM and p400. While this is the first time such an interaction has been identified, it is complicated by the fact that a diverse range of interacting proteins are present in a mammalian cells and these may act as a bridge to associate instead of a bon a fide direct interaction between ATM and p400. To further support the existence of the interaction, further experiments were carried out in a non-mammalian system where there is less chance of other bridging proteins that allow the interaction between ATM and p400. The SF9 expression system was chosen to visualise the interaction. SF9 are an immortalised cell line established from the moth Spodoptera frugiperda. Overexpression of proteins is achieved by introducing baculovirus that has been engineered to express a protein of interest. Baculoviral constructs for HA-p400 were produced in this study while FLAG-ATM, HA-TIP60 and HA-RAR had previously been produced by Dr Jeong Park and Chris Burrows. All of these constructs were used to investigate an interaction between p400 and ATM in this heterologous system.

4.2.2 Subcloning HA-p400 into pFastBac1

The Bac-to-Bac® baculovirus expression system is an efficient way of cloning cDNA of interest for protein expression in SF9 cells. cDNAs can be cloned into the multiple cloning site (MSC) of the pFastBac1 vector which is flanked by transposition sequences. When *E.coli* DH10Bac are transformed with pFastBac1 plasmids, there is transposition of the cassette containing the coding region of interest from the pFastBac1 vector into a baculovirus shuttle vector (bacmid). The bacmid contains a LacZ gene that is interrupted when the cassette from pFastBac1 will be inserted into the bacmid. This allows for blue-white selection of colonies.

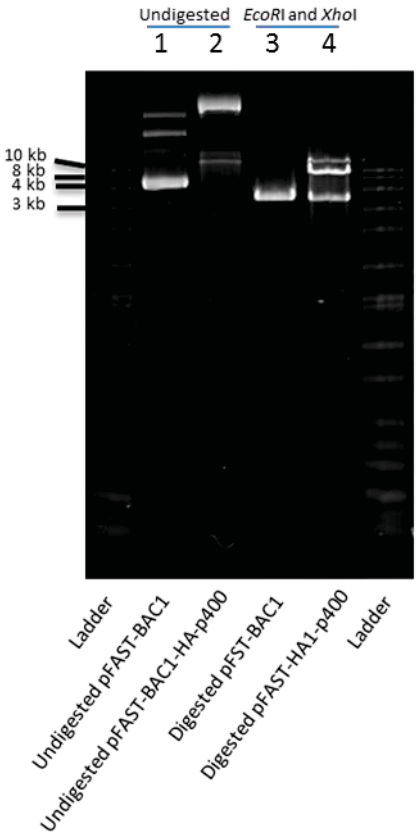

Figure 4.15 Subcloning HA-p400 into pFastBac1. pFastBac1 (200 ng) and pFastBac1-HA-p400 (200 ng) was digested with *Eco*RI or *Xho*I. Undigested and digested plasmids were subjected to electrophoresis on a 1% agarose in 0.5x TBE gel at 100 V for 1 h. Samples were visualised using ethidium bromide under UV light. L: Ladder, Lane 1: pFastBac1 undigested, Lane 2: pFastBac1-HA-p400 undigested, Lane 3: pFastBac1 digested, Lane 4: pFastBac1-HA-p400 digested.

Both CBS-HA-p400 and pFastBac1 were sequentially digested with *Eco*RI and *Xho*I as described in section 2.2.6 in order to sub-clone HA-p400 into pFastBac1. Neither *Eco*RI or *Xho*I cuts within the HA-p400 coding sequence but sites occur in the plasmid backbone of CBS-HA-p400 and within the MCS of pFastBac1. Digested HA-p400 insert and pFastBac1 vector backbone were purified by agarose gel electrophoresis and purification (section 2.2.4 and 2.2.5) before being used in a ligation reaction as described in section 2.2.8. *E.coli* DH5α were transformed with the ligation reaction and plated onto LB/agar plates containing ampicillin (50 µg/mL) as described in section 2.2.10. Colonies were screened for the inclusion of the insert by digestion with *Eco*RI and *Xho*I. Figure 4.15 shows digestion of pFastBac1 and pFastBac1-HA-p400 with *Eco*RI and *Xho*I. 200 ng of plasmid DNA was digested with *Eco*RI and *Xho*I according to section 2.2.6 before uncut (lane 1 and 2 for pFastBac1 and pFastBac1-HA-p400

respectively) or digested plasmid (lane 3 and 4 for pFastBac1 and pFastBac1-HA-p400 respectively) were separated on a 1% agarose gel (section 2.2.4). The pFastBac1-HA-p400 plasmid releases a band of 12 kb which is consistent with the size of the HA-p400 cDNA. The additional band seen in lane 4 is the vector backbone of pFastBac1. This can also be seen in lane 3.

E.coli DH10Bac were transformed with pFastBac1-HA-p400 plasmid DNA according to the manufacturer's instructions. Cells were grown on plates containing 50 µg/mL kanamycin, 7 µg/mL gentamycin, 10 µg/mL tetracycline, 40 µg/mL IPTG and 100 µg/mL X-gal to allow blue-white selection of bacmid containing colonies. Two white colonies were picked and grown in 5 mL of LB supplemented with 50 µg/mL kanamycin, 7 µg/mL gentamycin, 10 µg/mL tetracycline and the bacmid was prepared according to section 2.2.12. Purified Bacmid was used to transfect SF9 cells as described in section 2.2.12 and HA-p400 baculovirus was propagated to passage 3 (P3) according to sections 2.4.3 and 2.4.5.

4.2.3 Optimising expression of proteins from baculovirus

The SF9 expression system is robust and generally produces large quantities of protein. The downside to this is that there is also a large amount of degradation products which is more problematic in expression large proteins such as ATM or p400. A time course of expression was undertaken to maximise the amount of full length protein produced and minimise the amount of degradation products. In this study, three proteins were examined over a period of 72 h to visualise optimal expression of proteins.

To examine expression of HA-TIP60, SF9 cells were plated before being infected with 20 µL of P3 HA-TIP60 virus as described in section 2.4.6. Cells were incubated at 26^{o}C and harvested for whole cell extract with a total volume of 500 µL (section 2.4.10) every 12 hours between 36 and 72 h post infection. Samples (30 µL) were resolved on a 10% SDS polyacrylamide gel before being immunoblotted (section 2.3.1 and 2.3.2) or stained using Commassie blue as a loading control (section 2.3.5). Figure 4.16 shows the expression of HA-TIP60 over the 72 h time period. Lane 1 shows uninfected SF9 cells as a control that was harvested at the 72 h time point. Lane 2-5 represent the HA-TIP60 expression samples at 36 h, 48 h, 60 h and 72 h post infection respectively. A single band can be seen in the α-HA panel in lanes 3-5. This shows that HA-TIP60 peaks at 72 h post-infection but required a minimum of 48 h of infection to visualise

expression. The Coomassie blue stained gel was included as a loading control to show that each lane contained similar protein amounts.

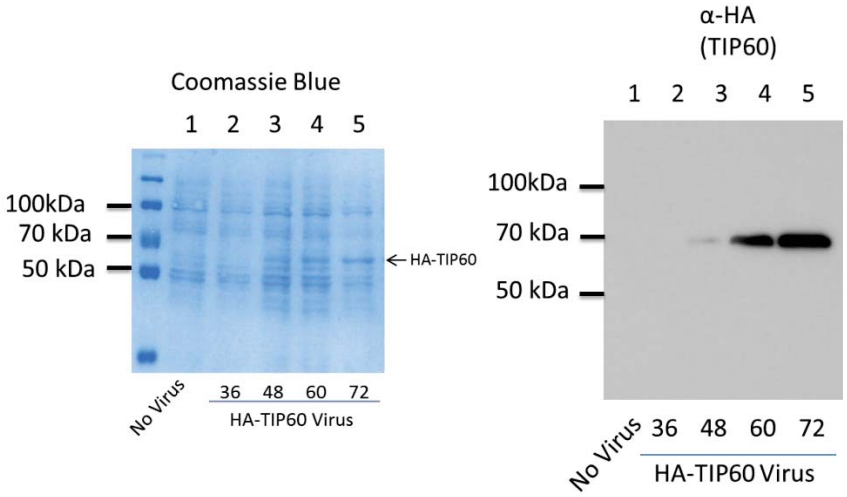

Figure 4.16 Time course of HA-TIP60 expression in SF9 cells. A 100 mm plate of SF9 cells that were plated at a density of $1x10^6$ cells/mL were infected with 20 µL of P3 HA-TIP60 virus or without virus (lane 1). Cells were incubated for 36, 48, 60 or 72 hours (lane 2-5 respectively) before being harvested for whole cell extract with a final volume of 500 µL. Samples (6% v/v) were resolved on a 10% SDS polyacrylamide gel for 1 h before being transferred to a PVDF membrane for two hours at 150 mA. Membranes were examined with α-HA to see HA-TIP60 expression while an additional gel was stained with Coomassie Blue to see equal loading. Lane 1: Non-infected SF9, Lane 2: HA-TIP60 36 h, Lane 3: HA-TIP60 48 h, Lane 4: HA-TIP60 60 h, Lane 5: HA-TIP60 72 h.

To examine the expression of FLAG-ATM SF9 cells were seeded before being infected with 0.5 mL of FLAG-ATM P3 virus as described in section 2.4.6. Cells were harvested to make whole cell extract (section 2.4.10) at 36 h, 48 h, 60 h, and 72 h with the uninfected sample harvested at 72 h. Samples were resolved on a 5% SDS polyacrylamide and either stained with Coomassie blue or used for western blotting (section 2.3.1, 2.3.2 and 2.3.5). Figure 4.17 shows the results of FLAG-ATM expression. Coomassie staining shows equal loading in each lane. The staining is quite light however bands can be seen around the 100 kDa mark. The α-FLAG panel shows the expression of a high molecular weight band above 260 kDa in lane 2-5 that represents FLAG-ATM. This band is absent in the non-infected control (lane 1). Expression of this large protein is optimal at 48 h and 60 h (lane 3 and 4) with lower levels seen at 36 h and 72 h (lane 2 and 5 respectively). There appears to be some level of degradation of FLAG-ATM at each time point.

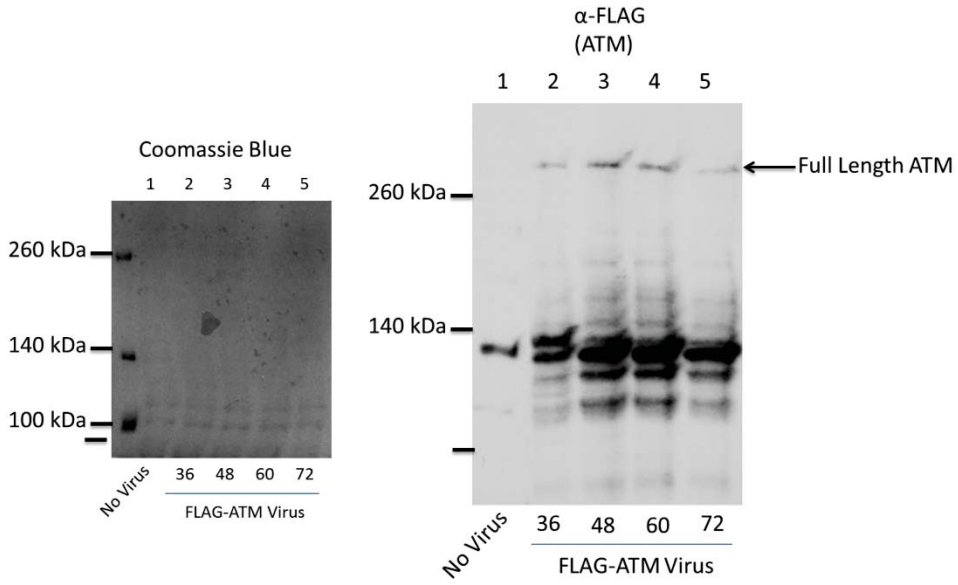

Figure 4.17 Time course of FLAG-ATM expression in SF9 cells. A 100 mm plate of SF9 cells that were plated at a density of $1x10^6$ cells/mL were infected with 20 µL of P3 FLAG-ATM virus or without virus (lane 1). Cells were incubated for 36, 48, 60 or 72 hours (lane 2-5 respectively) before being harvested for whole cell extract with a final volume of 500 µL. Samples (6% v/v) were resolved on a 5% SDS polyacrylamide gel for 1 h before being transferred to a PVDF membrane for four hours at 150 mA. Membranes were examined with α-FLAG to see FLAG-ATM expression while an additional gel was stained with Coomassie blue to confirm equal loading. Lane 1: Non-infected SF9, Lane 2: FLAG-ATM 36 h, Lane 3: FLAG-ATM 48 h, Lane 4: FLAG-ATM 60 h, Lane 5: FLAG-ATM 72 h.

To examine the expression of HA-p400, SF9 cells were seeded and infected with 1 mL of HA-p400 P3 virus per plate as described in section 2.4.6. Cells were harvested to make whole cell extract (section 2.4.10) at 24 h, 36 h, 48 h, 60 h, and 72 h with the uninfected sample harvested at 72 h. Samples were resolved on a 5% SDS polyacrylamide gel and either stained with Coomassie blue or used for immunoblotting (section 2.3.1, 2.3.2 and 2.3.5). Figure 4.17 shows the results of HA-p400 expression. Coomassie staining shows equal loading in each lane. p400 expression was examined using an antibody raised against p400 and can be seen in the α-p400 panel. There is little to no expression of p400 seen in lane 2, 3 or 6 which represent 24 h, 36 h and 72 h with significantly more p400 expressed in lanes 4 and 5 which represent 48 h and 60 h. There is a significant amount of degradation products seen in all lanes and a small amount of cross reacting protein which can be seen in lane 1 which is non-infected SF9 cells.

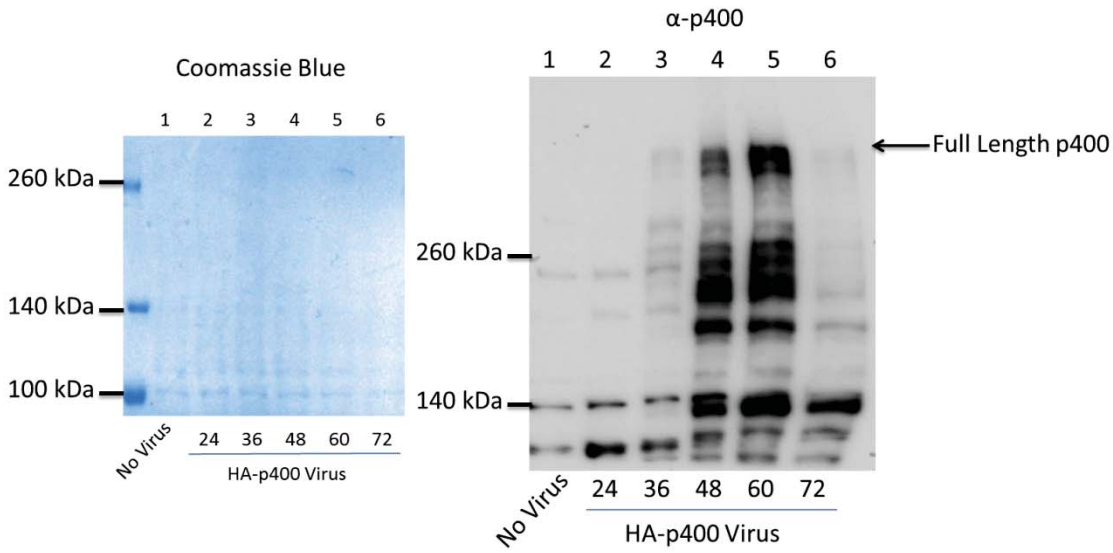

Figure 4.18 Time course of HA-p400 expression in SF9 cells. A 100 mm plate of SF9 cells that were plated at a density of $1x10^6$ cells/mL were infected with 20 µL of P3 HA-p400 virus or without virus (lane 1). Cells were incubated for 24, 36, 48, 60 or 72 h (lane 2-6 respectively) before being harvested for whole cell extract with a final volume of 500 µL. Samples (6% v/v) were resolved on a 5% SDS polyacrylamide gel for 1 h before being transferred to a PVDF membrane for four hours at 150 mA. Membranes were examined with α-HA antibody to see HA-p400 expression while an additional gel was stained with Coomassie blue to see equal loading. Lane 1: Non-infected SF9, Lane 2: HA-p400 24 h, Lane 3: HA-p400 36 h, Lane 4: HA-p400 48 h, Lane 5: HA-p400 60 h, Lane 6: HA-p400 72 h.

Overall, human recombinant proteins of HA-TIP60, FLAG-ATM and HA-p400 were all expressed in SF9 cells using the baculoviral system. The time points of 48 h and 60 h produced the highest level of expression for FLAG-ATM and HA-p400 with 48 h showing slight decreased levels for HA-TIP60 compared to 60 h. A significant protein degradation or truncated protein expression occurred regardless of time course in both FLAG-ATM and HA-p400. This was expected as they are significantly larger proteins compared to HA-TIP60 which did not exhibit any degradation products.

4.2.4 Examining the interaction between ATM and p400 in SF9 cells

The interaction between ATM and p400 has been identified by co-immunoprecipitation with proteins expressed in mammalian cells. To confirm this direct interaction it needs to be shown in a different system. Additionally, the co-immunoprecipitation in mammalian cells was only completed using a single type of antibody-conjugated beads as the reciprocal co-immunoprecipitation experiment failed to show an interaction (data not shown). Here, the interaction between ATM and p400 was investigated with reciprocal pull down experiments.

SF9 cells were plated at a density of $1x10^6$ cells/mL and allowed to adhere for 15 min before being infected with baculoviruses of HA-p400, FLAG-ATM, HA-TIP60, HA-RAR or a combination of these to investigate the interaction between ATM and p400. RAR was used as a negative control to show that the interaction seen between FLAG-ATM and HA-p400 was not dependent on the HA tag but rather on the interaction between the two proteins. RAR is a nuclear retinoic acid receptor that is expected not to interact with either ATM or p400. The cells were incubated for 48 h before being harvested to collect whole cell extract. The samples were split into two equal volumes and were subjected to immunoprecipitation using M2 agarose (for FLAG-tagged protein) or α-HA antibody conjugated beads. The samples were incubated overnight on an orbital rotator at 4^oC before being washed thoroughly with lysis buffer to remove any non-specific binding proteins. The samples were resolved on a 5-10% two-step gradient gel before being transferred to a PVDF membrane and examined with α-FLAG or α-HA antibody.

From the results shown in Figure 4.19, a reciprocal interaction between ATM and p400 has been established. The input panels show that protein is expressed in all appropriate lanes. The expression levels of p400 are relatively weak in the input panel (lanes 3 and 6). However the HA immunoprecipitation showed that HA-p400 was able to be pulled down in both samples indicating that HA-p400 was indeed expressed in these samples. The α-FLAG IP shows clearly that HA-p400 is able to precipitate with FLAG-ATM and that p400 is unable to be pulled down in the absence of FLAG-ATM (compare lane 3 with lane 6). Additionally, the positive control of FLAG-ATM interacting with HA-TIP60 can clearly be seen in lane 5. HA-TIP60 was unable to be pulled down in the absence of FLAG-ATM (see lane 2). The negative control of FLAG-ATM and HA-RAR (lane 8), was included to show that the interactions seen between ATM and p400 and ATM and TIP60 are specific and not due to an interaction between the HA and FLAG tags or any non-specific interaction. Additionally, HA-RAR was unable to bind to the α-FLAG antibody beads to be pulled down (lane 7). The reciprocal experiment using α-HA antibody conjugated beads showed complementary results to the α-FLAG IP. Here, HA-p400 was able to pull down FLAG-ATM (lane 6) while FLAG-ATM was unable to be pulled down by the α-HA antibody conjugated beads (lane 4). The positive control of HA-TIP60 interaction with FLAG-ATM can also be seen in lane 5. Additionally, the negative control of HA-RAR together with FLAG-ATM (lane 8)

failed to show ATM being pulled down by HA-RAR. HA-RAR was precipitated using α-HA beads (lane 7).

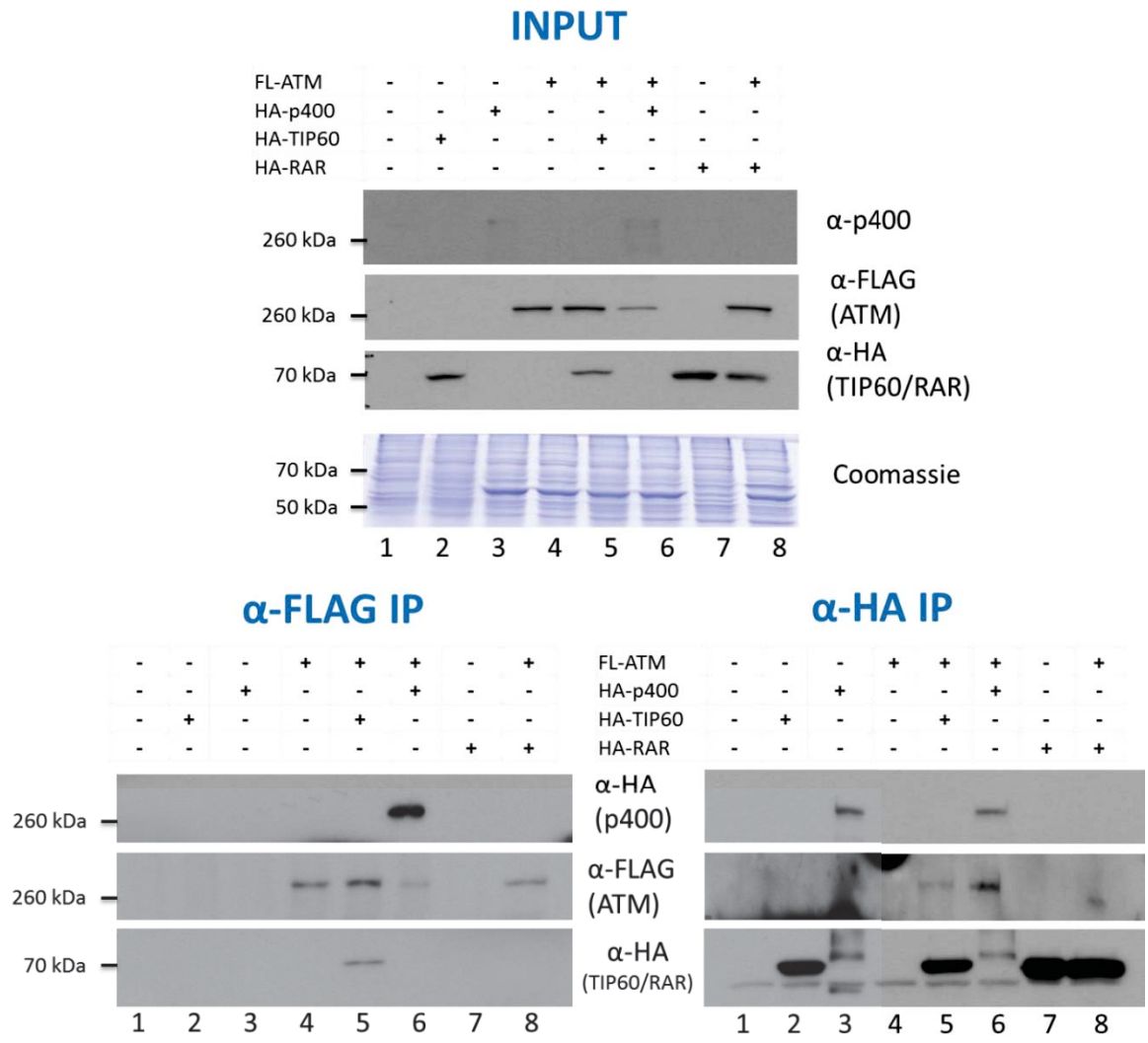

Figure 4.19 Co-immunoprecipitation between ATM and p400 in SF9 cells. Cells that were infected with a combination of FLAG-ATM, HA-p400, HA-TIP60 and HA-RAR baculovirus were incubated for 48 h before being subjected to whole cell extraction. Samples were immunoprecipitated with M2 agarose (α-FLAG) or with α-HA antibody conjugated beads. The samples were resolved on a 5-10% two-step gradient gel at 0.03 A for 1 h 15 min. Proteins were transferred to a PVDF membrane for 4 h at 150 mA before being examined using α-FLAG, α-HA or α-p400. Coomassie Blue stain was used for the input sample to show equal loading. . Lane 1: Non-infected SF9, Lane 2: HA-TIP60, Lane 3: HA-p400, Lane 4: FLAG-ATM, Lane 5: FLAG-ATM and HA-TIP60, Lane 6: FLAG-ATM and HA-p400, Lane 7: HA-RAR, Lane 8: FLAG-ATM and HA-RAR.

4.2.5 Localisation of FLAG-ATM and HA-p400 in SF9 cells

Confocal microscopy is a powerful technique that can be used to visualise the localisation of proteins within a cellular system. Here, FLAG-ATM and HA-p400 were

examined at different time points to determine their position with SF9 cells and if co-localisation could be seen. Here, SF9 cells were seeded onto coverslips as described in section 2.4.9 and infected with FLAG-ATM P3 virus, HA-p400 P3 virus or a combination of FLAG-ATM and HA-400 virus. Cells were stained according to section 2.4.9 and were imaged using a confocal microscope.

Figure 4.20 shows the localisation of FLAG-ATM 24 h, 36 h and 48 h post infection. FLAG-ATM, shown in red, is distributed throughout the cell in both nucleus and cytoplasm at each time point. There is staining that localises with DAPI, which stains DNA, indicating that there is ATM present in the nucleus of the cell. Additionally, a small amount of ATM staining appears in the cytoplasm surrounding the nucleus. Figure 4.21 shows the staining of HA-p400 24 h, 36 h and 48 h post infection. Here, p400 is shown in green and at 24 h stains throughout the cell in both the nucleus and cytoplasm. At 36 h and 48 h post infection, p400 is found solely in the cytoplasm. This is shown by a distinct lack of staining in the nuclear region in the α-p400 panel and there is no co-localisation of DAPI with HA-p400 staining. Interestingly, when the two proteins are co-expressed as in Figure 4.22, both proteins are initially expressed throughout the cell including the nucleus (Figure 4.22, 24 h panel). At the later time points, 36 h and 48 h, ATM is no longer localised in the nucleus and is completely sequestered in the cytoplasm with p400. This change in localisation supports the hypothesis that there is an interaction between ATM and p400 resulting in p400 binding to ATM, sequestering it in the cytoplasm. All experiments were repeated on three separate occasions and representative images from these are shown. For all time points, at least 30 cells were examined.

Figure 4.20 FLAG-ATM localisation in SF9 cells. SF9 cells were seeded on 22 x 22 mm coverslips at a density of $8x10^5$ cells/mL and infected with FLAG-ATM P3 virus. Cells were incubated for between 24 h and 48 h before being stained for imaging on the confocal microscope (section 2.4.9). FLAG-ATM is shown in red. DAPI was used to stain nuclei and is shown in blue. DIC was used to show the overall size and shape of the imaged cell. Images were taken at 630 x optical zoom with 6.5 x digital zoom.

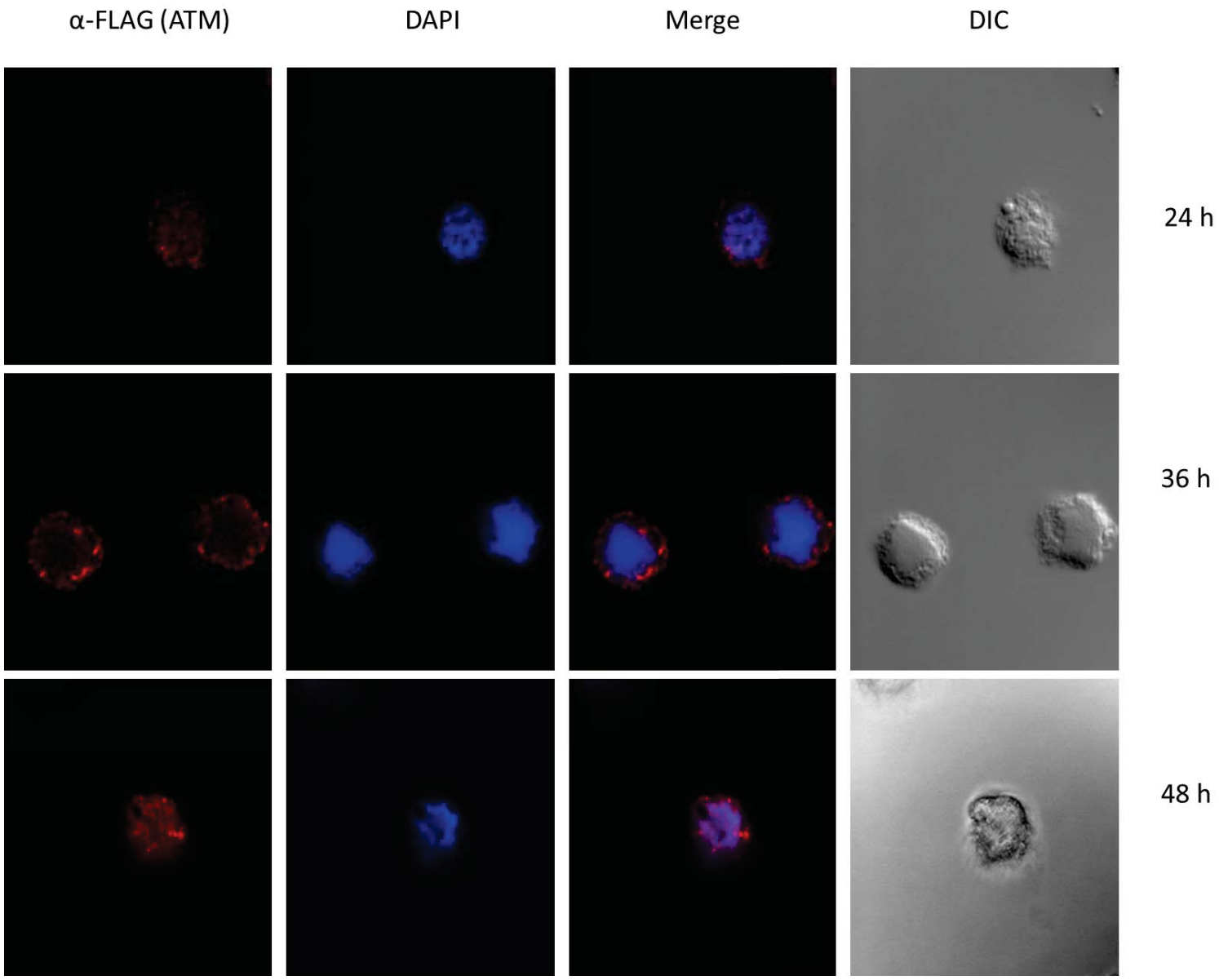
α-FLAG (ATM)
DAPI
Merge
DIC
24 h
36 h
48 h

Figure 4.21 HA-p400 localisation in SF9 cells. SF9 cells were seeded on 22 x 22 mm coverslips at a density of $8x10^5$ cells/mL and infected with HA-p400 P3 virus. Cells were incubated for between 24 h and 48 h before being stained for imaging on the confocal microscope (section 2.4.9). HA-p400 is shown in green. DAPI was used to stain nuclei and is shown in blue. DIC was used to show the overall size and shape of the imaged cell. Images were taken at 630 x optical zoom with 6.5 x digital zoom.

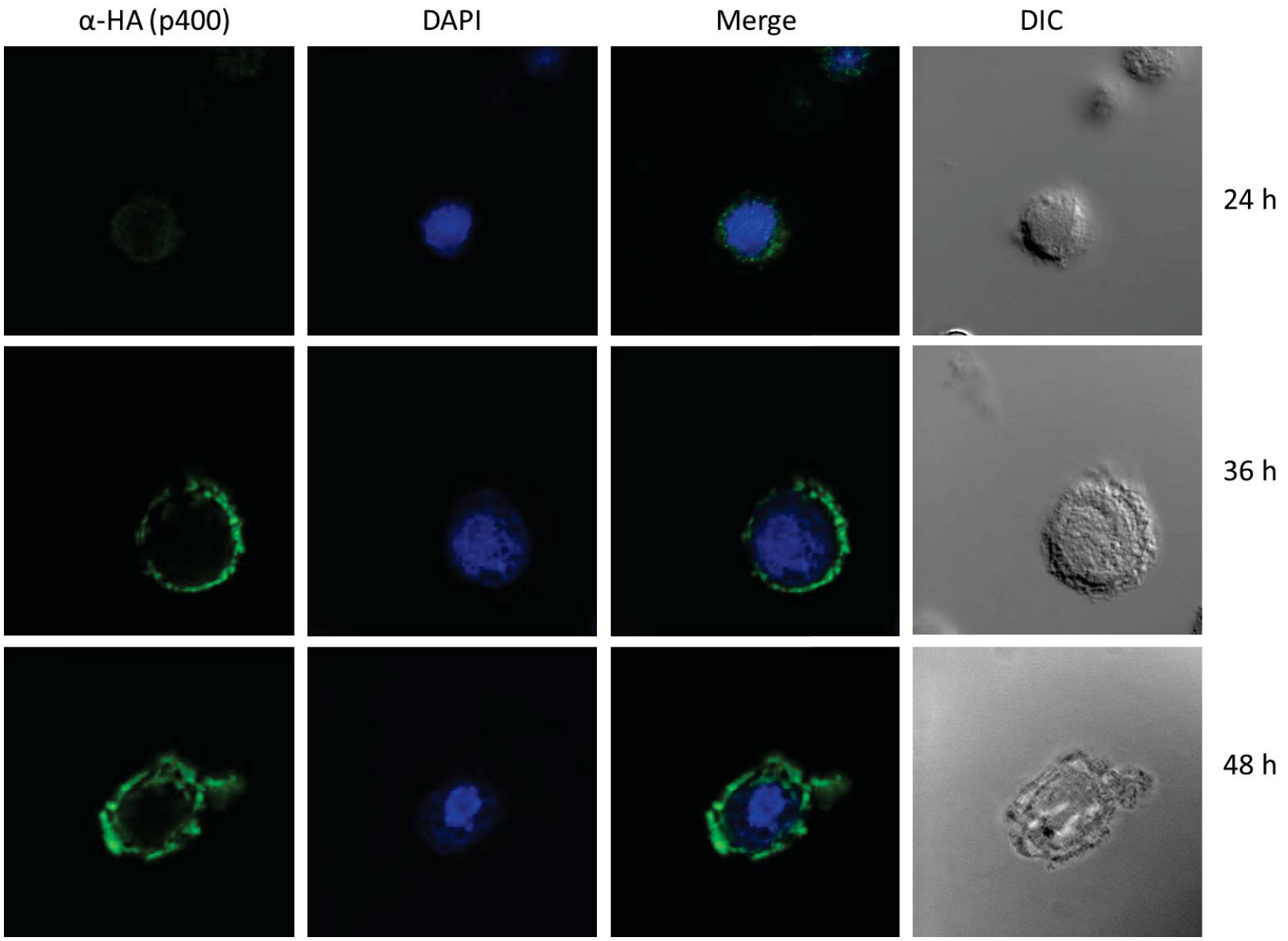
α-HA (p400)
DAPI
Merge
DIC
24 h
36 h
48 h

Figure 4.22 FLAG-ATM and HA-p400 localisation in SF9 cells. SF9 cells were seeded on 22 x 22 mm coverslips at a density of $8x10^5$ cells/mL and infected with FLAG-ATM and HA-p400 P3 virus. Cells were incubated for between 24 h and 48 h before being stained for imaging on the confocal microscope (section 2.4.9). FLAG-ATM is shown in red while HA-p400 is shown in green. DAPI was used to stain nuclei and is shown in blue. DIC was used to show the overall size and shape of the imaged cell. Images were taken at 630 x optical zoom with 6.5 x digital zoom.

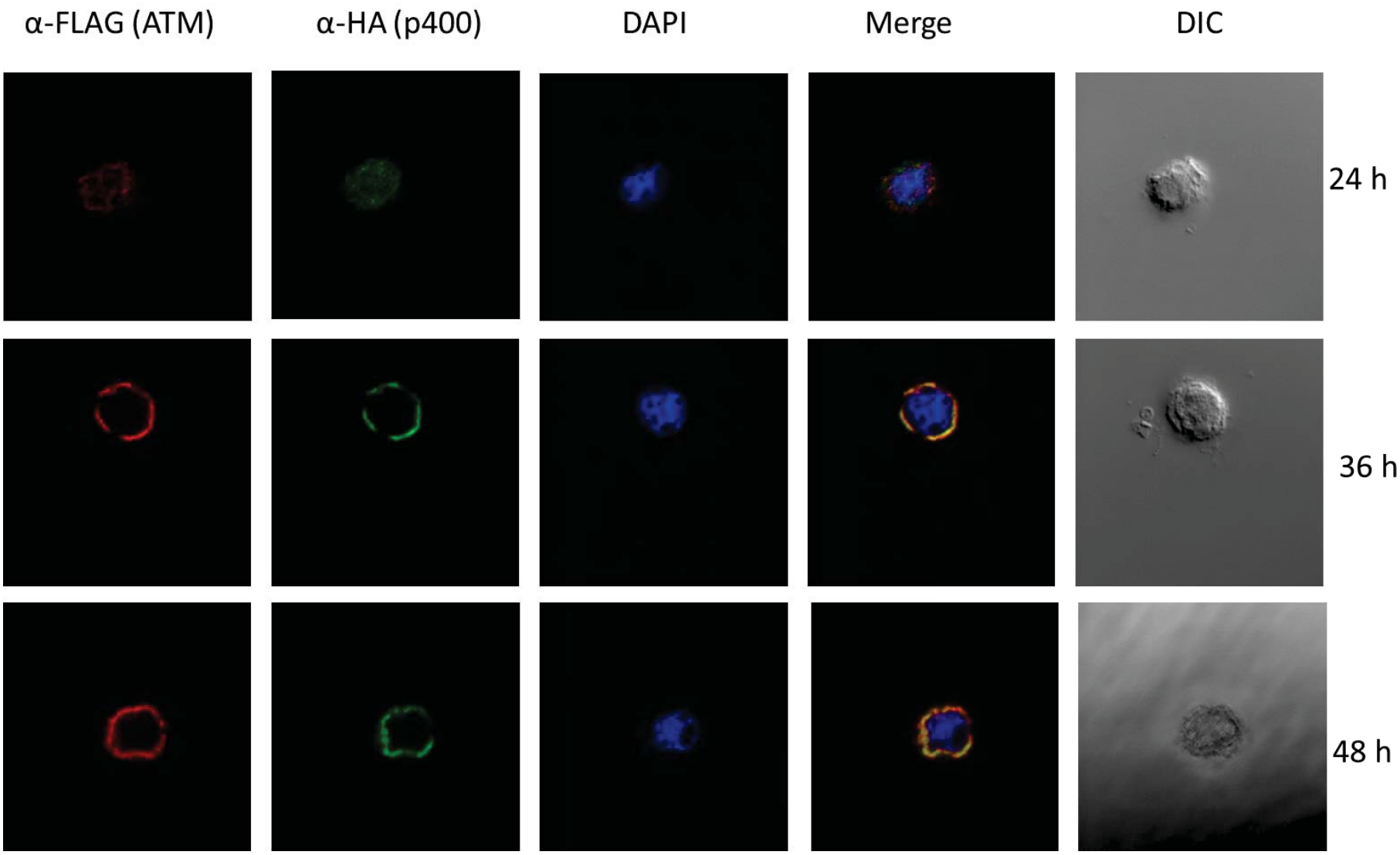
α-FLAG (ATM)
α-HA (p400)
DAPI
Merge
DIC
24 h
36 h
48 h

4.3 Functional analysis of the p400-ATM interaction

4.3.1 Introduction

The potential interaction between ATM and p400 has been established through several different methodologies including co-immunoprecipitation in mammalian cells and SF9 cells, as well as by colocalisation in SF9 cells by confocal microscopy. It is hypothesised that the interaction between ATM and p400 will be significant in regulating several functions of ATM and p400 within the cellular system. These include; p400 will alter the activity of ATM kinase in the presence or absence of DNA damage; ATM kinase will alter the activity of p400 chromatin exchange in the presence or absence of DNA damage; or finally, that the interaction between ATM and p400 is a means of bringing both proteins to the site of DNA damage. The kinase activity of ATM was assessed in the presence of DNA damage and in the presence of p400.

4.3.2 ATM kinase activity

To investigate the autophosphorylation of ATM in the presence and absence of DNA damage HEK293T cells were transfected with pcDNA-HA-ATM (4 µg) using and were incubated for 48 h before being harvested for whole cell extract (section 2.4.10). Prior to harvest, cells were treated with UV for 2 min and allowed to recover for 1 h. Samples were subjected to immunoprecipitation using α-HA antibody conjugated beads (2.3.3) and used in a kinase assay with [P^{33}] ATP as a phosphate source (section 2.3.4). Samples were resolved on a 5-10% two-step gradient SDS polyacrylamide gel and transferred to a membrane as in section 2.3.1 and 2.3.2. Phosphorylation of proteins was examined by X-ray film. Membranes were also examined for ATM expression using antibodies raised against HA.

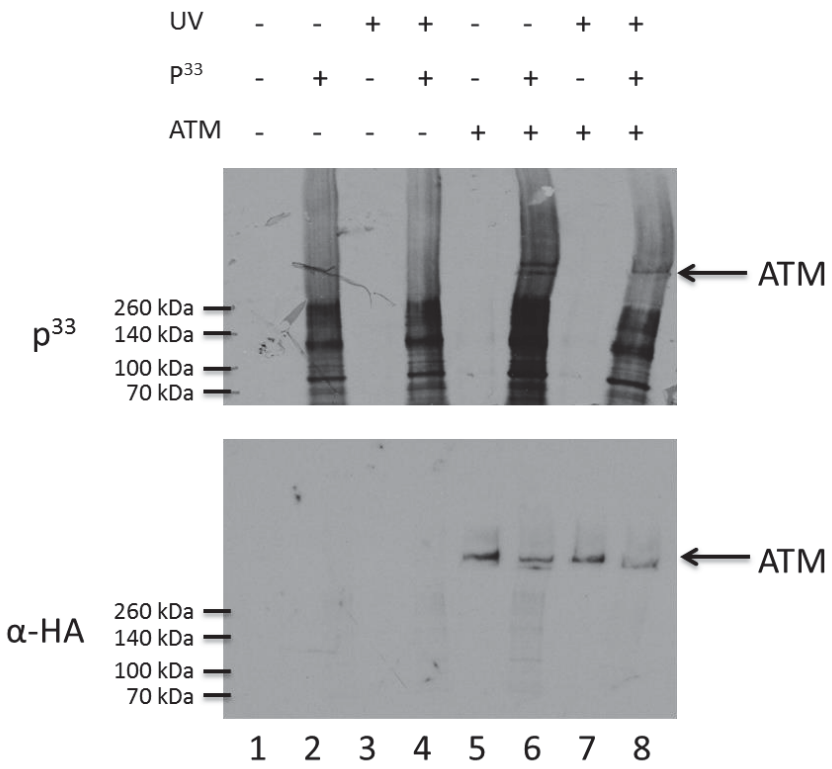

Figure 4.23 ATM autophosphorylation in the presence of UV induced DNA damage. HEK293T cells were transfected with ATM (4 µg) with FuGENE™ HD. Prior to harvest, samples were treated with UV for 2 min and left to recover for 60 min. Whole cell extract was made (2.4.10) and samples were subjected to immunoprecipitation with α-HA conjugated beads before being used in an autophosphorylation kinase assay (2.3.3 and 2.3.4). Samples were resolved on a 5-10% two-step gradient SDS polyacrylamide gel and resolved at 30 mA for 1 h 15 min. Samples were transferred to PVDF membrane at 150 mA for 4 h before being examined for phosphorylation and immunoblot using α-HA antibody. Lane 1 and 2: non-transfected 293T cells in the absence and presence of [P^{33}] ATP respectively, Lane 3 and 4: non-transfected 293T cells treated with UV in the absence and presence of [P^{33}] ATP respectively, Lane 5 and 6: immunoprecipitated ATM in absence and presence of [P^{33}] ATP respectively, Lane 7 and 8: immunoprecipitated ATM treated with UV in absence and presence of [P^{33}] ATP respectively.

Figure 4.23 shows the autophosphorylation of ATM in the presence and absence of UV induced DNA damage. Lane 1 and 2 shows non-transfected 293T cells in the absence and presence of [P^{33}] ATP respectively and lane 3 and 4 shows non-transfected 293T cells treated with UV in the absence and presence of [P33] ATP respectively. Lane 5 and 6 show immunoprecipitated ATM in absence and presence of [P^{33}] ATP respectively while lane 7 and 8 show immunoprecipitated ATM treated with UV in absence and presence of [P^{33}] ATP respectively. In the samples that have no [P^{33}] ATP in the reaction there is no background signal indicating that what is seen in the [P^{33}]

ATP samples occurred during the kinase reaction (Lane 1, 3, 5 and 7). Lane 2 and 4 which do not express ATM show some lower weight proteins are phosphorylated. This suggests that some non-specific kinases are pulled down and will phosphorylate proteins in the immunoprecipitated sample. There appears to be no difference between samples treated with UV compared to those that have not been treated. Lane 6 and 8 show some extra bands above the 260 kDa mark that represent HA-ATM. When examined with α-HA, bands of the same size are seen. The amount of HA-ATM in lane 5 -8 is relatively equal. The P^{33} panel shows ATM is phosphorylated in lanes 6 and 8 however, there is no way to distinguish whether the observed phosphorylation occurs by autophosphorylation or due to non-specific kinases pulled down in the reaction. There appears to be no increase in ATM phosphorylation in the presence of UV induced DNA damage. Additionally, an immunoblot of histone H2AX-P showed the increase in H2AX phosphorylation associated with DNA damage and ATM activation (data not shown).

Immunoprecipitated ATM or co-immunoprecipitated ATM/TIP60 or ATM/p400 were examined for autophosphorylation of ATM to investigate whether ATM can be activated in the absence of DNA damage by an interaction between ATM and p400. SF9 cells were plated in 100 mm plates at a density of $1x10^6$ cells/mL and allowed to adhere for 15 min before being infected with P3 HA-TIP60 virus (20 μL), P3 FLAG-ATM virus (0.5 mL) or P3 HA-p400 virus (1 mL) or a combination of the viruses. Cells were incubated for 48 h before being used to make whole cell extract (section 2.4.10). Whole cell extract was subjected to immunoprecipitation and then used for a kinase assay (section 2.3.3 ad 2.3.4).

Figure 4.24 shows the results of the kinase assay. The input samples show the expression of the proteins used in each sample. Lane 1 is a negative control. Lane 2, 3 and 4 show the single expression of HA-TIP60, HA-p400 and FLAG-ATM respectively while lane 5 shows the co-expression of HA-TIP60 and FLAG-ATM and lane 6 shows the co-expression of HA-p400 and FLAG-ATM. The IP panel shows the immunoprecipitation of proteins that was used in the kinase assay in the P^{33} panel below. Lane 1 is a kinase assay with no immunoprecipitated material to act as a negative control. Lane 2 and 3 show the kinase assay completed using immunoprecipitates with α-HA and α-FLAG beads with SF9 extract respectively. This was used because samples 4 and 5 were performed using α-HA beads to pull down HA-

TIP60 and HA-p400 while lanes 6-8 use α-FLAG beads to pull down FLAG-ATM and its co-immunoprecipitation partners HA-TIP60 and HA-p400. The IP panel successfully shows the immunoprecipitation and co-immunoprecipitation of all proteins. p400 in lane 5 appears as a large smear however, a bulge can be seen at the same place as p400 in lane 8 showing that p400 was precipitated in this sample. The large smear may have occurred from precipitation of a large amount of cross reacting proteins. When looking at the P^{33} panel, there appears to be no phosphorylation of ATM in any of the samples (lane 6-8) however, p400 appears to be heavily phosphorylated in lane 5. This likely comes from non-specific kinases immunoprecipitated in the samples. The amount of p400 immunoprecipitated in lane 8 compared to lane 5 is very low, therefore it is unlikely that any phosphorylation of p400 would be seen in this sample. ATM failed to become phosphorylated in this assay possibly because ATM expressed in SF9 cells may not be active due to incorrect folding or incorrect signalling for activation.

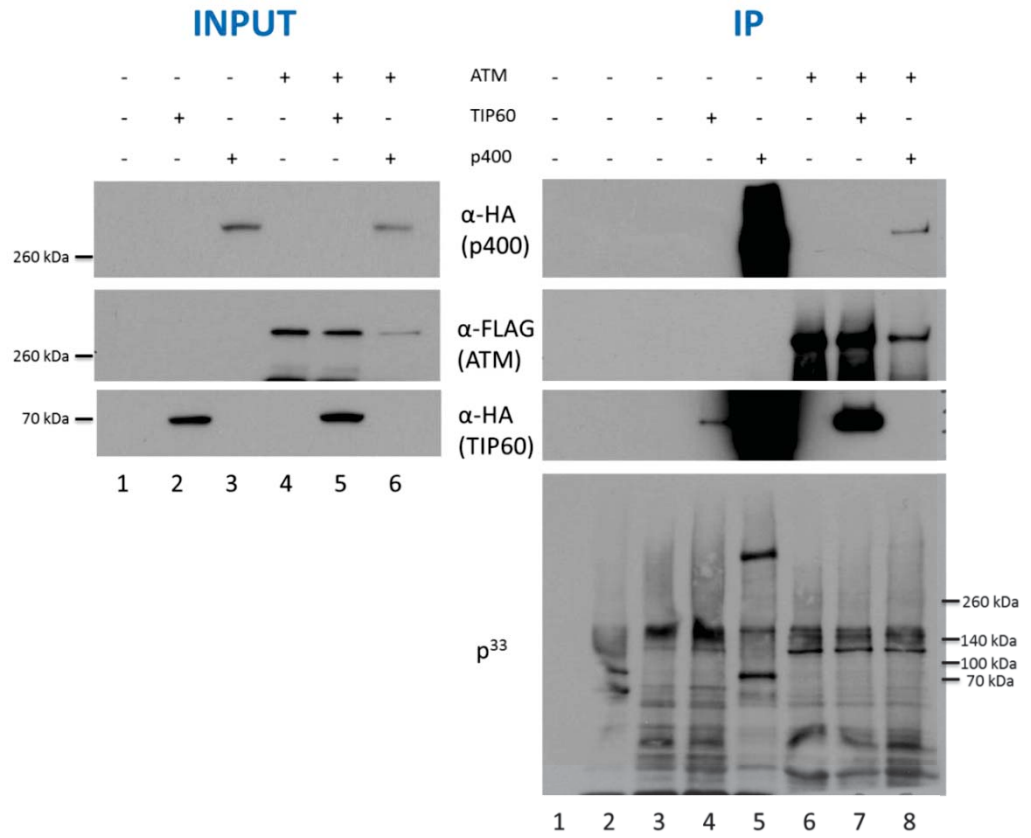

Figure 4.24 Autophosphorylation of recombinant ATM expressed in SF9 cells. SF9 cells were plated in 100 mm plates at a density of $1x10^6$ cells/mL and allowed to adhere for 15 min before being infected with P3 HA-TIP60 virus (20 µL), P3 FLAG-ATM virus (0.5 mL) or P3 HA-p400 virus (1 mL) or a combination of the viruses. Cells were incubated for 48 h before being used to make whole cell extract (section 2.4.10). Whole cell extract was subjected to immunoprecipitation with α- HA or α-FLAG conjugated beads and then used for a kinase assay (section 2.3.3 ad 2.3.4). Samples were resolved on a 5-10% two-step gradient SDS polyacrylamide gel and resolved at 30 mA for 1 h 15 min. Samples were transferred to PVDF membrane at 150 mA for 4 h before being examined for phosphorylation and immunoblotting using α-HA antibody. Input panel shows expression of proteins in SF9 cells. Lane 1: non-infected, Lane 2: HA-TIP60, Lane 3: HA-p400, Lane 4: FLAG-ATM, Lane 5: FLAG-ATM, Lane 6: FLAG-ATM and HA-TIP60, Lane 6: FLAG-ATM and HA-p400. IP panel shows; Lane 1: No immunoprecipitated material, Lane 2: Non-infected SF9 cells immunoprecipitated with α-HA beads, Lane 3: Non-infected SF9 cells immunoprecipitated with α-FLAG beads, Lane 4: HA-TIP60, Lane 5: HA-p400, Lane 6: FLAG-ATM, Lane 7: FLAG-ATM, Lane 7: FLAG-ATM and HA-TIP60, Lane 8: FLAG-ATM and HA-p400.

4.4 Discussion

Protein-protein interactions govern many processes within a cell. This is exemplified through DNA repair pathways where a coordinated effort of proteins strives to maintain the integrity of DNA and reduce the probability of cellular transformation. One of the key proteins involved in double-strand break repair is ATM kinase. This protein is responsible for phosphorylating histone H2AX at break sites as well as a vast number of proteins involved in DNA repair or checkpoint control (Burma et al., 2001; Geng et al., 2007; B. Xu et al., 2002). As a regulator of ATM, histone acetyl transferase TIP60 is known to acetylate ATM in the presence of DNA double-strand breaks facilitating ATM activation (Sun et al., 2007). This study investigated the interaction of ATM with the p400 ATPase for which there are several lines of evidence to suggest that the ATM-p400 interaction was likely to occur. Firstly, ATM is a member of the PIKK family of kinases. These family members share a similar domain structure including FAT (FRAP-ATM-TRRAP) domain, a FATC domain (a FAT domain located at the C-terminus of the protein), a PIKK regulatory domain and a PI3K kinase domain (Shiloh, 2003). Interestingly there appears to be functional redundancy of these domains. If the FATC domain of ATM is exchanged for the homologous domain from ATR, TRRAP or DNA-PKcs, the overall function of the protein is retained (Jiang et al., 2006). This suggests that there may be common binding partners for the domains within PIKK proteins. Further evidence for an interaction between ATM and p400 is supported by TIP60. TIP60 has been shown to interact with the SANT domain of p400 and as well as ATM (Park et al., 2010; Sun et al., 2007). Additionally, a paper in 2010 suggested a relationship between ATM and p400 as knockdown of p400 was able to induce the activity of ATM (Lise Mattera et al., 2010). Interestingly, mice generated to knockout either ATM and p400 prove to be embryonic lethal serves to emphasise the importance of these two repair proteins and the difficulty in determining their function (Daniel et al., 2012; Ueda et al., 2007).

Co-immunoprecipitation experiments were carried out to visualize the interaction between ATM and p400 (Figure 4.9). HA-tagged p400 was pulled down by α-HA conjugated agarose beads and FLAG-tagged ATM was shown to coimmunoprecipitate. An attempt to perform the reciprocal experiment pulling down ATM and coimmunoprecipitating p400 was unsuccessful in mammalian cells. When examining the interaction between ATM and p400 in a reverse co-immunoprecipitation

experiment, only a small amount of ATM was pulled down and the reciprocal interaction was not consistently detectable due to the low interaction amount (data not shown). In order to confirm the interaction, ATM and p400 were expressed in an insect system using SF9 cells. Coimmunoprecipitation experiments were carried out and the interaction between ATM and p400 could be observed (Figure 4.19). In this set of experiments, the interaction was shown using a reciprocal coimmunoprecipitation assay. While proteins expressed in insect cells showed a large amount of degradation products (Figure 4.16 and 4.18) which may have facilitated the interaction between ATM and p400, the proteins expressed in mammalian cells (figure 4.4 and 4.8) showed a single band consistent with the size of full length ATM or p400. This suggests that the interaction between ATM and p400 is through the full length protein and not through the smaller degradation products.

An additional method to observe the interaction between ATM and p400 was confocal microscopy to examine protein localization. Recombinant human ATM expressed in SF9 cells localized to both the nucleus and cytoplasm over the 48 h time period examined while recombinant human p400 expressed in SF9 cells initially localizes to the nucleus and cytoplasm at 24 h post-infection but became solely cytoplasmic at 36 h post-infection (Figure 4.20 and 4.21). Interestingly, when recombinant human ATM and p400 are co-expressed in SF9 cells, a clear change in localization of ATM could be seen at 36 h and 48 h post infection (Figure 4.22) where ATM is only found in the cytoplasm. This suggests that the p400 restricts ATM to the cytoplasm through a direct interaction. While ATM and p400 are both nuclear proteins in mammalian cells, it appears that the nuclear localization sequence in p400 may not be functioning for localization to the nucleus of SF9 cells. Examination of the literature did not yield a consensus nuclear localization sequence for SF9 cells as these cells are primarily used for protein expression and not as a model system for examining protein function. The change in localization of ATM upon p400 coexpression may be an artifact of protein expression in SF9 cells as ATM has been described to be a nuclear protein with small amounts in cytoplasmic vesicles in mammalian cells (Dar et al., 2006; Gately et al., 1998; Watters et al., 1997). This localization does not change upon DNA damage by UV irradiation. However, to confirm that p400 is not involved in localization of ATM in mammalian cells, the localization of ATM can be investigated in the presence of p400 that has undergone mutagenesis of the nuclear localization signal.

To elucidate the potential role of the ATM-p400 interaction, the dynamics of the interaction was examined. p400 is known to act as part of the larger TIP60/p400 complex in DNA repair (Kobor et al., 2004; Kusch et al., 2004). The interaction of p400 with ATM suggests two possible scenarios. Firstly, ATM may be associated with the TIP60 complex or alternatively, p400 may be associated with a distinct ATM-TIP60 complex. The coimmunoprecipitation between ATM and members of the TIP60 complex was examined to determine if the interaction between ATM and p400 was in the context of the TIP60 complex, or part of the ATM-TIP60 complex. GAS41 and BAF53 are two integral members of the TIP60 complex that if pulled down, should bring down the additional members of the complex. Figure 4.10 illustrated that immunoprecipitated BAF53 or GAS41 were not capable of pulling down ATM suggesting that the interaction between ATM and p400 is not through the TIP60 complex. As the interaction between ATM and TIP60 is not altered in the presence or absence of DNA damage (Sun et al., 2007), the interaction between ATM and p400 was examined under these same conditions. Figure 4.11 confirmed that as the ATM-TIP60 interaction remains unaltered in the presence and absence of DNA damage, the interaction between ATM and p400 also remains in the presence and absence of damage. Interestingly, the observation of expression of p400 and ATM in SF9 cells using confocal microscopy was conducted in the absence of DNA damage and showed that there was a change in localization of ATM when expressed with p400 presumably due to an interaction. This supports the hypothesis that the interaction occurs in the presence and absence of DNA damage, however this result may be confounded by the fact that SF9 cells do not express the complete set of mammalian proteins involved in DNA repair.

The SANT domain of p400 has previously been shown to interact with TIP60 and cause an inhibition of TIP60 acetyl transferase activity (Park et al., 2010). As p400 has been shown to interact with ATM (Figure 4.9) presumably through the ATM-TIP60 complex, mapping the interacting domain of p400 to ATM could help provide evidence as to whether the ATM-p400 interaction is facilitated through TIP60 or in an independent manner. Initially coimmunoprecipitation between ATM and the N- and C-termini of p400 were examined. Both domains showed ATM was able to be precipitated (Figure 4.13). The N-terminal p400 construct appeared to precipitate a larger amount of ATM compared to the C-terminal construct of p400. The small amount of ATM that was

pulled down using the C-terminus construct may have been due to the small amount of N-terminal p400 that was included in this construct. To examine this further, six fragments of p400 were used to precipitate ATM (Figure 4.14). The three N-terminal fragments (F1, F2 and F3) all precipitated a significant amount of ATM while two C-terminal fragments (F4 (SANT) and F5) showed weak precipitation. F6 failed to show any precipitation of ATM. The ability of multiple domains of p400 to interact with a single protein has previously been reported with Fragment 1-4 all showing the ability to precipitate with TIP60 (Park et al., 2010). The N-terminal fragments contain both the HSA domain and regions of the SWI2/SNF2 homology domains while fragment 4 contains the SANT domain of p400. While the SWI2/SNF2 homology domain is associated with the nucleosome exchange function of p400 (Kobor et al., 2004), there is no literature provided suggesting a role for the HSA domain or any of the associated regions within the N-terminal region of p400. The weak interaction between ATM and fragment 4 and 5 suggests that it is the N-terminus of p400 that is responsible for the reaction. Importantly, fragment 2 of p400 showed both a strong interaction with ATM (this study, Figure 4.14) and with TIP60 (Park et al., 2010). While fragment 2 did not show an effect on TIP60 acetylase activity (Park et al., 2010), it may be important for bridging the interaction between ATM and p400 and hence requires further investigation.

Protein-protein interactions facilitate a variety of functions including signalling, regulation of activity and acting as bridging moieties. With the interaction of p400 and ATM established, the function of the interaction needed to be assessed. Three possible functions were suggested but due to time constraints, only one was examined. The possibilities include; p400 affects ATM kinase activity directly or indirectly through inhibiting TIP60 activity; ATM affects p400 nucleosome exchange activity; or the interaction acts to facilitate bringing either ATM or p400 to the break sites. In this study, the kinase activity of ATM was assessed in the presence and absence of p400. Initially, the autophosphorylation of ATM was assessed in the presence and absence of DNA damage. No visible difference in phosphorylation levels of ATM was detected regardless of DNA damage induction (Figure 4.23). This is potentially an experimental design error as ATM activation occurs rapidly after DNA damage induction and in this experiment the cells were not harvested for several hours after the addition of doxorubicin. ATM may have already been phosphorylated at the DNA dependent sites

and the small amount of phosphorylation seen in the assay may have been due to a non-specific kinase pulled down in association with the proteins. In an attempt to remove the confounding effects of the ATM kinase assay in a mammalian system, the intrinsic activity of ATM was assessed using recombinant protein expressed in SF9 cells (Figure 4.24). Here ATM and/or p400 was immunoprecipitated and used in a kinase assay. No visible ATM phosphorylation was seen, however p400 phosphorylation was observed. This p400 phosphorylation was present in the absence of ATM and is likely caused through non-specific kinases but poses several questions; do p400 post-translational modifications occur in mammalian cells, what are they and what are their functions?

With the kinase assay producing inconclusive results, attention turns to the areas that could be investigated further. Acetylation of ATM by TIP60 is required for ATM activation in the presence of DNA damage and the SANT domain of p400 has been previously shown to inhibit the histone acetyl transferase activity of TIP60 (Park et al., 2010; Sun et al., 2005; Sun et al., 2007). The novel interaction between ATM and p400 may represent an additional method of regulation by inhibiting the acetylase activity of TIP60. Examination of TIP60 acetylase function on ATM in the presence and absence of p400 or the SANT domain of p400 may provide valuable information regarding the effect of p400 on ATM activity. Interestingly, p400 appears to be capable of being phosphorylated (Figure 4.24). While no p400 post-translation modifications have been reported, it is possible that some of these modifications will alter the activity of p400. It would be interesting to identify sites of post-translational modification and investigate roles of these modifications in regard to p400 activity. Finally, the interaction between ATM and p400 may provide a mechanism for recruitment of proteins to the DNA break site. A study conducted in 2010 has identified a role for p400 in nucleosome destabilisation at the initial steps of DNA repair with knockdown of p400 resulting in an increase in radiosensitivity and overall reduction in repair (Ye Xu et al., 2010). The completion of ChIP at sites of DNA damage combined with knockdown of ATM or p400 may provide data to confirm the dependency of either protein in the recruitment to break sites.

Examination of the literature may indirectly support the possibility of a functional ATM/p400 interaction in the process of DNA repair. Both enzymes have been implicated with proper signalling, modification and localisation of RAD51 at sites of DNA damage (Chen et al., 1999; Celine Courilleau et al., 2012; Yuan, Chang, & Lee,

2003). RAD51 is a protein that plays several roles during homologous recombination including binding single stranded DNA and strand invasion (Sung, Krejci, Van Komen, & Sehorn, 2003). In 2003, Chen et al illustrated how ATM knockout cells had decreased formation of RAD51 foci, while in 2012 Courilleau et al. described how depletion of p400 resulted in delayed RAD51 foci formation (Chen et al., 1999; Celine Courilleau et al., 2012). These independent investigations suggest that there is a relationship between the two enzymes, which could be a result of the interaction described in this study. A potential mechanism to examine if the interaction between ATM and p400 is required for RAD51 formation at sites of DNA damage is to produce mutants that abolish the interaction between ATM and p400 and examine RAD51 foci formation when these proteins are overexpressed. This would provide a mechanism to investigate function of the interaction in vivo, adding validity to the presence of the ATM/p400 interaction.

The identification of a novel interaction between ATM kinase and the ATPase p400 provides insight to the complexity of DNA repair. While no evidence could be provided for the function of the interaction, this study provides a platform for more in depth investigation into the influence of p400 on DNA repair.

5 Summary and Future directions

5.1 Summary

The DNA double-strand break response is arguably one of the most important cellular processes with its ability to repair breaks and prevent genetic instability that is associated with the development of cancer. A plethora of proteins with a variety of functions is involved in DNA repair. This study focuses on three major proteins involved in DNA repair; TIP60, a histone acetyl transferase; ATM, a serine/threonine kinase from the PIKK family; and p400, a chromatin remodeler.

In a previous study, overexpression of TIP60 or the SANT domain of p400 resulted in the phosphorylation of H2AX in the absence of a DNA damaging agent. This phosphorylation is a sign of activation of the DNA double-strand break response. It was hypothesised that the activation of this pathway was due to overexpressed TIP60 or the SANT domain of p400 being able to sequester a negative regulator associated with the ATM-TIP60 complex resulting in activation of ATM. This study was aimed at examining in greater detail the ability of TIP60 and the SANT domain of p400 to induce the activation of the DSB response. Therefore, individual domains of TIP60 were cloned and examined for their ability to induce H2AX phosphorylation. Additionally, deletions were introduced into each of the three helices of the SANT domain to determine if a single helix was responsible for the induction of H2AX phosphorylation. Unfortunately, H2AX phosphorylation induced by TIP60 and SANT domain overexpression was not consistently reproduced. Similarly, expression of the TIP60 domains and SANT domain helix deletions failed to show any meaningful results.

Protein-protein interactions are found throughout the cell in various pathways and DNA repair is no exception. ATM has previously been shown to interact with TIP60 and this interaction proves essential for ATM activation during DNA repair which involves TIP60 acetylation of ATM resulting in autophosphorylation and activation of ATM. TIP60 has also been shown to interact with p400, presumably in the context of the TIP60 chromatin remodeling complex. TRRAP, another member of the PIKK family has previously been shown to interact with p400. Interestingly, members of the PIKK family show functional redundancy in their domains. For example, when the FATC

domain of ATM was replaced with the homologous domain from ATR, DNA-PKcs, or TRRAP, ATM retained the ability to interact with TIP60 (Jiang et al., 2006). This study hypothesised that p400 was able to interact with ATM, given that TRRAP and ATM share common domains found within the PIKK proteins. The present study used co-immunoprecipitation in mammalian cells and in SF9 cells to confirm the interaction between ATM and p400. Additionally, co-immunoprecipitation showed that ATM could precipitate with both the N-terminal and C-terminal regions of p400 with a stronger interaction with the N-terminal region. This was reflected in the interaction of ATM and fragments 1-6 of p400. There appeared to be a strong interaction between ATM and fragments 1-3 which are N-terminal fragments and fragment 4 and 5 pulling down less ATM. Confocal microscopy also supports the hypothesis of an interaction between ATM and p400. The ATM localisation was altered from a uniform distribution throughout the whole cell to completely cytosolic localisation upon coexpression of p400.

While the function of the ATM-p400 interaction was not determined during this study, the results in this study provide a platform for a more in depth investigation into the function of the interaction during DNA repair. Limitations and some future experiments are discussed below.

5.2 Limitations

It is important to recognise several limitations that were encountered during this study. The DNA damage response encompasses a range of pathways and the mechanisms used to recognise them are often redundant. For example, both homologous recombination and non-homologous end joining use histone H2AX phosphorylation as a marker of the break site however the protein kinase responsible for phosphorylation vary and include ATM, ATR and DNA-PKcs. In the case of the experiment described in chapter 3, the increase in H2AX phosphorylation that was seen with TIP60 or SANT domain expression may have been due to activation of any of these proteins. As these experiments were performed *in vivo,* identifying the pathway involved poses a challenge.

The original experiment examining the induction of H2AX phosphorylation with overexpression of TIP60 or the SANT domain of p400 was completed using the same cell line as in this study. However, due to the time interval between experiments the age

and passage number of the cells varied considerably. The genetic homogeneity and protein composition between the two groups of cells may have been markedly different resulting in the variable results between studies. This problem represents a major issue when comparing similar studies. It also needs to be considered when comparing work between different authors and previous studies. The difference in cellular protein composition could result in inconsistencies.

The experiments planned in this study were performed *in vivo* where the interaction between ATM and p400 may have been influenced by any number of proteins in the cell. The following describes strategies that could be used to validate the interaction between ATM and p400 and methods to investigate the function of the interaction.

5.3 Future Directions

5.3.1 Functional analysis of SANT domain Helix deletion constructs

In a previous study it was suggested that the SANT domain of p400 was able to induce the phosphorylation of H2AX in the absence of a DNA damaging agent, possibly through the activation of ATM. This study examined the ability of three helix deletion mutants of the SANT domain of p400 for their ability to induce a similar effect. The SANT domain and the SANT domain helix deletions were however, unable to provide reproducible results. The SANT domain of p400 could still be playing a role in the DNA damage response through the interaction with the histone acetyl transferase TIP60. Previously the SANT domain of p400 was shown to produce a robust inhibition of TIP60 HAT activity (Park et al., 2010). Investigation into the SANT domain of other chromatin remodeling proteins has suggested that the majority of function is associated with the third helix within the domain (Barbaric et al., 2003; Pinson et al., 1998; Sterner et al., 2002). To investigate the importance of each of the helices within the SANT domain of p400, the helix deletion constructs produced in this study could first be examined for their ability to immunoprecipitate with TIP60. Following this the HAT activity of TIP60 can be assessed in the presence of the SANT domain helix deletion mutants to assess their ability to inhibit TIP60 associated HAT activity as described by Park et al 2010.

It is possible that the H2AX phosphorylation assay used in this study was an inappropriate method to examine the effect on the DNA damage response. An

alternative method to assess the involvement of the SANT domain of p400 in the DNA damage response could be to assess the viability of cells expressing the various helix deletion constructs in the presence of a DNA damaging agent. If the SANT domain is able to activate the DNA double-strand break repair pathway in the absence of damage, this may translate to increased viability of cells in the presence of DNA damage. Examination of the viability of cells expressing the SANT domain or helix deletion constructs may provide some insight into the protective effect of the domains. Several methods are available to examine the viability of cells including the xCELLigence system from Roche which allows real-time monitoring of cell viability as well as the ability to distinguish cellular states such as cellular senescence and apoptosis. Chemical based assays are also available to examine cell viability including the ApoTox-Glo™ Triplex Assay and CellTiter 96® AQueous One Solution Cell Proliferation Assay System, both from Promega, that can be used to determine proliferation, viability and apoptosis. Comparing the viability of cells expressing WT SANT domain or a helix deletion mutant to non-transfected cells in the presence or absence of DNA damage could be used to test whether the SANT domain has an effect on the DNA damage response and if one or more of the helices within the domain play a major role in this function.

If the function of the helix deletions appears to show a significant effect, it will also need to be characterised in a whole protein context. To examine this, the mutations could be introduced into full length p400 and used to see if the full length protein with mutations has the same effect as the smaller helix deletion mutants.

5.3.2 Confirming the ATM-p400 interaction

This study used several methods to examine an interaction between ATM and p400 including co-immunoprecipitation between overexpressed proteins in a mammalian system and an insect cell system as well as examining the change in localisation of ATM and p400 when co-expressed in SF9 insect cells. To confirm the interaction in the absence of overexpressed proteins, immunoprecipitation experiments pulling down endogenously expressed proteins should be completed. While this experiment was attempted in this study (data not shown), the combination of the ATM and p400 antibodies was not conducive to obtaining clear results as the p400 antibody produces a non-specific band at the size of ATM. Additionally, it is ideal to immunoprecipitate with an antibody raised in one animal and complete the immunoblot with an antibody

raised in another animal to prevent background signals. These were not available for this study.

Another method that could be used to confirm the interaction between ATM and p400 is a GST pulldown assay. While cloning and expressing p400 in *E.coli* is not feasible due to its size, expression of GST-tagged Fragment 1-6 of p400 could be expressed and used in conjunction with FLAG-ATM expressed in SF9 cells. This assay could be used to identify which domains of p400 are able to interact with ATM and support the results shown in Figure 4.14. If it were possible to identify specific interacting domains, the next step could be to examine the ability of these domains to alter the DNA damage response. This could be examined through cell viability or apoptosis assays as described in section 5.3.1.

It was hypothesised that there was an interaction between ATM and p400 because TRRAP, another member of the PIKK family, has the ability to interact with p400 and the domains within the PIKK family members are functionally equivalent. Additionally, TIP60 has the ability to interact with both ATM and p400. This study used immunoprecipitation as a means to assess the interaction between ATM and p400 and while they can co-immunoprecipitate this may be due to an interaction with a bridging protein such as TIP60. To assess this, tandem immunoprecipitation could be used. Here, TIP60, ATM and p400, each with a different tag would need to be coexpressed. The first immunoprecipitation would pull down TIP60 as this is known to pull down both ATM and p400. TIP60 could be eluted from the beads to produce a solution with TIP60 and the associated ATM and p400 and this solution could be subjected to a second immunoprecipitation pulling down either ATM or p400. If the ATM-p400 interaction is bridged by TIP60, all three proteins should be present in the precipitate. If ATM-TIP60 and p400-TIP60 are two separate complexes only TIP60 would be coimmunoprecipitated. Alternatively, the immunoprecipitation of ATM and p400 could be investigated in the presence of siRNA targeting TIP60. If TIP60 can facilite the interaction between ATM and p400, the absence of TIP60 may result in the inability of ATM and p400 to coimmunoprecipitate.

5.3.3 Functional assays associated with the ATM-p400 interaction

While a novel interaction between ATM and p400 was identified, the functional analysis attempted in this study was not able to define a specific role for interaction.

The interaction may regulate ATM kinase activity, p400 histone exchange or may act as a mechanism for bringing ATM and p400 together at DNA break sites.

ATM is a serine/threonine kinase that is responsible for phosphorylating a range of proteins involved in DNA repair. It is possible that the interaction between ATM and p400 may alter the kinase activity of ATM. The kinase assay that was used in this study did not provide any information regarding ATM kinase activity as nonspecific kinases appeared to be copurified. To more efficiently examine the kinase activity, an *in vitro* kinase assay could be developed that will reduce the amount of background while being able to clearly show the activity of ATM. In this study, the autophosphorylation of ATM was examined through immunoprecipitating ATM and using the protein on the beads to assess activity. This resulted in a large amount of background phosphorylation. Elution of ATM from the beads to produce a pure ATM sample may help overcome this background noise. Additionally, as well as being able to examine autophosphorylation, the purified ATM sample could be used to assess the phosphorylation of ATM target proteins such as H2AX and p53. The phosphorylation could be examined through the use of phospho specific antibodies or by [P^{33}] ATP. Examining the activity of ATM in the presence of p400 and in the presence and absence of DNA damage could assess the importance of p400 on ATM kinase activity.

Both ATM and p400 have been described independently to have an effect on RAD51 with knockdown or depletion of either protein reducing RAD51 foci formation in the presence of DNA damage (Chen et al., 1999; Celine Courilleau et al., 2012). It is possible that these effects may be due to the ATM-p400 complex described in this study. To investigate this, mutagenesis to prevent the interaction between ATM and p400 can be completed and confirmed through coimmunoprecipitation. If the formation of RAD51 foci at break sites is reliant on the ATM-p400 complex, disruption to the interaction should reduce the foci formation. This can be examined using live cell imaging to observe the formation of RAD50 at DNA break sites.

The SANT domain of p400 has been shown to inhibit the HAT activity of TIP60 using core histones purified from HeLa cells (Park et al., 2010). The current study has identified an interaction between ATM and p400 and suggests that the p400 SANT domain may affect the acetylation of ATM through inhibiting the HAT activity of TIP60. The *in vitro* HAT assay that was described in Park et al, 2010 paper could be

altered to use purified ATM as the target. Alternatively, the acetylation status of ATM could be assessed *in vivo* through an antibody specific to lysine acetylation at 3016 of ATM in the presence and absence of the SANT domain of p400.

p400 is a chromatin remodeler that is responsible for exchanging H2A-H2B dimers for H2AZ-H2B dimers throughout the genome. While p400 has been found to be essential in DNA repair, its actual function is unclear. A homologous protein Domino in Drosophila is responsible for exchanging the H2AX/H2AZ homologue H2AV at break sites after repair. This function was also assessed in the *Saccharomyces cerevisiae* homologue SWR1 (Mizuguchi, Wu, Alami, & Luk, 2012). The Mizuguchi study provides a method for an *in vitro* chromatin exchange assay which could be used to examine the effect ATM may have on p400 chromatin exchange.

Interestingly, the phosphorylation status of p400 has not been discussed in literature. The results of the kinase assay performed in section 4.3 showed that p400 is capable of being phosphorylated. Examination of the phosphorylation status of p400 in the presence and absence of DNA damage could elucidate if phosphorylation of p400 has any effect on its activity. Purification of p400 in the presence and absence of DNA damage followed by mass spectrophotometry could be used to identify phosphorylation sites on p400. Examining these sites may provide an idea of what type of kinase is responsible for the phosphorylation of p400. If specific sites within p400 are found to be differentially phosphorylated, production of phospho-mimic constructs or non-phosphorylatable constructs and their effect on the DNA damage response could provide information regarding the activation. One such assay that could be used to assess the effect of phosphorylation of p400 is a chromatin exchange assay asking the question; does phosphorylation of p400 affect chromatin exchange?

An interesting observation was seen when examining the localisation of p400 and ATM expressed in SF9 cells. ATM was found to be sequestered in the cytoplasm my p400 when the two proteins were coexpressed as opposed to a more general localisation throughout the cytoplasm and nucleus when only ATM was expressed. While this phenomenon was observed in a nonmammalian system, how the localisation of ATM and p400 in mammalian cells in the presence and absence of DNA damage remains to be examined. The combination of fluorescently tagged ATM and p400 and live cell imaging will provide an efficient system to examine the localisation of these proteins.

Additionally, treatments such ATM inhibitors, siRNA mediated knockdown of protein, or expression of kinase- or ATPase-deficient mutants can be used to determine if any change in localisation is dependent on activity of specific proteins.

Chromatin immunoprecipitation (ChIP) is a technique that identifies protein interation sites on DNA *in vivo*. In this study, the interaction between ATM and p400 was identified using immunoprecipitation and subcellular localisation via confocal microscopy. A method that could be used to identify if the ATM-p400 interaction occurs at break sites is ChIP in conjunction with zinc finger nuclease technology. Zinc finger nucleases are generally used for site-directed mutagenesis within the genome through the introduction of DNA double-strand breaks and homologous recombination. The use of zinc finger nucleases in this case could be used to introduce DNA double-strand breaks at a known region in the genome. This method has been previously described to investigate the accumulation of proteins at a specific break site (Ye Xu et al., 2010). ChIP could be performed pulling down either ATM or p400 and examining the break site targeted by the zinc finger nuclease. This could elucidate whether ATM and p400 are localising to the break sites at the same time. ChIP could be repeated with the knock down of ATM or p400 and the ability of these proteins to localise to the break sites in the absence of one or the other could help to shed light on whether one protein is responsible for bringing the other to the site of DNA damage.

Live cell imaging is a powerful technique that can be used to study DNA break sites in real time. Fluorescence resonance energy transfer (FRET) is a technique used to examine the proximity of fluorescent coupling. This technique requires two proteins that are fluorescently labelled to be in close proximity to each other. When one fluorescent tag is excited, if the second tag is in close proximity, the excitation energy of the primary tag will excite the second tag which will produce a signal. FRET will only occur if the two proteins are within approximately 200 nm of each other. The FRET signal could be examined in the presence and absence of DNA damage to provide information about the interaction between ATM and p400. That is, whether the interaction is dynamic and only present under the stress of DNA damage or if the interaction persists under non-stressed conditions.

To examine the accumulation of ATM and p400 at DNA break sites in real time, live cell imaging using fluorescence recovery after photobleaching (FRAP) could be used to

examine protein dynamics with the use of photoactive tags. This technique would use p400 or ATM that has been tagged with a photoactive motif that is stably expressed in cells. When cells are photobleached to induce DNA damage, the accumulation and spread of the photoactively tagged proteins could be examined. Examining this process with the knockdown of ATM or p400 could provide information about the interaction and if it is necessary for bringing one or the other protein to the site of DNA damage.

5.5 Conclusion

While this study failed to reproduce the induction of H2AX phosphorylation seen with overexpression of TIP60 or the SANT domain of p400, it has provided evidence for a novel interaction between ATM kinase and p400 ATPase. This study provides a platform for further investigation into the function associated with this interaction and a number of methods by which this could be assessed have been suggested. Both ATM and p400 have previously been shown to have essential functions during DNA damage and understanding the biology behind DNA repair may provide a new target for pharmacological intervention in cancer therapies.

6 References

Aasland, R., Stewart, A. F., & Gibson, T. (1996). The SANT domain: A putative DNA-binding domain in the SWI-SNF and ADA complexes, the transcriptional corepressor N-CoR and TFIIIB. *Trends in Biochemical Sciences, 21*(3), 87-88. doi: 10.1016/s0968-0004(96)30009-1

Acharya, S., Foster, P. L., Brooks, P., & Fishel, R. (2003). The coordinated functions of the E-coli MutS and MutL proteins in mismatch repair. *Molecular Cell, 12*(1), 233-246. doi: 10.1016/s1097-2765(03)00219-3

Adam, M., Robert, F., Larochelle, M., & Gaudreau, L. (2001). H2A.Z is required for global chromatin integrity and for recruitment of RNA polymerase II under specific conditions. *Molecular and Cellular Biology, 21*(18), 6270-6279. doi: 10.1128/mcb.21.18.6270-6279.2001

Bakkenist, C. J., & Kastan, M. B. (2003). DNA damage activates ATM through intermolecular autophosphorylation and dimer dissociation. *Nature, 421*(6922), 499-506. doi: 10.1038/nature01368

Barbaric, S., Reinke, H., & Horz, W. (2003). Multiple mechanistically distinct functions of SAGA at the PH05 promoter. *Molecular and Cellular Biology, 23*(10), 3468-3476. doi: 10.1128/mcb.23.10.3468-3476.2003

Barlow, C., Hirotsune, S., Paylor, R., Liyanage, M., Eckhaus, M., Collins, F., . . . WynshawBoris, A. (1996). Atm-deficient mice: A paradigm of ataxia telangiectasia. *Cell, 86*(1), 159-171. doi: 10.1016/s0092-8674(00)80086-0

Bassing, C. H., Chua, K. F., Sekiguchi, J., Suh, H., Whitlow, S. R., Fleming, J. C., . . . Alt, F. W. (2002). Increased ionizing radiation sensitivity and genomic instability in the absence of histone H2AX. *Proceedings of the National Academy of Sciences of the United States of America, 99*(12), 8173-8178. doi: 10.1073/pnas.122228699

Batty, D. P., & Wood, R. D. (2000). Damage recognition in nucleotide excision repair of DNA. *Gene, 241*(2), 193-204. doi: 10.1016/s0378-1119(99)00489-8

Berkovich, E., Monnat, R. J., Jr., & Kastan, M. B. (2007). Roles of ATM and NBS1 in chromatin structure modulation and DNA double-strand break repair. *Nature Cell Biology, 9*(6), 683-U137. doi: 10.1038/ncb1599

Bhaskara, V., Dupre, A., Lengsfeld, B., Hopkins, B. B., Chan, A., Lee, J.-H., . . . Paull, T. T. (2007). Rad50 adenylate kinase activity regulates DNA tethering by Mre11/Rad50 complexes. *Molecular Cell, 25*(5), 647-661. doi: 10.1016/j.molcel.2007.01.028

Bird, A. W., Yu, D. Y., Pray-Grant, M. G., Qiu, Q. F., Harmon, K. E., Megee, P. C., . . . Christman, M. F. (2002). Acetylation of histone H4 by Esa1 is required for DNA double-strand break repair. *Nature, 419*(6905), 411-415. doi: 10.1038/nature01035

Boyer, L. A., Langer, M. R., Crowley, K. A., Tan, S., Denu, J. M., & Peterson, C. L. (2002). Essential role for the SANT domain in the functioning of multiple chromatin remodeling enzymes. *Molecular Cell, 10*(4), 935-942. doi: 10.1016/s1097-2765(02)00634-2

Boyer, L. A., Latek, R. R., & Peterson, C. L. (2004). The SANT domain: a unique histone-tail-binding module? *Nature Reviews Molecular Cell Biology, 5*(2), 158-163. doi: 10.1038/nrm1314

Burma, S., Chen, B. P., Murphy, M., Kurimasa, A., & Chen, D. J. (2001). ATM phosphorylates histone H2AX in response to DNA double-strand breaks. *Journal of Biological Chemistry, 276*(45), 42462-42467.

Canman, C. E., Lim, D. S., Cimprich, K. A., Taya, Y., Tamai, K., Sakaguchi, K., . . . Siliciano, J. D. (1998). Activation of the ATM kinase by ionizing radiation and phosphorylation of p53. *Science, 281*(5383), 1677-1679. doi: 10.1126/science.281.5383.1677

Canzio, D., Chang, E. Y., Shankar, S., Kuchenbecker, K. M., Simon, M. D., Madhani, H. D., . . . Al-Sady, B. (2011). Chromodomain-Mediated Oligomerization of HP1 Suggests a

Nucleosome-Bridging Mechanism for Heterochromatin Assembly. *Molecular Cell, 41*(1), 67-81. doi: 10.1016/j.molcel.2010.12.016

Cavialli, G., & Paro, R. (1998). Chromo-domain proteins: Linking chromatin structure to epigenetic regulation. *Current Opinion in Cell Biology, 10*(3), 354-360.

Celeste, A., Difilippantonio, S., Difilippantonio, M. J., Fernandez-Capetillo, O., Pilch, D. R., Sedelnikova, O. A., . . . Nussenzweig, A. (2003). H2AX haploinsufficiency modifies genomic stability and tumor susceptibility. *Cell, 114*(3), 371-383. doi: 10.1016/s0092-8674(03)00567-1

Chailleux, C., Tyteca, S., Papin, C., Boudsocq, F., Puget, N., Courilleau, C., . . . Trouche, D. (2010). Physical interaction between the histone acetyl transferase Tip60 and the DNA double-strand breaks sensor MRN complex. *Biochemical Journal, 426*, 365-371. doi: 10.1042/bj20091329

Chan, H. M., Narita, M., Lowe, S. W., & Livingstone, D. M. (2005). The p400 E1A-associated protein is a novel component of the p53 -> p21 senescence pathway. *Genes & Development, 19*(2), 196-201. doi: 10.1101/gad.1280205

Chen, G., Yuan, S. S. F., Liu, W., Xu, Y., Trujillo, K., Song, B. W., . . . Lee, E. (1999). Radiation-induced assembly of Rad51 and Rad52 recombination complex requires ATM and c-Abl. *Journal of Biological Chemistry, 274*(18), 12748-12752. doi: 10.1074/jbc.274.18.12748

Courilleau, C., Chailleux, C., Jauneau, A., Grimal, F., Briois, S., Boutet-Robinet, E., . . . Canitrot, Y. (2012). The chromatin remodeler p400 ATPase facilitates Rad51-mediated repair of DNA double-strand breaks. *Journal of Cell Biology, 199*(7), 1067-1081. doi: 10.1083/jcb.201205059

Courilleau, C., Mattera, L., Legube, G., Ueda, T., Fukunaga, R., Chevillard-Briet, M., . . . Trouche, D. (2010). ATPase p400 module the cellular future through regulation of ROS homeostasis. *Bulletin Du Cancer, 97*, S39-S39.

Daniel, J. A., Pellegrini, M., Lee, B.-S., Guo, Z., Filsuf, D., Belkina, N. V., . . . Nussenzweig, A. (2012). Loss of ATM kinase activity leads to embryonic lethality in mice. *Journal of Cell Biology, 198*(3), 295-304. doi: 10.1083/jcb.201204035

Dar, I., Biton, S., Shiloh, Y., & Barzilai, A. (2006). Analysis of the ataxia telangiectasia mutated-mediated DNA damage response in murine cerebellar neurons. *Journal of Neuroscience, 26*(29), 7767-7774. doi: 10.1523/jneurosci.2055-06.2006

David, S. S., O'Shea, V. L., & Kundu, S. (2007). Base-excision repair of oxidative DNA damage. *Nature, 447*(7147), 941-950.

de Jager, M., Dronkert, M. L. G., Modesti, M., Beerens, C., Kanaar, R., & van Gent, D. C. (2001). DNA-binding and strand-annealing activities of human Mre11: implications for its roles in DNA double-strand break repair pathways. *Nucleic Acids Research, 29*(6), 1317-1325. doi: 10.1093/nar/29.6.1317

de Laat, W. L., Jaspers, N. G. J., & Hoeijmakers, J. H. J. (1999). Molecular mechanism of nucleotide excision repair. *Genes & Development, 13*(7), 768-785. doi: 10.1101/gad.13.7.768

Derheimer, F. A., & Kastan, M. B. (2010). Multiple roles of ATM in monitoring and maintaining DNA integrity. *Febs Letters, 584*(17), 3675-3681. doi: 10.1016/j.febslet.2010.05.031

Downs, J. A., Allard, S., Jobin-Robitaille, O., Javaheri, A., Auger, A., Bouchard, N., . . . Cote, J. (2004). Binding of chromatin-modifying activities to phosphorylated histone H2A at DNA damage sites. *Molecular Cell, 16*(6), 979-990. doi: 10.1016/j.molcel.2004.12.003

Doyon, Y., & Cote, J. (2004). The highly conserved and multifunctional NuA4 HAT complex. *Current Opinion in Genetics & Development, 14*(2), 147-154. doi: 10.1016/j.gde.2004.02.009

Doyon, Y., Selleck, W., Lane, W. S., Tan, S., & Cote, J. (2004). Structural and functional conservation of the NuA4 histone acetylytransferase complex from yeast to humans. *Molecular and Cellular Biology, 24*, 1884-1896.

Draker, R., Sarcinella, E., & Cheung, P. (2011). USP10 deubiquitylates the histone variant H2A.Z and both are required for androgen receptor-mediated gene activation. *Nucleic Acids Research, 39*(9), 3529-3542. doi: 10.1093/nar/gkq1352

Elsaesser, S. J., Goldberg, A. D., & Allis, C. D. (2010). New functions for an old variant: no substitute for histone H3.3. *Current Opinion in Genetics and Development, 20*, 110-117.

Elson, A., Wang, Y. Q., Daugherty, C. J., Morton, C. C., Zhou, F., CamposTorres, J., & Leder, P. (1996). Pleiotropic defects in ataxia-telangiectasia protein-deficient mice. *Proceedings of the National Academy of Sciences of the United States of America, 93*(23), 13084-13089. doi: 10.1073/pnas.93.23.13084

Engelke, D. R., Krikos, A., Bruck, M. E., & Ginsburg, D. (1990). Purification of thermus-aquaticus DNA-polymerase expressed in escherichia-coli. *Analytical Biochemistry, 191*(2), 396-400. doi: 10.1016/0003-2697(90)90238-5

Falck, J., Coates, J., & Jackson, S. P. (2005). Conserved modes of recruitment of ATM, ATR and DNA-PKcs to sites of DNA damage. *Nature, 434*(7033), 605-611.

Filippo, J. S., Sung, P., & Klein, H. (2008). Mechanism of eukaryotic homologous recombination *Annual Review of Biochemistry* (Vol. 77, pp. 229-257).

Fischle, W., Tseng, B. S., Dormann, H. L., Ueberheide, B. M., Garcia, B. A., Shabanowitz, J., . . . Allis, C. D. (2005). Regulation of HP1-chromatin binding by histone H3 methylation and phosphorylation. *Nature, 438*(7071), 1116-1122. doi: 10.1038/nature04219

Frank, S. R., Parisi, T., Taubert, S., Fernandez, P., Fuchs, M., Chan, H. M., . . . Amati, B. (2003). MYC recruits the TIP60 histone acetyltransferase complex to chromatin. *Embo Reports, 4*(6), 575-580. doi: 10.1038/sj.embor.embor861

Fuchs, M., Gerber, J., Drapkin, R., Sif, S., Ikura, T., Ogryzko, V., . . . Livingston, D. M. (2001). The p400 complex is an essential E1A transformation target. *Cell, 106*(3), 297-307.

Gao, Y., Hayes, R. B., Huang, W.-Y., Caporaso, N. E., Burdette, L., Yeager, M., . . . Berndt, S. I. (2011). DNA repair gene polymorphisms and tobacco smoking in the risk for colorectal adenomas. *Carcinogenesis, 32*(6), 882-887. doi: 10.1093/carcin/bgr071

Gatei, M., Jakob, B., Chen, P., Kijas, A. W., Becherel, O. J., Gueven, N., . . . Lavin, M. F. (2011). ATM Protein-dependent Phosphorylation of Rad50 Protein Regulates DNA Repair and Cell Cycle Control. *Journal of Biological Chemistry, 286*(36), 31542-31556. doi: 10.1074/jbc.M111.258152

Gately, D. P., Hittle, J. C., Chan, G. K. T., & Yen, T. J. (1998). Characterization of ATM expression, localization, and associated DNA-dependent protein kinase activity. *Molecular Biology of the Cell, 9*(9), 2361-2374.

Geng, L. Y., Zhang, X. S., Zheng, S., & Legerski, R. J. (2007). Artemis links ATM to G(2)/M checkpoint recovery via regulation of Cdk1-cyclin B. *Molecular and Cellular Biology, 27*(7), 2625-2635. doi: 10.1128/mcb.02072-06

Gevry, N., Chan, H. M., Laflamme, L., Livingston, D. M., & Gaudreau, L. (2007). p21 transcription is regulated by differential localization of histone H2A.Z. *Genes & Development, 21*(15), 1869-1881. doi: 10.1101/gad.1545707

Goldgar, D. E., Healey, S., Dowty, J. G., Da Silva, L., Chen, X., Spurdle, A. B., . . . kConFab. (2011). Rare variants in the ATM gene and risk of breast cancer. *Breast Cancer Research, 13*(4). doi: 10.1186/bcr2919

Gorrini, C., Squatrito, M., Luise, C., Syed, N., Perna, D., Wark, L., . . . Amati, B. (2007). Tip60 is a haplo-insufficient tumour suppressor required for an oncogene-induced DNA damage response. *Nature, 448*(7157), 1063-1067.

Grune, T., Brzeski, J., Eberharter, A., Clapier, C. R., Corona, D. F. V., Becker, P. B., & Muller, C. W. (2003). Crystal structure and functional analysis of a nucleosome recognition module of the remodeling factor ISWI. *Molecular Cell, 12*(2), 449-460. doi: 10.1016/s1097-2765(03)00273-9

Halazonetis, T. D., Gorgoulis, V. G., & Bartek, J. (2008). An oncogene-induced DNA damage model for cancer development. *Science, 319*(5868), 1352-1355. doi: 10.1126/science.1140735

Hardy, S., Jacques, P.-E., Gevry, N., Forest, A., Fortin, M.-E., Laflamme, L., . . . Robert, F. (2009). The Euchromatic and Heterochromatic Landscapes Are Shaped by Antagonizing Effects of Transcription on H2A.Z Deposition. *Plos Genetics, 5*(10). doi: 10.1371/journal.pgen.1000687

Hlubek, F., Lohberg, C., Meiler, J., Jung, A., Kirchner, T., & Brabletz, T. (2001). Tip60 is a cell-type-specific transcriptional regulator. *Journal of Biochemistry, 129*(4), 635-641.

Hopfner, K. P., Karcher, A., Craig, L., Woo, T. T., Carney, J. P., & Tainer, J. A. (2001). Structural biochemistry and interaction architecture of the DNA double-strand break repair Mre11 nuclease and Rad50-ATPase. *Cell, 105*(4), 473-485. doi: 10.1016/s0092-8674(01)00335-x

Humphrey, G. W., Wang, Y. H., Russanova, V. R., Hirai, T., Qin, J., Nakatani, Y., & Howard, B. H. (2001). Stable histone deacetylase complexes distinguished by the presence of SANT domain proteins CoREST/kiaa0071 and Mta-L1. *Journal of Biological Chemistry, 276*(9), 6817-6824. doi: 10.1074/jbc.M007372200

Ikura, T., Ogryzko, V. V., Grigoriev, M., Groisman, R., Wang, J., Horikoshi, M., . . . Nakatani, Y. (2000). Involvement of the TIP60 histone acetylase complex in DNA repair and apoptosis. *Cell, 102*(4), 463-473.

Ikura, T., Tashiro, S., Kakino, A., Shima, H., Jacob, N., Amunugarna, R., . . . Kamiya, K. (2007). DNA damage-dependent acetylation and ubiquitination of H2AX enhances chromatin dynamics. *Molecular and Cellular Biology, 27*(20), 7028-7040. doi: 10.1128/mcb.00579-07

Jiang, X., Xu, Y., & Price, B. D. (2010). Acetylation of H2AX on lysine 36 plays a key role in the DNA double-strand break repair pathway. *Febs Letters, 584*(13), 2926-2930. doi: 10.1016/j.febslet.2010.05.017

Jiang, X. F., Sun, Y. L., Chen, S. J., Roy, K., & Price, B. D. (2006). The FATC domains of PIKK proteins are functionally equivalent and participate in the Tip60-dependent activation of DNA-PKcs and ATM. *Journal of Biological Chemistry, 281*(23), 15741-15746. doi: 10.1074/jbc.M513172200

Jiang, X. F., Xu, Y., & Price, B. D. (2010). Acetylation of H2AX on lysine 36 plays a key role in the DNA double-strand break repair pathway. *Febs Letters, 584*(13), 2926-2930. doi: 10.1016/j.febslet.2010.05.017

Jiricny, J. (2006). The multifaceted mismatch-repair system. *Nat Rev Mol Cell Biol, 7*(5), 335-346.

Kaidi, A., & Jackson, S. P. (2013). KAT5 tyrosine phosphorylation couples chromatin sensing to ATM signalling. *Nature, 498*(7452), 70-+. doi: 10.1038/nature12201

Kamine, J., Elangovan, B., Subramanian, T., Coleman, D., & Chinnadurai, G. (1996). Identification of a cellular protein that specifically interacts with the essential cysteine region of the HIV-1 tat transactivator. *Virology, 216*(2), 357-366. doi: 10.1006/viro.1996.0071

Kao, J., Milano, M. T., Javaheri, A., Garofalo, M. C., Chmura, S. J., Weichselbaum, R. R., & Kron, S. J. (2006). gamma-H2AX as a therapeutic target for improving the efficacy of radiation therapy. *Current Cancer Drug Targets, 6*(3), 197-205. doi: 10.2174/156800906776842957

Kastan, M. B., & Lim, D. S. (2000). The many substrates and functions of ATM. *Nature Reviews Molecular Cell Biology, 1*(3), 179-186. doi: 10.1038/35043058

Keogh, M. C., Mennella, T. A., Sawa, C., Berthelet, S., Krogan, N. J., Wolek, A., . . . Buratowski, S. (2006). The Saccharomyces cerevisiae histone H2A variant Htz1 is acetylated by NuA4. *Genes & Development, 20*(6), 660-665. doi: 10.1101/gad.1388106

Kim, J.-W., Song, P. I., Jeong, M.-H., An, J.-H., Lee, S.-Y., Jang, S.-M., . . . Choi, K.-H. (2008). TIP60 represses transcriptional activity of p73 beta via an MDM2-bridged ternary complex. *Journal of Biological Chemistry, 283*(29), 20077-20086. doi: 10.1074/jbc.M800161200

Kim, M.-Y., Ann, E.-J., Kim, J.-Y., Mo, J.-S., Park, J.-H., Kim, S.-Y., . . . Park, H.-S. (2007). Tip60 histone acetyltransferase acts as a negative regulator of notch1 signaling by

means of acetylation. *Molecular and Cellular Biology, 27*(18), 6506-6519. doi: 10.1128/mcb.01515-06

Kimura, A., & Horikoshi, M. (1998). Tip60 acetylates six lysines of a specific class in core histones in vitro. *Genes to Cells, 3*(12), 789-800. doi: 10.1046/j.1365-2443.1998.00229.x

Kinner, A., Wu, W., Staudt, C., & Iliakis, G. (2008). gamma-H2AX in recognition and signaling of DNA double-strand breaks in the context of chromatin. *Nucleic Acids Research, 36*(17), 5678-5694. doi: 10.1093/nar/gkn550

Kobayashi, J., Tauchi, H., Chen, B., Burma, S., Tashiro, S., Matsuura, S., . . . Komatsu, K. (2009). Histone H2AX participates the DNA damage-induced ATM activation through interaction with NBS1 (vol 380, pg 752, 2009). *Biochemical and Biophysical Research Communications, 384*(2), 271-271. doi: 10.1016/j.bbrc.2009.04.086

Kobor, M. S., Venkatasubrahmanyam, S., Meneghini, M. D., Gin, J. W., Jennings, J. L., Link, A. J., . . . Rine, J. (2004). A protein complex containing the conserved Swi2/Snf2-related ATPase Swr1p deposits histone variant H2A.Z into euchromatin. *Plos Biology, 2*(5), 587-599. doi: e131 10.1371/journal.pbio.0020131

Kramer, B., Kramer, W., & Fritz, H. J. (1984). Different base base mismatches are corrected with different efficiencies by the methyl-directed DNA mismatch-repair system of escherichia-coli. *Cell, 38*(3), 879-887. doi: 10.1016/0092-8674(84)90283-6

Kusch, T., Florens, L., MacDonald, W. H., Swanson, S. K., Glaser, R. L., Yates, J. R., . . . Workman, J. L. (2004). Acetylation by Tip60 is required for selective histone variant exchange at DNA lesions. *Science, 306*(5704), 2084-2087. doi: 10.1126/science.1103455

Lahue, R. S., Au, K. G., & Modrich, P. (1989). DNA mismatch correction in a defined system. *Science, 245*(4914), 160-164. doi: 10.1126/science.2665076

Larochelle, M., & Gaudreau, L. (2003). H2A.Z has a function reminiscent of an activator required for preferential binding to intergenic DNA. *Embo Journal, 22*(17), 4512-4522. doi: 10.1093/emboj/cdg427

Lavin, M. F., & Shiloh, Y. (1997). The genetic defect in ataxia-telangiectasia. *Annual Reviews of Immunology, 15*, 177-202.

Lee, J. H., & Paull, T. T. (2004). Direct activation of the ATM protein kinase by the Mre11/Rad50/Nbs1 complex. *Science, 304*(5667), 93-96. doi: 10.1126/science.1091496

Li, Y., Jenkins, C. W., Nichols, M. A., & Xiong, Y. (1994). Cell-cycle expression and p53 regulation of the cyclin-dependent kinase inhibitor p21. *Oncogene, 9*(8), 2261-2268.

Lieber, M. R. (2008). The mechanism of human nonhomologous DNA end joining. *Journal of Biological Chemistry, 283*(1), 1-5. doi: 10.1074/jbc.R700039200

Lim, D. S., Kim, S. T., Xu, B., Maser, R. S., Lin, J. Y., Petrini, J. H. J., & Kastan, M. B. (2000). ATM phosphorylates p95/nbs1 in an S-phase checkpoint pathway. *Nature, 404*(6778), 613-+.

Luger, K. (1997). Crystal structure of the nucleosome core particle at 2.8 angstrom resolution. *Nature, 389*(6684), 251-260.

Luger, K. (1998). The histone tails of the nucleosome. . *Current Opinion in Genetics and Development, 8*(2), 140-146.

Mattera, L., Courilleau, C., Legube, G., Ueda, T., Fukunaga, R., Chevillard-Briet, M., . . . Trouche, D. (2010). The E1A-Associated p400 Protein Modulates Cell Fate Decisions by the Regulation of ROS Homeostasis. *Plos Genetics, 6*(6). doi: 10.1371/journal.pgen.1000983

Mattera, L., Escaffit, F., Pillaire, M. J., Selves, J., Tyteca, S., Hoffmann, J. S., . . . Trouche, D. (2009). The p400/Tip60 ratio is critical for colorectal cancer cell proliferation through DNA damage response pathways. *Oncogene, 28*(12), 1506-1517. doi: 10.1038/onc.2008.499

Meneghini, M. D., Wu, M., & Madhani, H. D. (2003). Conserved histone variant H2A.Z protects euchromatin from the ectopic spread of silent heterochromatin. *Cell, 112*(5), 725-736. doi: 10.1016/s0092-8674(03)00123-5

Messner, S., & Hottiger, M. O. (2011). Histone ADP-ribosylation in DNA repair, replication and transcription. *Trends in Cell Biology, 21*(9), 534-542. doi: 10.1016/j.tcb.2011.06.001

Mizuguchi, G., Wu, W.-H., Alami, S., & Luk, E. (2012). Biochemical Assay for Histone H2A.Z Replacement by the Yeast SWR1 Chromatin Remodeling Complex. In C. Wu, & C. D. Allis (Eds.), *Nucleosomes, Histones & Chromatin, Pt A* (Vol. 512, pp. 275-291).

Mohrmann, L., Kal, A. J., & Verrijzer, C. P. (2002). Characterization of the extended Myb-like DNA-binding domain of trithorax group protein zeste. *Journal of Biological Chemistry, 277*(49), 47385-47392. doi: 10.1074/jbc.M202341200

Murr, R., Loizou, J. I., Yang, Y.-G., Cuenin, C., Li, H., Wang, Z.-Q., & Herceg, Z. (2006). Histone acetylation by Trrap-Tip60 modulates loading of repair proteins and repair of DNA double-strand breaks. *Nat Cell Biol, 8*(1), 91-99.

Murr, R., Loizou, J. I., Yang, Y. G., Cuenin, C., Li, H., Wang, Z. Q., & Herceg, Z. (2006). Histone acetylation by Trrap-Tip60 modulates loading of repair proteins and repair of DNA double-strand breaks. *Nature Cell Biology, 8*(1), 91-U36. doi: 10.1038/ncb1343

Nakagawa, K., Taya, Y., Tamai, K., & Yamaizumi, M. (1999). Requirement of ATM in phosphorylation of the human p53 protein at serine 15 following DNA double-strand breaks. *Molecular and Cellular Biology, 19*(4), 2828-2834.

Nordentoft, I., & Jorgensen, P. (2003). The acetyltransferase 60 kDa trans-acting regulatory protein of HIV type 1-interacting protein (Tip60) interacts with the translocation E26 transforming-specific leukaemia gene (TEL) and functions as a transcriptional co-repressor. *Biochemical Journal, 374*, 165-173. doi: 10.1042/bj20030087

Ogata, K., Morikawa, S., Nakamura, H., Sekikawa, A., Inoue, T., Kanai, H., . . . Nishimura, Y. (1994). Solution structure of a specific DNA complex of the myb DNA-binding domain with cooperative recognition helices. *Cell, 79*(4), 639-648. doi: 10.1016/0092-8674(94)90549-5

Oliner, J. D., Pietenpol, J. A., Thiagalingam, S., Gvuris, J., Kinzler, K. W., & Vogelstein, B. (1993). Oncoprotein mdm2 conceals the activation domain of tumor suppressor-p53. *Nature, 362*(6423), 857-860. doi: 10.1038/362857a0

Park, J. H., Sun, X. J., & Roeder, R. G. (2010). The SANT domain of p400 ATPase represses acetyltransferase activity and coactivator function of TIP60 in basal p21 gene expression. *Mol Cell Biol, 30*(11), 2750-2761. doi: 10.1128/MCB.00804-09

Pinson, B., Sagot, I., Borne, F., Gabrielsen, O. S., & Daignan-Fornier, B. (1998). Mutations in the yeast Myb-like protein Bas1p resulting in discrimination between promoters in vivo but not in vitro. *Nucleic Acids Research, 26*(17), 3977-3985. doi: 10.1093/nar/26.17.3977

Pinto, D. M. S., & Flaus, A. (2010). Structure and Function of Histone H2AX. In H. P. Nasheuer (Ed.), *Genome Stability and Human Diseases* (Vol. 50, pp. 55-78).

Prokopcova, J., Kleibl, Z., Banwell, C. M., & Pohlreich, P. (2007). The role of ATM in breast cancer development. *Breast Cancer Research and Treatment, 104*(2), 121-128. doi: 10.1007/s10549-006-9406-6

Robinson, P. J. J., An, W., Routh, A., Martino, F., Chapman, L., Roeder, R. G., & Rhodes, D. (2008). 30 nm chromatin fibre decompaction requires both H4-K16 acetylation and linker histone eviction. *Journal of Molecular Biology, 381*(4), 816-825. doi: 10.1016/j.jmb.2008.04.050

Robinson, P. J. J., Fairall, L., Huynh, V. A. T., & Rhodes, D. (2006). EM measurements define the dimensions of the "30-nm" chromatin fiber: Evidence for a compact, interdigitated structure. *Proceedings of the National Academy of Sciences of the United States of America, 103*(17), 6506-6511. doi: 10.1073/pnas.0601212103

Rogakou, E. P., Pilch, D. R., Orr, A. H., Ivanova, V. S., & Bonner, W. M. (1998). DNA double-stranded breaks induce histone H2AX phosphorylation on serine 139. *Journal of Biological Chemistry, 273*(10), 5858-5868. doi: 10.1074/jbc.273.10.5858

Sarcinella, E., Zuzarte, P. C., Lau, P. N. I., Draker, R., & Cheung, P. (2007). Monoubiquitylation of H2A.Z distinguishes its association with euchromatin or

facultative heterochromatin. *Molecular and Cellular Biology, 27*(18), 6457-6468. doi: 10.1128/mcb.00241-07

Shieh, S. Y., Ikeda, M., Taya, Y., & Prives, C. (1997). DNA damage-induced phosphorylation of p53 alleviates inhibition by MDM2. *Cell, 91*(3), 325-334. doi: 10.1016/s0092-8674(00)80416-x

Shiio, Y., & Eisenman, R. N. (2003). Histone sumoylation is associated with transcriptional repression. *Proceedings of the National Academy of Sciences of the United States of America, 100*(23), 13225-13230. doi: 10.1073/pnas.1735528100

Shiloh, Y. (2003). ATM and related protein kinases: Safeguarding genome integrity. *Nature Reviews Cancer, 3*, 155-168.

Shiota, M., Yokomizo, A., Masubuchi, D., Tada, Y., Inokuchi, J., Eto, M., . . . Naito, S. (2010). Tip60 Promotes Prostate Cancer Cell Proliferation by Translocation of Androgen Receptor into the Nucleus. *Prostate, 70*(5), 540-554. doi: 10.1002/pros.21088

Shiotani, B., & Zou, L. (2009). Single-Stranded DNA Orchestrates an ATM-to-ATR Switch at DNA Breaks. *Molecular Cell, 33*(5), 547-558. doi: 10.1016/j.molcel.2009.01.024

Shogren-Knaak, M., Ishii, H., Sun, J. M., Pazin, M. J., Davie, J. R., & Peterson, C. L. (2006). Histone H4-K16 acetylation controls chromatin structure and protein interactions. *Science, 311*(5762), 844-847. doi: 10.1126/science.1124000

Shroff, R., Arbel-Eden, A., Pilch, D., Ira, G., Bonner, W. M., Petrini, J. H., . . . Lichten, M. (2004). Distribution and dynamics of chromatin modification induced by a defined DNA double-strand break. *Current Biology, 14*(19), 1703-1711. doi: 10.1016/j.cub.2004.09.047

Smith, R. J. (2010). *Activation of the DNA double-strand break response by a chromatin remodeler.* (Bachelor of Science with Honours), Massey University, Palmerston North, New Zealand.

Soutoglou, E., & Misteli, T. (2010). Activation of the cellular DNA damage response in the absence of DNA lesions (vol 320, pg 1507, 2008). *Science, 327*(5968), 959-959.

Sterner, D. E., Wang, X., Bloom, M. H., Simon, G. M., & Berger, S. L. (2002). The SANT domain of Ada2 is required for normal acetylation of histones by the yeast SAGA complex. *The journal of biological chemistry, 277*(10), 8178-8186.

Stiff, T., O'Driscoll, M., Rief, N., Iwabuchi, K., Lobrich, M., & Jeggo, P. A. (2004). ATM and DNA-PK function redundantly to phosphorylate H2AX after exposure to ionizing radiation. *Cancer Research, 64*(7), 2390-2396. doi: 10.1158/0008-5472.can-03-3207

Stratton, M. R., Campbell, P. J., & Futreal, P. A. (2009). The cancer genome. *Nature, 458*(7239), 719-724.

Stucki, M., Clapperton, J. A., Mohammad, D., Yaffe, M. B., Smerdon, S. J., & Jackson, S. P. (2005). MDC1 directly binds phosphorylated histone H2AX to regulate cellular responses to DNA double-strand breaks. *Cell, 123*(7), 1213-1226. doi: 10.1016/j.cell.2005.09.038

Stucki, M., Clapperton, J. A., Mohammad, D., Yaffe, M. B., Smerdon, S. J., & Jackson, S. P. (2008). MDC1 directly binds phosphorylated histone H2AX to regulate cellular responses to DNA double-strand breaks (vol 123, pg 1213, 2005). *Cell, 133*(3), 549-549. doi: 10.1016/j.cell.2008.04.021

Sun, Y. L., Jiang, X. F., Chen, S. J., Fernandes, N., & Price, B. D. (2005). A role for the Tip60 histone acetyltransferase in the acetylation and activation of ATM. *Proceedings of the National Academy of Sciences of the United States of America, 102*(37), 13182-13187. doi: 10.1073/pnas.0504211102

Sun, Y. L., Jiang, X. F., Xu, Y., Ayrapetov, M. K., Moreau, L. A., Whetstine, J. R., & Price, B. D. (2009). Histone H3 methylation links DNA damage detection to activation of the tumour suppressor Tip60. *Nature Cell Biology, 11*(11), 1376-U1273. doi: 10.1038/ncb1982

Sun, Y. L., Xu, Y., Roy, K., & Price, B. D. (2007). DNA damage-induced acetylation of lysine 3016 of ATM activated ATM kinase activity. *Molecular and Cellular Biology, 27*(24), 8502-8509.

Sung, P., Krejci, L., Van Komen, S., & Sehorn, M. G. (2003). Rad51 recombinase and recombination mediators. *Journal of Biological Chemistry, 278*(44), 42729-42732. doi: 10.1074/jbc.R300027200

Sykes, S. M., Mellert, H. S., Holbert, M. A., Li, K., Marmorstein, R., Lane, W. S., & McMahon, S. B. (2006). Acetylation of the p53 DNA-binding domain regulates apoptosis induction. *Molecular Cell, 24*(6), 841-851. doi: 10.1016/j.molcel.2006.11.026

Tang, Y., Luo, J. Y., Zhang, W. Z., & Gu, W. (2006). Tip60-dependent acetylation of p53 modulates the decision between cell-cycle arrest and apoptosis. *Molecular Cell, 24*(6), 827-839. doi: 10.1016/j.molcel.2006.11.021

Tyteca, S., Vandromme, M., Legube, G., Chevillard-Briet, M., & Trouche, D. (2006). Tip60 and p400 are both required for UV-induced apoptosis but play antagonistic roles in cell cycle progression. *Embo Journal, 25*(8), 1680-1689. doi: 10.1038/sj.emboj.7601066

Ueda, T., Watanabe-Fukunaga, R., Ogawa, H., Fukuyama, H., Higashi, Y., Nagata, S., & Fukunaga, R. (2007). Critical role of the p400/mDomino chromatin-remodeling ATPase in embryonic hematopoiesis. *Genes to Cells, 12*(5), 581-592. doi: 10.1111/j.1365-2443.2007.01080.x

Umesako, S., Fujisawa, K., Iiga, S., Mori, N., Takahashi, M., Hong, D. P., . . . Okumoto, M. (2005). Atm heterozygous deficiency enhances development of mammary carcinomas in p53 heterozygous knockout mice. *Breast Cancer Research, 7*(1), R164-R170. doi: 10.1186/bcr968

Uziel, T., Lerenthal, Y., Moyal, L., Andegeko, Y., Mittelman, L., & Shiloh, Y. (2003). Requirement of the MRN complex for ATM activation by DNA damage. *Embo Journal, 22*(20), 5612-5621.

Valdes-Mora, F., Song, J. Z., Statham, A. L., Strbenac, D., Robinson, M. D., Nair, S. S., . . . Clark, S. J. (2012). Acetylation of H2A.Z is a key epigenetic modification associated with gene deregulation and epigenetic remodeling in cancer. *Genome Research, 22*(2), 307-321. doi: 10.1101/gr.118919.110

Ward, I. M., & Chen, J. (2001). Histone H2AX is phosphorylated in an ATR-dependent manner in resonpose to replicational stress. *The journal of biological chemistry, 276*(51), 47759-47762.

Ward, I. M., Minn, K., Jorda, K. G., & Chen, J. J. (2003). Accumulation of checkpoint protein 53BP1 at DNA breaks involves its binding to phosphorylated histone H2AX. *Journal of Biological Chemistry, 278*(22), 19579-19582. doi: 10.1074/jbc.C300117200

Watters, D., Khanna, K. K., Beamish, H., Birrell, G., Spring, K., Kedar, P., . . . Lavin, M. (1997). Cellular localisation of the ataxia-telangiectasia (ATM) gene product and discrimination between mutated and normal forms. *Oncogene, 14*(16), 1911-1921. doi: 10.1038/sj.onc.1201037

West, M. H. P., & Bonner, W. M. (1980). Histone-2a, a heteromorphous family of 8 protein species. *Biochemistry, 19*(14), 3238-3245. doi: 10.1021/bi00555a022

Williams, R. S., Dodson, G. E., Limbo, O., Yamada, Y., Williams, J. S., Guenther, G., . . . Tainer, J. A. (2009). Nbs1 Flexibly Tethers Ctp1 and Mre11-Rad50 to Coordinate DNA Double-Strand Break Processing and Repair. *Cell, 139*(1), 87-99. doi: 10.1016/j.cell.2009.07.033

Wong, M. M., Cox, L. K., & Chrivia, J. C. (2007). The chromatin remodeling protein, SRCAP, is critical for deposition of the histone variant H2A.Z at promoters. *Journal of Biological Chemistry, 282*(36), 26132-26139. doi: 10.1074/jbc.M703418200

Wu, L., Luo, K., Lou, Z., & Chen, J. (2008). MDC1 regulates intra-S-phase checkpoint by targeting NBS1 to DNA double-strand breaks. *Proceedings of the National Academy of Sciences of the United States of America, 105*(32), 11200-11205. doi: 10.1073/pnas.0802885105

Xiao, H., Chung, J., Kao, H. Y., & Yang, Y. C. (2003). Tip60 is a co-repressor for STAT3. *Journal of Biological Chemistry, 278*(13), 11197-11204. doi: 10.1074/jbc.M210816200

Xu, B., Kim, S. T., Lim, D. S., & Kastan, M. B. (2002). Two molecularly distinct G(2)/M checkpoints are induced by ionizing irradiation. *Molecular and Cellular Biology, 22*(4), 1049-1059. doi: 10.1128/mcb.22.4.1049-1059.2002

Xu, Y., Ashley, T., Brainerd, E. E., Bronson, R. T., Meyn, M. S., & Baltimore, D. (1996). Targeted disruption of ATM leads to growth retardation, chromosomal fragmentation during meiosis, immune defects, and thymic lymphoma. *Genes & Development, 10*(19), 2411-2422. doi: 10.1101/gad.10.19.2411

Xu, Y., Sun, Y., Jiang, X., Ayrapetov, M. K., Moskwa, P., Yang, S., . . . Price, B. D. (2010). The p400 ATPase regulates nucleosome stability and chromatin ubiquitination during DNA repair. *Journal of Cell Biology, 191*(1), 31-43. doi: 10.1083/jcb.201001160

Yamamoto, T., & Horikoshi, M. (1997). Novel substrate specificity of the histone acetyltransferase activity of HIV-1-Tat interactive protein Tip60. *Journal of Biological Chemistry, 272*(49), 30595-30598. doi: 10.1074/jbc.272.49.30595

You, Z., Bailis, J. M., Johnson, S. A., Dilworth, S. M., & Hunter, T. (2007). Rapid activation of ATM on DNA flanking double-strand breaks. *Nature Cell Biology, 9*(11), 311-U193. doi: 10.1038/ncb1651

Yuan, S. S. F., Chang, H. L., Hou, M. F., Chan, T. F., Kao, Y. H., Wu, Y. C., & Su, J. H. (2002). Neocarzinostatin induces Mre11 phosphorylation and focus formation through an ATM- and NBS1-dependent mechanism. *Toxicology, 177*(2-3), 123-130. doi: 10.1016/s0300-483x(02)00220-2

Yuan, S. S. F., Chang, H. L., & Lee, E. (2003). Ionizing radiation-induced Rad51 nuclear focus formation is cell cycle-regulated and defective in both ATM(-/-) and c-Abl(-/-) cells. *Mutation Research-Fundamental and Molecular Mechanisms of Mutagenesis, 525*(1-2), 85-92. doi: 10.1016/s0027-5107(03)00009-5

Zhang, Y. (2003). Transcriptional regulation by histone ubiquitination and deubiquitination. *Genes & Development, 17*(22), 2733-2740. doi: 10.1101/gad.1156403

Zilberman, D., Coleman-Derr, D., Ballinger, T., & Henikoff, S. (2008). Histone H2A.Z and DNA methylation are mutually antagonistic chromatin marks. *Nature, 456*(7218), 125-129.

Appendix 1 PCR Primers and Protocols

Name	Orientation	Sequence (5' → 3')	Annealing Temp(°C)
CBS sequencing	Forward	CGTGACGGTTGTTGTGCT	
	Reverse	CTAGAAGGCACAGTCGAGG	
Chromo	Forward	AAGGAATTCATGGCGGAGGTGGGGGAGATAATC	52
	Reverse	GGAATCGATCTAAACCTTCTTTCTCTTCTTCTTGGGCTGGTCAGGCTCGCCACCGGGAAT	
Chromozinc	Forward	AAGGAATTCATGGCGGAGGTGGGGGAGATAATC	52
	Reverse	GGAATCGATCTAAACCTTCTTTCTCTTCTTCTTGGGGGAGATGGTGCCCTTGCGGTAAAT	
Zinc	Forward	GACGAATTCCTCTCCTCCAGCTCCTGCCTGCAG	52
	Reverse	GGAATCGATCTAAACCTTCTTTCTCTTCTTCTTGGGGGAGATGGTGCCCTTGCGGTAAAT	
ZincHAT	Forward	GACGAATTCCTCTCCTCCAGCTCCTGCCTGCAG	52
	Reverse	GATATCGATCTAAACCTTCTTTCTCTTCTTCTTGGGGGTCTGGGACCAGTAGCTTCGATA	
HAT	Forward	CGTGAATTCACCAAGTGTGACCTACGACATCCT	52
	Reverse	GATATCGATCTAAACCTTCTTTCTCTTCTTCTTGGGGGTCTGGGACCAGTAGCTTCGATA	
ΔH1	Forward	TGCAGCAGCGCACTGATGAGCCACTCGGGGTTG	60
	Reverse	GGCTCATCAGTGCGCTGCTGCAGGCTGTAAAGC	
ΔH2	Forward	ACGTCACTGACATTAGGTGTGTGAGCAGGTGAC	60
	Reverse	ACACACCTAATGTCAGTGACGTTGTTAACTCCTG	
ΔH3	Forward	TCCTGTAGCCGAATCGATGTCATCATTCCACGAGAGGAG	63
	Reverse	TGGAATGATGACATCGATTCGGCTACAGGAGTTAACAAC	
HA-p400	Forward	ATCGAATTCGGTACCATGTACCCATACGATGTTCCTGACTATGCGGGGATGCACCATGGCACTGGCCCCCAG	55
	Reverse	TGCAGGCCGGCCCCACCCGCGGCT	
HA-ATM	Forward	TTCTTCGATATCGGTACCATGTACCCATACGATGTTCCTGACTATGCGGGGATGAGTCTAGTACTTAATGATCTG	55
	Reverse	ACTACTGATATCTGCCATCAATTCAATC	

Table A.1 Primer sequences and annealing temperatures used in this study.

PCR protocol HA-ATM. Reactions were carried out using KAPA HiFi HotStart polymerase as described below. Annealing temperatures for primer pairs are shown in table A.1.

Component	Volume (µL)
2x KAPA HiFi HotStart ReadyMix	25
Forward Primer (10 µM)	1.5
Reverse Primer (10 µM)	1.5
Template DNA (10 ng/µL)	1
PCR Grade Water	21

Table A.2 KAPA HiFi HotStart PCR reaction composition

Temperature	Time	Repeats
95^{0}C	3 min	1
98^{0}C	20 sec	
55^{0}C	15 sec	30x
72^{0}C	30 sec	
72^{0}C	5 min	1x
4^{0}C	Hold	

Table A.3 KAPA HiFi HotStart PCR protocol

PCR protocol for HA-p400. Reactions were carried out using FastStart Taq from Roche. Annealing temperatures for primer pairs are shown in table A.1.

Component	Volume (µL)
10 X PCR reaction buffer (20 mM $MgCl_2$)	5
Forward Primer (10 µM)	2.5
Reverse Primer (10 µM)	2.5
dNTPs (10 mM)	5
Template DNA (10 ng/µL)	2.5
Phusion Polymerase (5 U/µL)	0.5
PCR Grade Water	32

Table A.4 FastStart Taq PCR reaction composition

Temperature	Time	Repeats
95^{0}C	4 min	1
95^{0}C	30 sec	
55^{0}C	35 sec	30x
72^{0}C	1.5 min	
72^{0}C	7 min	1x
4^{0}C	Hold	

Table A.5 FastStart Taq PCR protocol

Appendix 2 Antibodies used in immunoblotting

Antibody	Company	Catalogue number	Initial concentration	Immunoblot concentration	Rabbit or Mouse
H2AX	Milipore	07-627	1 mg/mL	5 µg/mL	Rabbit
H2AX S139P	Milipore	07-164	1 mg/mL	5 µg/mL	Rabbit
β-actin	Sigma	A5316	1 mg/mL	1 µg/mL	Mouse
ATM	Calbiochem	819844	0.1 mg/mL	1 µg/mL	Rabbit
FLAG	Sigma	F3165	1 mg/mL	2 µg/mL	Mouse
HA	Sigma	SAB4300603	1 mg/mL	2 µg/mL	Rabbit
TIP60	N/A	N/A	1 mg/mL	5 µg/mL	Rabbit
p400	N/A	N/A	0.7 mg/mL	0.7 µg/mL	Rabbit
Ku86	Santa Curz	E0307	0.2 mg/mL	0.4 µg/mL	Mouse

Antibodies raised against TIP60 and p400 were custom antibodies raised by Dr Jeong Park.

Secondary antibodies that were used in this study were SC2054 and SC2055 (α-rabbit and α-mouse respectively) were purchased at a concentration of 2 mg/mL and used at a final concentration of 0.2 µg/mL.

Appendix 3 Plasmid Maps

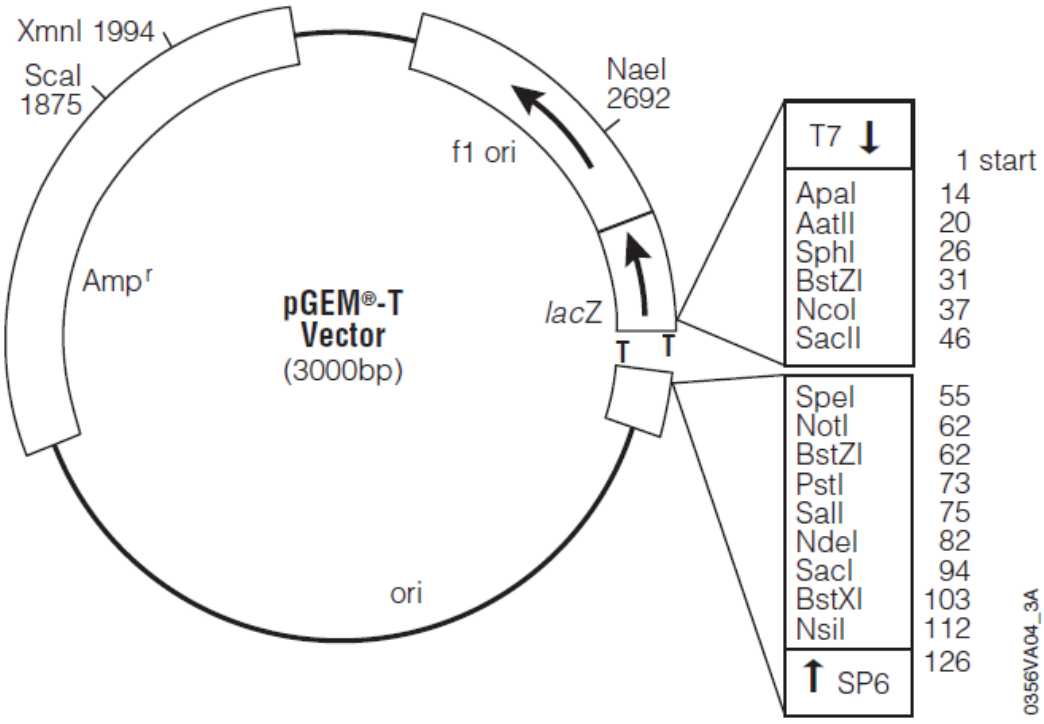

Figure A3.1 Plasmid map of pGEM-T Vector.

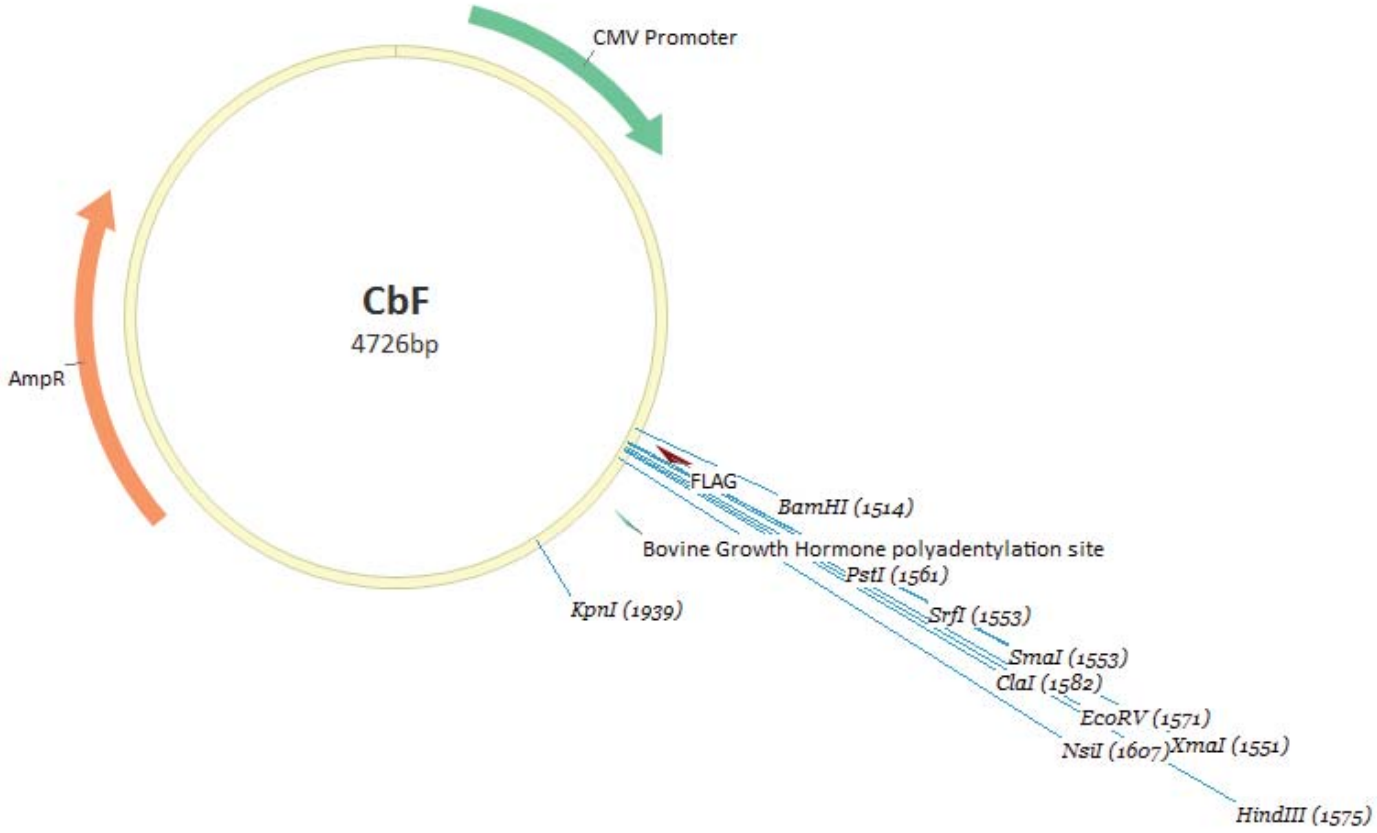

Figure A3.2 Plasmid map of CbF vector

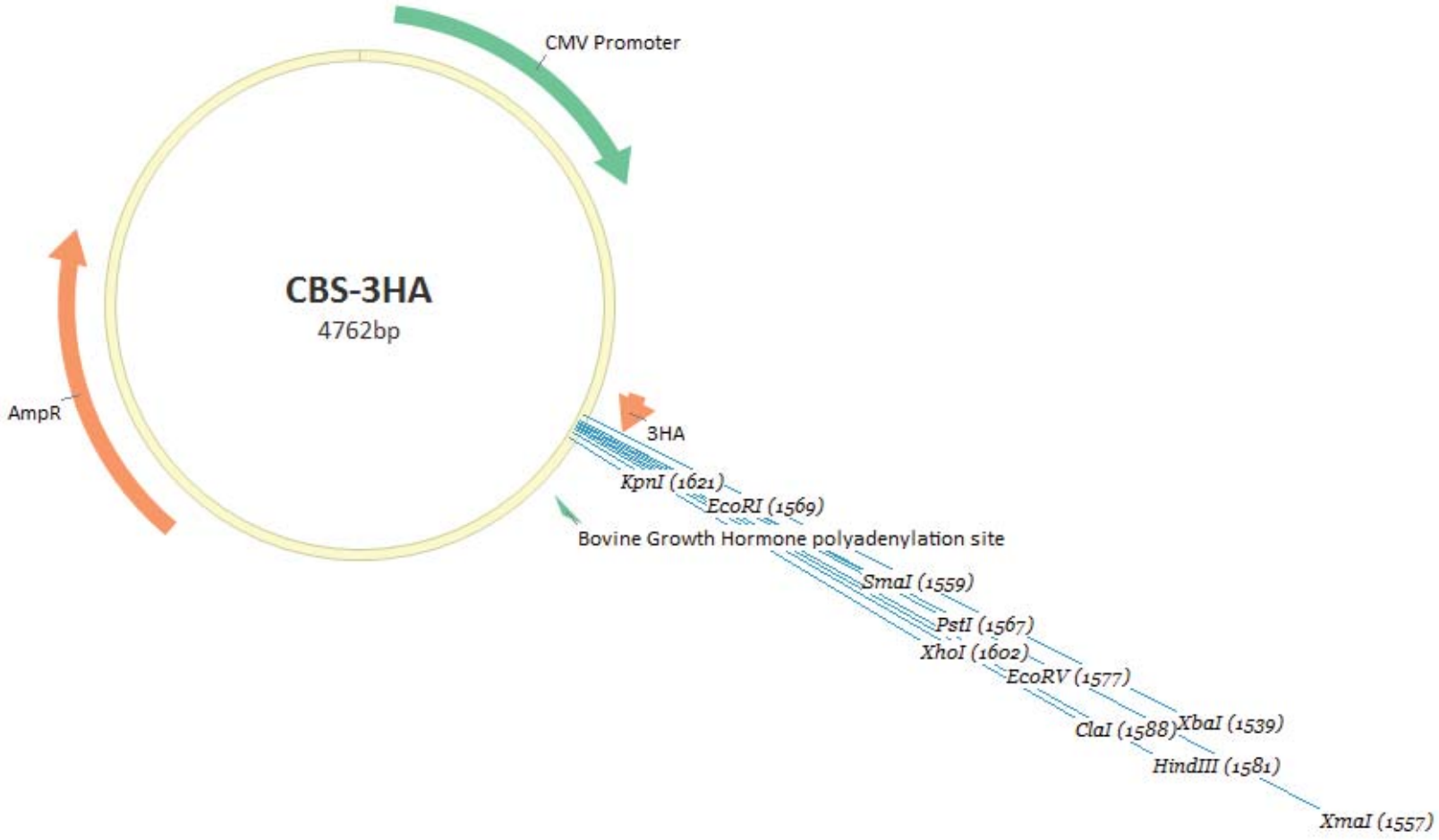

Figure A3.3 Plasmid map of CBS-3HA vector

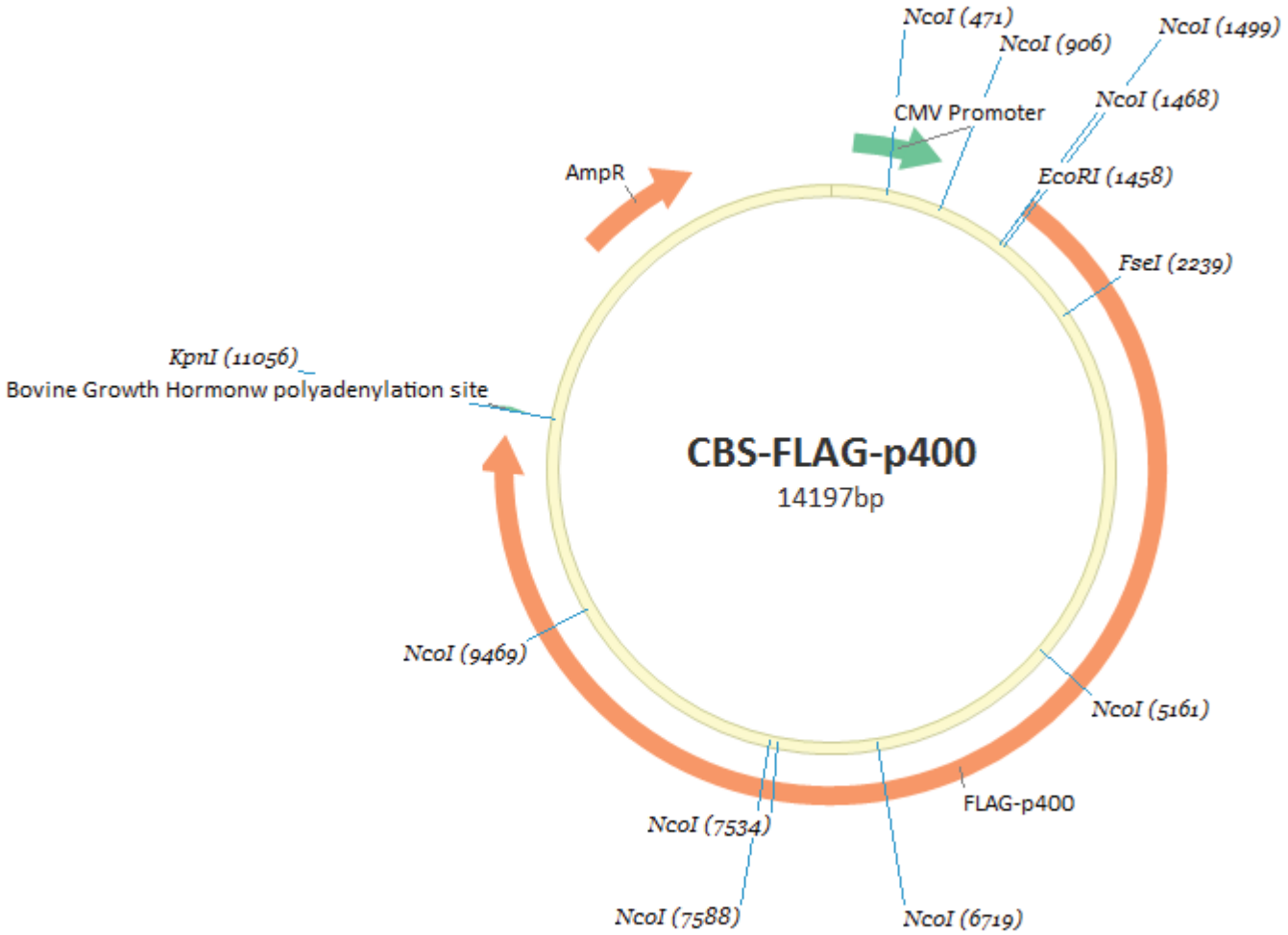

Figure A3.4 Plasmid map of CBS-FLAG-p400

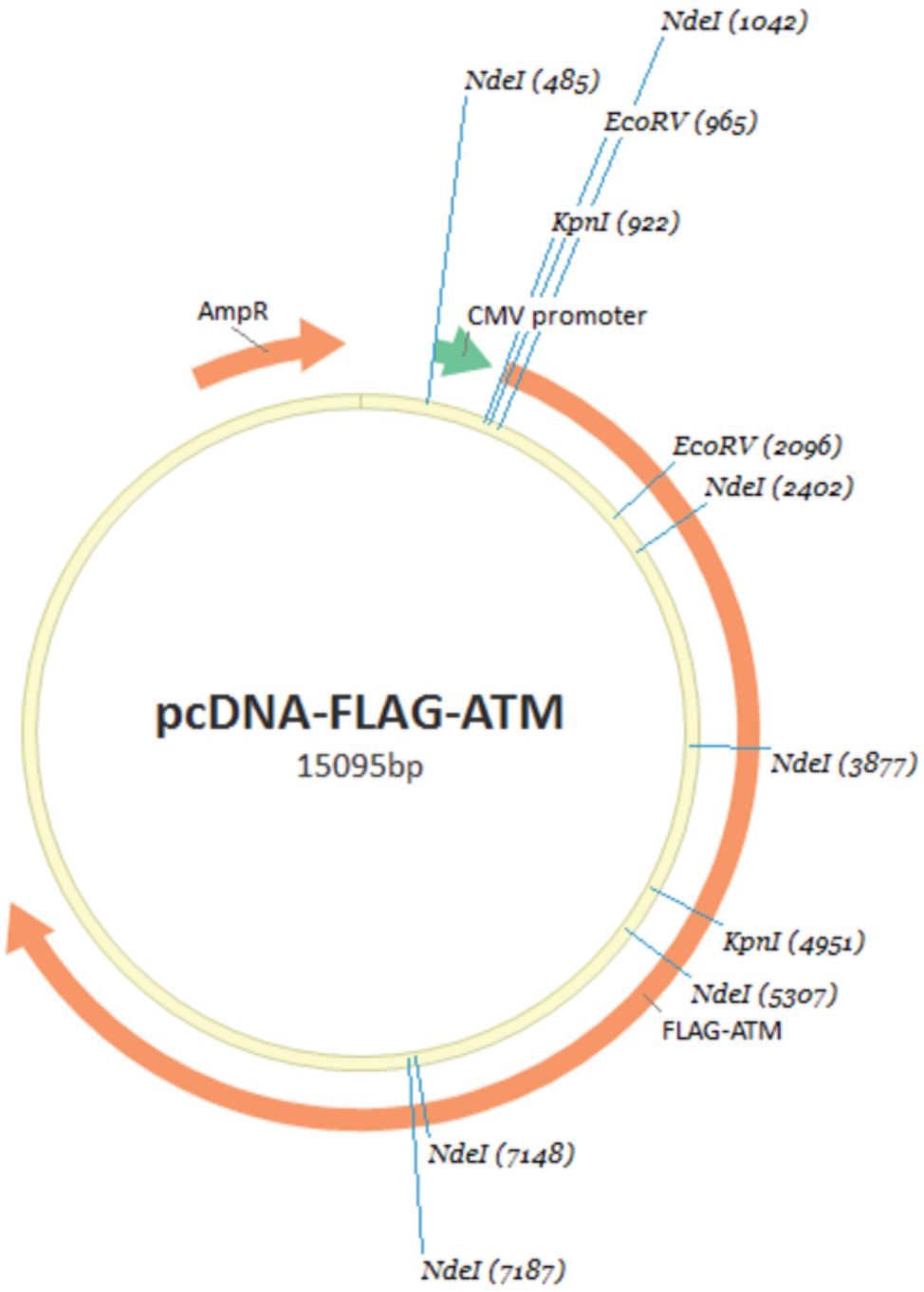

Figure A3.5 Plasmid map of pcDNA-FLAG-ATM

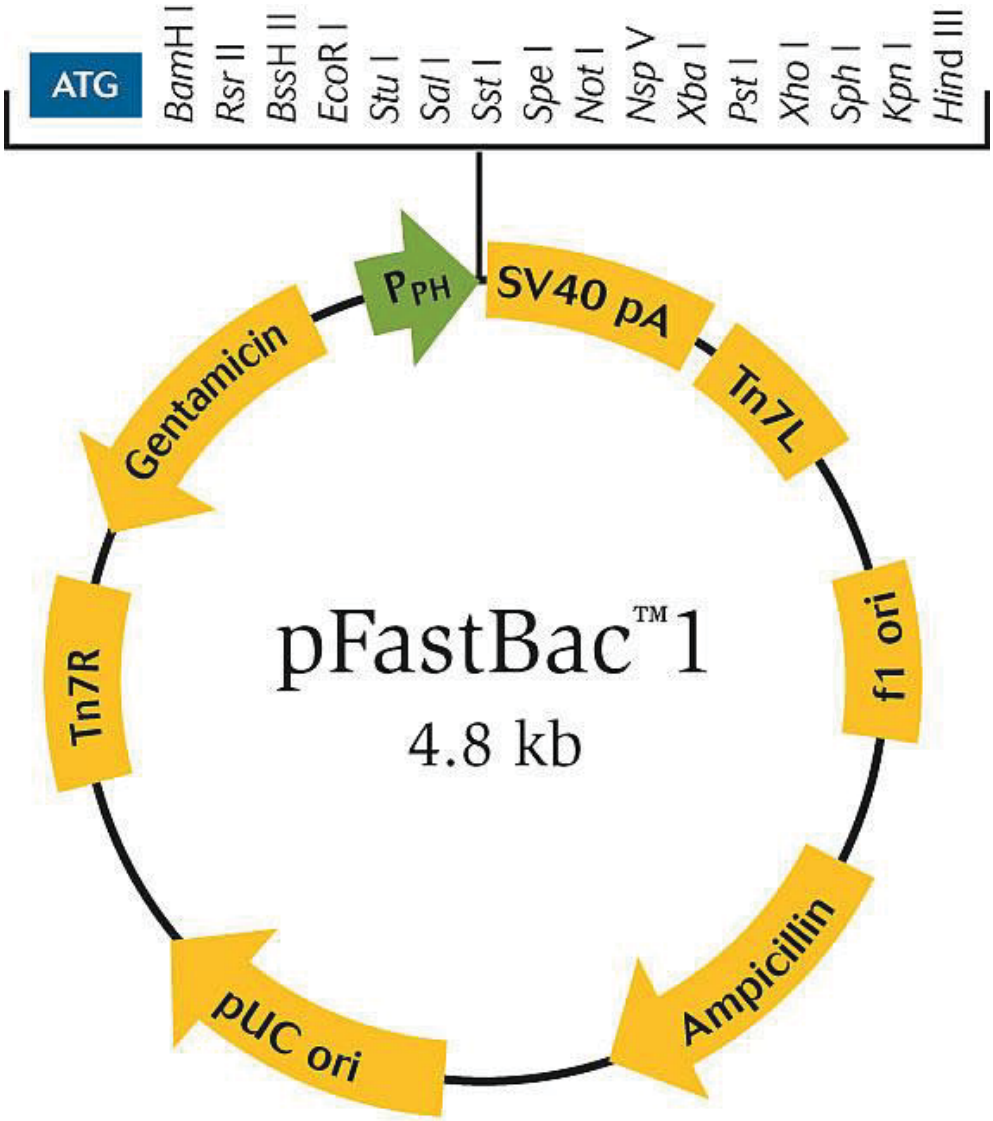

Figure A3.6 Plasmid map of pFastBac1